International
Progress Report

IPR-01-26

Äspö Hard Rock Laboratory

Integrated stress analysis of hydraulic stress data in the Äspö region, Sweden

Analys of hydraulic fracturing stress measurements and hydraulic test in pre-existing fractures (HTPF) in boreholes KAS02, KAS03 and KLX02

Daniel Ask, KTH
Ove Stephansson, KTH

Francois H Cornet, Institut de Physique du Globe de Paris

May 2001

Svensk Kärnbränslehantering AB
Swedish Nuclear Fuel
and Waste Management Co
Box 5864
SE-102 40 Stockholm Sweden
Tel +46 8 459 84 00
Fax +46 8 661 57 19

Äspö Hard Rock
Laboratory

Report no.
IPR-01-26

No.
F86K

Author
Ask, Stephansson, Cornet

Date
01-05-01

Checked by
Rolf Christiansson

Date
2001-07-10

Approved
Christer Svemar

Date
01-08-02

Äspö Hard Rock Laboratory

Integrated stress analysis of hydraulic stress data in the Äspö region, Sweden

Analysis of hydraulic fracturing stress measurements and hydraulic test in pre-existing fractures (HTPF) in boreholes KAS02, KAS03 and KLX02

Daniel Ask, KTH
Ove Stephansson, KTH

Francois H Cornet, Institut de Physique du Globe de Paris

May 2001

Keywords: Rock mechanics, rock stress, hydraulic fracturing, integrated stress analysis, chevron notches

ABSTRACT

We have conducted an integrated stress analysis study of in-situ hydraulic rock stress measurements in the Äspö region, Sweden. The inversion method, which was developed by Cornet and Valette (1984) based on the least squares criterion, is applied to determine the regional stress field. A three-, six-, and seven-parameter inversion program have been made and successfully calibrated. Totally, six calibrations and comparisons have been performed using published data from Sweden (Ljunggren and Raillard, 1987) and France (Cornet and Burlet, 1992). Later, the program has been applied to the Äspö data.

The studied in-situ stress data from Äspö consist of 5 hydraulic tests of pre-existing fractures (HTPF) and 80 hydraulic fracturing measurements (HF) down to 1337 m depth in boreholes KAS02, KAS03 and KLX02 (Bjarnason et al., 1989; Ljunggren and Klasson, 1997; Ekman, 1997; Ekman et al., 1997). Altogether, 85 successful in-situ stress measurements have been performed. The in-situ data has been re-analyzed, based on the assumption that all measurements obey Gaussian distribution. The inversion indicates that the first shut-in pressure from HF measurements is preferable when using the integrated stress determination method.

The results indicate that the magnitude of minimum horizontal stress is of the same order of magnitude as the vertical stress down to approximately 400-500 m depth. Below 500 m depth the vertical stress is the minimum stress at least down to approximately 900 m depth. The orientation of maximum horizontal stress is NW-SE.

The inversion results are in some cases associated with rather large uncertainties, especially regarding the magnitude and orientation of maximum horizontal stress. The most probable reason for this is that the number of HF data greatly exceeds the number of HTPF data. Normally, when applying the integrated stress analysis method to hydraulic stress measurements, this relationship is the opposite. During the coarse of inversion analysis, it has been evident that the resolutions of the unknowns are greatly improved with increasing number of HTPF data. Further complications of analyses are test sections that have more than one fracture, the existence of chevron notches, and the high flow rate pumping procedure used in the HF measurements.

The study also includes an investigation of geological structures influencing the regional stress field. Based on the hydraulic stress data, it is suggested that one (or more) sub-horizontal zone(s), consisting of fine-grained granite (aplite), disturb(s) the stress field below the island of Äspö. In borehole KLX02, the redistribution of the stress field between 700-1100 m depth is caused by either: (i) two intersection sub-vertical zones, SFZ04 and SFZ07 (Eriksson et al., 1997); or (ii) two sub-horizontal zones (Bergman et al., 2001). The stress analysis of borehole KLX02 is partly based on interpretation of fractures detected from BIPS-pictures, which proved to be very difficult and associated with great uncertainties. Therefore, the state of stress in the deeper sections in KLX02 is discussed only tentatively.

SAMMANFATTNING

Vi har utfört en integrerad spänningsanalys med hjälp av in-situ hydrauliska spänningsdata för området kring Äspö, Sverige. Spänningsdata från Äspö har analyserats med en inversionsmetod som utvecklats av Cornet och Valette (1984) och är baserad på minsta kvadrat metoden. En tre-, sex- och sju-parametersmodell har utvecklats och kalibrerats. Totalt har sex kalibreringar och jämförelser utförts med publiserade data från Sverige (Ljunggren and Raillard, 1987) och Frankrike (Cornet and Burlet, 1992). Därefter har programmen applicerats på spänningsdata från Äspö.

In-situ data från Äspö består av 5 hydrauliska tester på existerande sprickor (HTPF) och 80 hydrauliska spräckningsmätningar (HF) i borrhål KAS02, KAS03 och KLX02 (Bjarnason et al., 1989; Ljunggren and Klasson, 1997; Ekman, 1997; Ekman et al., 1997). Tillsammans har 85 in-situ spänningsmätningar utförts. In-situ spänningsdata har granskats baserat på antagandet att alla mätningar är Gauss fördelade. Inversionsresultaten indikerar att det första shut-in trycket från HF mätningar är att föredra vid användandet av den integrerade spänningsanalysen.

Analysen indikerar generellt att minsta horisontalspänning är av samma storleksordning som vertikalspänningen ned till ca 400-500 m djup. Under 500 m djup är vertikalspänningen den minsta spänningen, åtminstone ned till 900 m djup. Orienteringen av största horisontalspänning är NV-SO.

Inversionresultaten är i vissa fall associerade med relativt stora osäkerheter, speciellt för storlek och orientering av största horisontalspänning. Den troligaste orsaken till detta är att antalet data från HF är betydligt större än antalet HTPF data. Normalt, när man använder den integrerade spänningsmetoden för hydrauliska spänningsdata, är förhållandet det motsatta. Under analysen visade det sig att upplösningen på de okända parametrarna förbättrades betydligt med ökat antal HTPF mätningar. Ytterligare osäkerheter i ursprungliga data är att ett antal mätningar har mer än en spricka i sektionen, att vissa sektioner visar spår av sk chervon notches samt det höga pumpflödet under HF mätningar.

I studien har också geologiska stukturer analyserats. Baserat på hydrauliska spänningsdata, har vi funnit stöd för antagandet att en/flera sub-horisontell(a) zon(er), bestående av en uppsprucken finkornig granit (aplit), påverkar spänningarna under Äspö. I borrhål KLX02, utgörs diskontinuiteten vid 700-1100 m djup av antingen (i) två korsande sub-vertikala zoner, SFZ04 och SFZ07 (Eriksson m fl, 1997) eller (ii) av två sub-horisontella zoner (Bergman m fl., 2001). Spänningsanalysen av de djupare sektionerna i borrhål KLX02 involverar analys av BIPS-orienterade sprickor. Dessa visade sig vara mycket svårtolkade och är således mycket osäkra. Med anledning av detta diskuteras endast spänningstillståndet i de djupare delarna av KLX02.

TABLE OF CONTENTS

SUMMARY AND CONCLUSIONS

This report considers the results from an integrated stress analysis using existing hydraulic stress measurement data from the Äspö region (Bjarnason et al., 1989; Ljunggren and Klasson, 1997; Ekman, 1997; Ekman et al., 1997). The stress data consists of 80 hydraulic fracturing measurements and 5 hydraulic test in pre-existing fractures in the three core drilled boreholes KAS02 and KAS03 and KLX02, drilled from the surface.

The objective of the analysis is to improve the interpretation of the regional stress field in the Äspö region using an integrated stress analysis method. The analysis is based on the least square criterion and is an iterative inversion method (Cornet and Valette, 1984; Tarantola and Valette, 1982). The method assumes that the stress data follow Gaussian distribution, thus may be described by their expected value, their variance and covariance's, respectively. Furthermore, *a priori* knowledge of the unknowns is assumed to exist that can be formulated in terms of expected value, variance and covariances. The quality of the inversion result was mainly controlled by: 1) comparing the *a priori* and the *a posteriori* measurement data. These must not differ more than about 1.5 times the standard deviation; 2) the resolution of unknown parameters. If the *a posteriori* variance is small, the value has been well resolved; if it is nearly equal to the *a priori* variance the corresponding unknowns has not been resolved.

A three-, six- and seven-parameter model for hydraulic stress data have been developed and successfully calibrated on both Swedish and French data. The calculation of horizontal stresses and the orientation of maximum horizontal stress in the test intervals are in accordance with the published data.

The results of the inversion analysis using data from the Äspö area are reasonable. However, all inversions are associated with uncertainties, in some cases large, which mean that the state of stress in some cases should only be used as a guideline. The analysis indicates discrepancies regarding the magnitudes and orientations of the stresses. The magnitudes are non-linear with depth and are strongly influenced by discontinuities (Bjarnason et al., 1989; Leijon, 1995; Ljunggren and Klasson, 1997; Ekman, 1997; Ekman et al., 1997). These discontinuities occur below 600 m depth in KAS02; between 575 and 750 m depth in KAS03; and between 700 and 1100 m depth in KLX02. We suggest that the redistribution of the stress field in the Äspö boreholes is due to one (or more) sub-horizontal zone(s). Possibly, also the shear zone EW-1 effects the regional stress field on the Äspö island. However, firm conclusions regarding the effects of the EW-1 zone cannot be made. In KLX02, two contradictory suggestions have been made concerning the structures between 700-1100 m depth. Eriksson et al. (1997) suggested that a discontinuity, consisting of two intersecting major fracture zones (SFZ04 and SFZ07), is located at 700-1100 m depth. However, Bergman et al. (2001) found two sub-horizontal reflectors at 650 and 900 m depth (orientation 308°/9° and 351°/10°, respectively), assuming a p-wave velocity of 5500 m/s. We hope that further research is conducted to verify/reject these suggestions.

The inversion results indicate that the minimum horizontal stress is very close to the vertical stress down to approximately 400-500 m depth. This result has been verified by Ask et al. (2001), who made an analysis of overcoring data in borehole KA3579G, Prototype Repository, Äspö HRL. The orientation of maximum horizontal stress is NW-SE. Below the discontinuities the analysis was based on a three-parameter model. In boreholes KAS02 and KAS03, thrust regimes are indicated at least down to approximately 900 m depth. The results from the integrated stress analysis (Cornet and Valette, 1984) have been compiled into six figures, S-1 to S-3, showing the state of stress in boreholes KAS02, KAS03, and KLX02 using the first shut-in pressure from the existing hydraulic stress data.

The analysis of the existing BIPS-pictures from KLX02 gave one possible borehole breakout oriented ENE-WSW at 1341-1342 m depth, indicating a NNW-SSE orientation of maximum horizontal stress. This suggested breakout was also identified using a forward-viewing camera and has a depth of approximately 1-2 cm. A possible borehole breakout in KLX02 have also been found between 750-820 m depth oriented NW-S with a maximum depth of 5 mm, i.e. indicating an orientation of maximum horizontal stress approximately ENE-WSW. The dominating elongation is in the NW direction and the less dominant in the S direction (M. Ask, personal communication). Furthermore, white colored small aperture fractures (probably calcite filled) appear in NE-SW direction between 1070-1080 m depth and rotating towards NW-SE with depth down to approximately 1300 m depth. Below 1300 m the fractures turn towards NNW-SSE. We suggest that these fractures are drilling induced tensile fracture and may be used to constrain the orientation of maximum horizontal stress. Conclusively, we suggest that the discontinuity at 700-1100 m depth in borehole KLX02, composed of either two sub-horizontal zones (Bergman et al., 2000) or two intersecting zones, SFZ04 and SFZ07 (Eriksson et al., 1999), cause a strong re-orientation of the stress field. The orientation of maximum horizontal stress above the discontinuity is NW-SE turning towards ENE-WSW within the zone and turning back to NW-SE below the discontinuity. However, the BIPS-measurements and the analysis of BIPS-pictures are associated with great uncertainties and these results should be considered the author's point of view. Due to these uncertainties and the contradictory results concerning the orientation of maximum horizontal stress compared to Ljunggren and Klasson (1997) in the deeper section of KLX02, we suggest that further research is conducted to verify/reject our interpretation, see Ch. 6.4 and 8.

Applications of the inversion results indicate that the first shut-in pressure from the hydraulic fracturing measurements is preferable when using the integrated stress determination method. Perhaps this is due to the fact that the fracture tested later connects with another fractures, thereby changing the hydraulic response resulting in erroneous fracture normal stress, during the propagation in the following pumping cycles. Another explanation may be that more fractures in the test section are opened during the propagation phase of the pump test. A third explanation may be the fact that the induced fracture turns from vertical to horizontal as it propagates away from the borehole (Zoback et al., 1977; Evans et al., 1989).

The fact that the majority of the stress measurements at Äspö are hydraulic fracturing measurements, means that the normal high flow rate pumping test has been used. This pumping procedure does not give as well defined fracture normal stress as compared to

the low flow rate hydraulic jacking tests, which in turn effects the resolution of the unknown parameters during inversion.

The most likely reason for the relatively poor results of the inversion analysis is that the number of hydraulic fracturing data greatly exceeds the number of HTPF data. Normally, the integrated stress analysis method is applied using a majority of HTPF data, with fractures located at different depths and, more important, with different orientations. The major drawback when using a majority of hydraulic fracturing measurements is that the induced fractures have similar orientations. During the coarse of inversion analysis, it was concluded that the resolution of the unknown parameters was greatly improved with increasing number of tests on inclined fractures.

Another reason for the relatively poor result is that many hydraulic fracturing tests were performed in sections that had more than one fracture. This implies that several fracture combinations had to be tested and more important, the fracture normal stress may not be representative since it includes pumping in two or more fracture simultaneously. The occurrence of the induced and pre-existing fracture were probably the result of the high flow rate pumping tests involved in the hydraulic fracturing method. Most probably, the pre-existing fracture was sealed in the beginning of the test and opened simultaneously with the induced fracture. The following pumping test subsequently involved both the induced and pre-existing fracture and the data were in some cases rejected as outflyers during the inversion analysis.

Additionally, the analysis of existing data reveals existence of chevron notches on the impression packer. The occurrence of chevron notches indicates that the vertical stress is inclined with respect to the borehole axis or that an induced fracture turns from vertical to horizontal as it propagates away from the borehole. The latter implies that the shut-in pressure may only afflict the vertical stress and not the minimum horizontal stress. Thus, the maximum horizontal stress remains undetermined (Zoback et al., 1977; Evans et al., 1989). The latter effect could possibly also explain why the minimum horizontal stress is close to the weight of the overburden in the Äspö region. Data that indicated chevron notches was however not deviating strongly from the remainder of the data and consequently were not excluded during the inversion analysis. They are though still a source of uncertainty.

The HF method also includes uncertainties that should be kept in mind during the comparison with the inversion result. These are mainly the pore and reopening pressure, the effect of non-vertical induced fractures and scattered orientations, and the assumptions concerning vertical stress component.

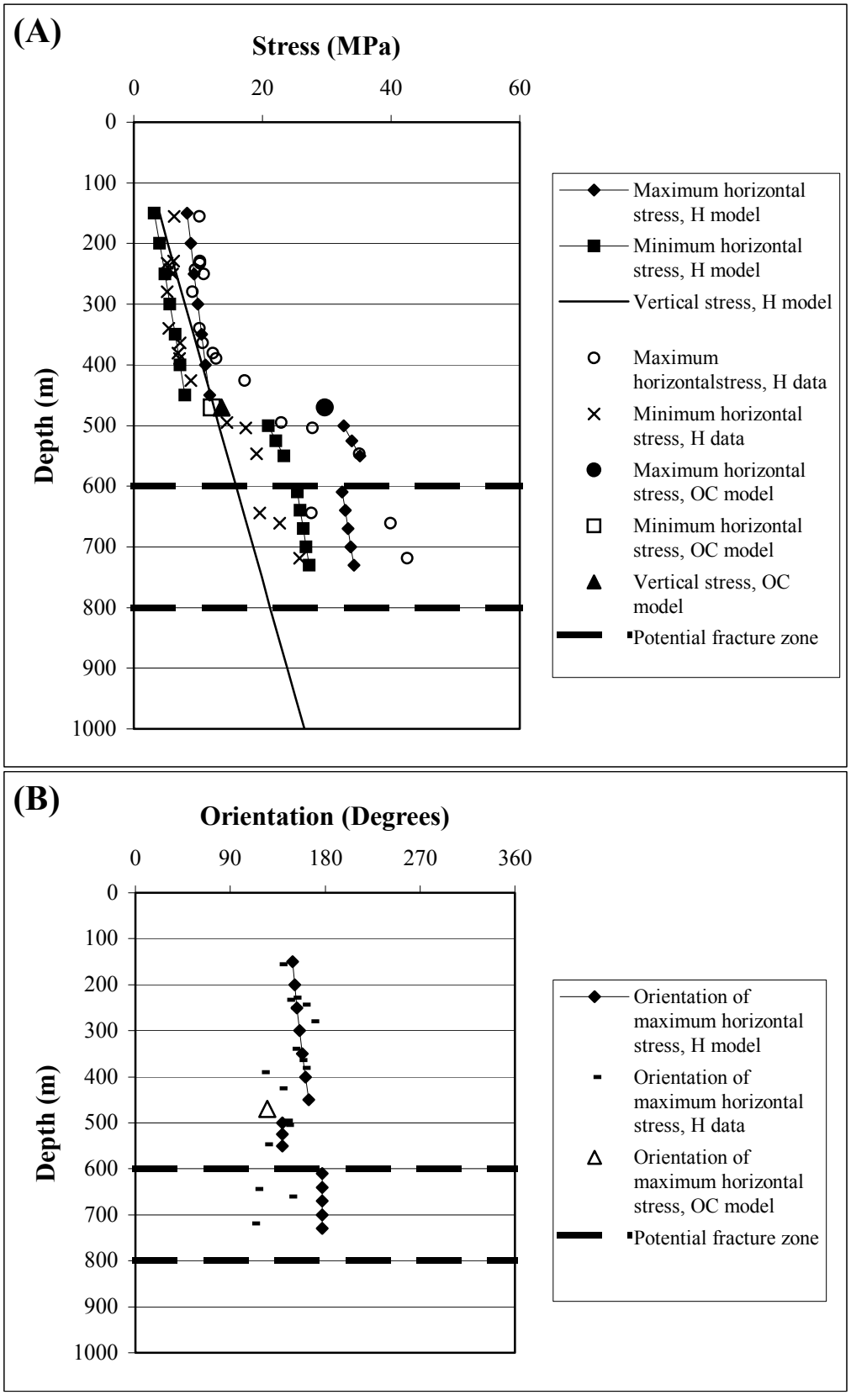

Figure S-1. *Summary of inversion results from borehole KAS02; (A) magnitudes and (B) orientation of* S_h.

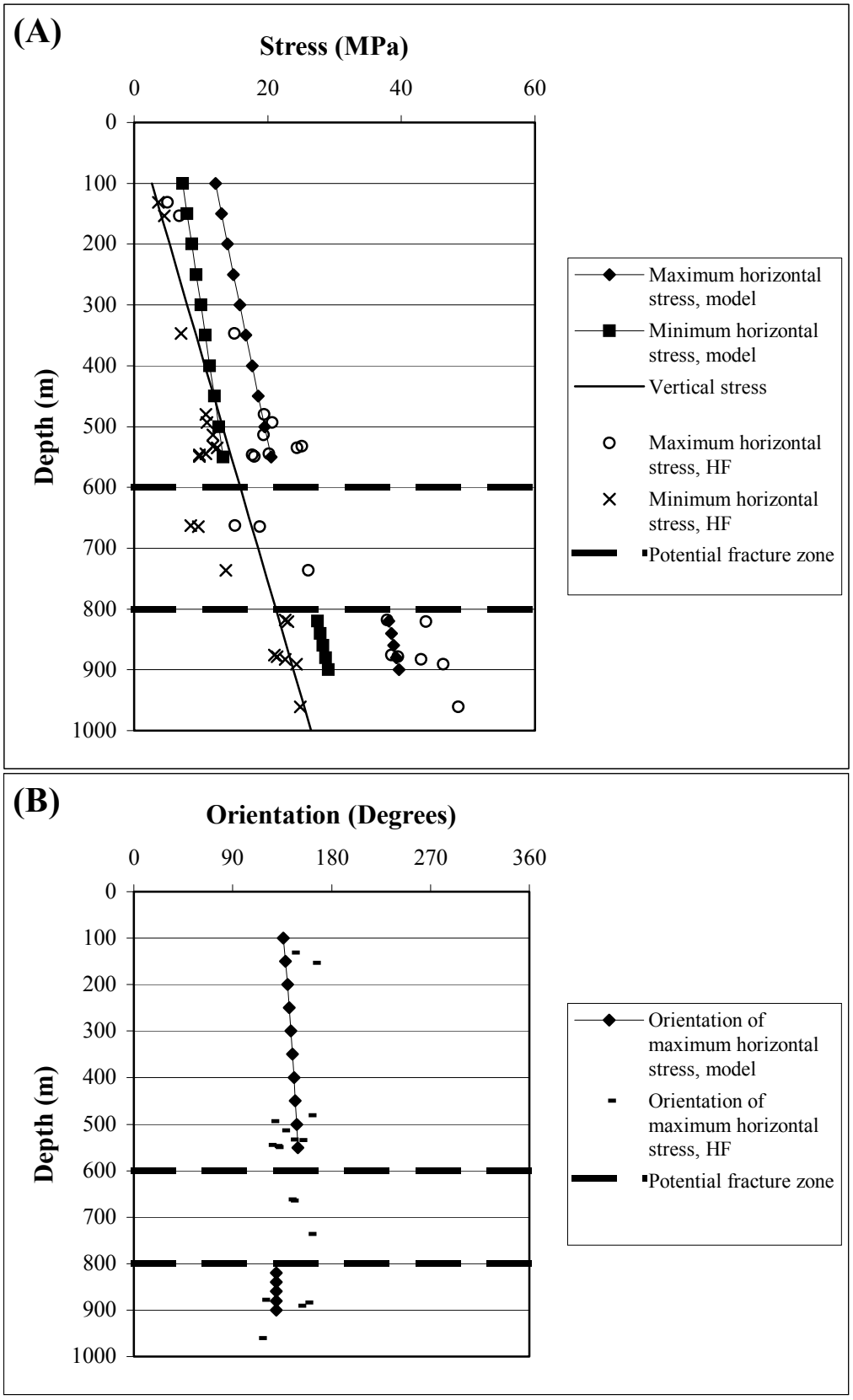

Figure S-2. *Summary of inversion results from borehole KAS03; (A) magnitudes and (B) orientation of* S_h.

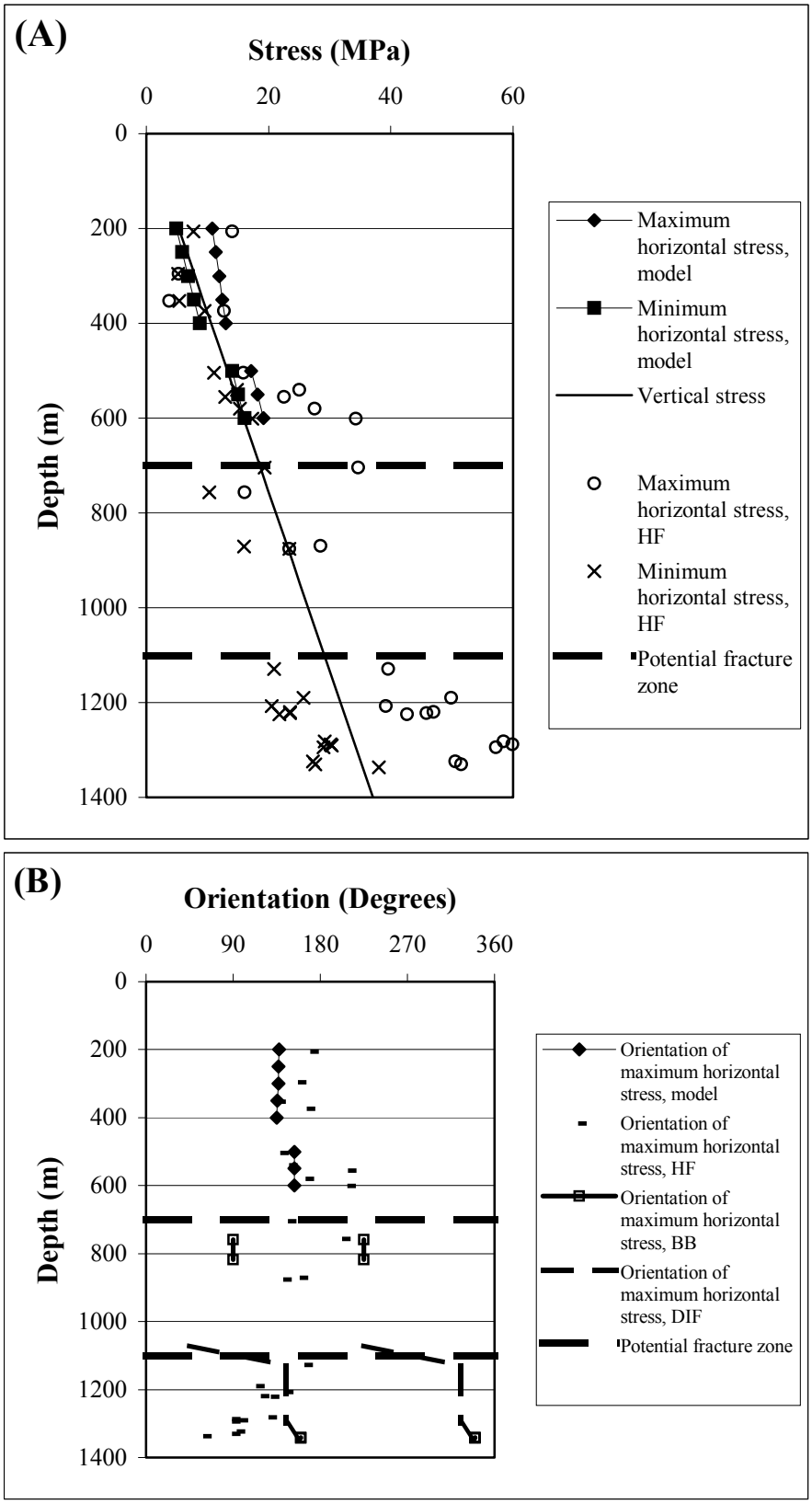

Figure S-3. *Summary of inversion results from borehole KLX02; (A) magnitudes and (B) orientation of S_h. The results below 700 m depth should be regarded as preliminary.*

1 INTRODUCTION

The Äspö Hard Rock Laboratory (HRL) of the Swedish Nuclear Fuel and Waste Management Co. (SKB) has been a geoscientific research area since 1986 (Fig. 1-1). This underground laboratory provides an implementation and operation basis for a future deep repository in Sweden. The vast number of research projects conducted has enabled valuable development and verification of site characterization methods from ground surface, boreholes and underground excavations, among them in-situ rock stress measurements.

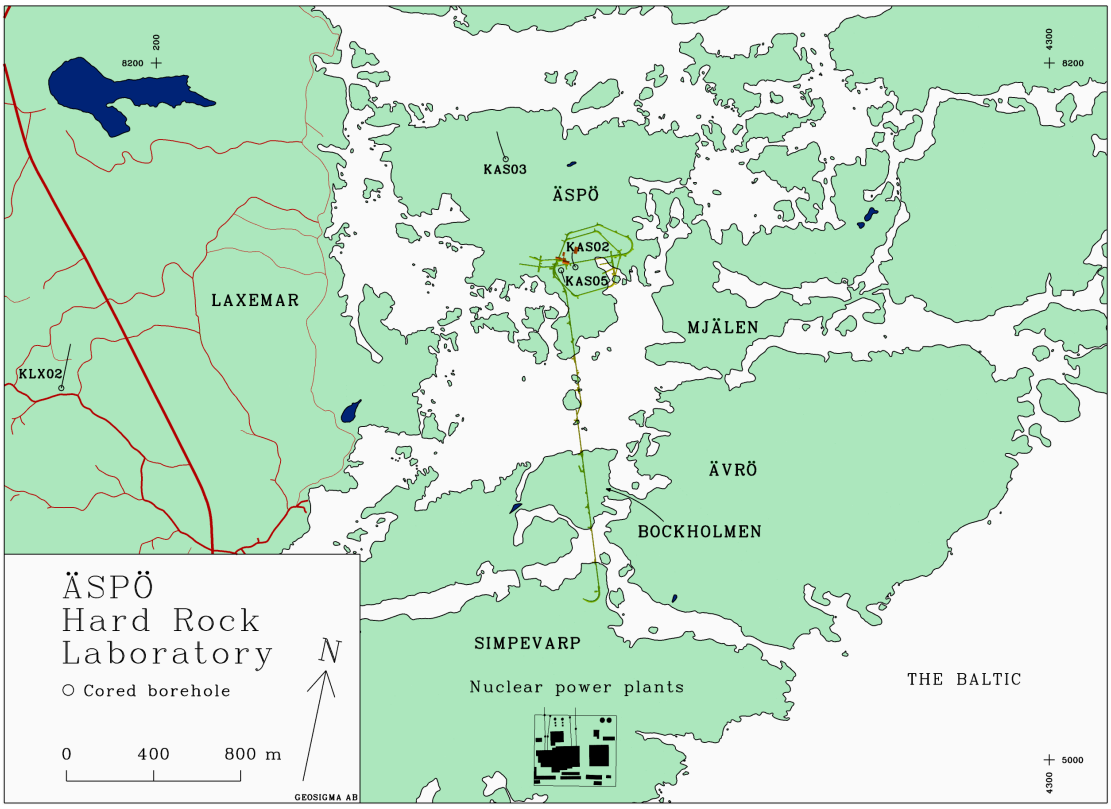

Figure 1-1. *Borehole locations in the Äspö region, Sweden (Modified after Ekman (2001)).*

A detailed knowledge of the in-situ stress field is important for several rock engineering aspects, including investigation, design, construction, and performance of engineered structures built on, in or of rock. Storage facilities for hazardous waste, e.g. spent nuclear fuel, are suggested to be located in rock at great depth. A full understanding of the stresses is essential in order to provide (i) boundary conditions for the storage facility; (ii) means to make a proper design and to analyze the mechanical response and possible failure of the rock mass; and (iii) some insight on how fluids flow underground (Stephansson, 1997).

The magnitude and orientation of stresses, independent of siting depth, control the orientation, geometry, dimension sequence of excavation, and in case of HLW waste, heat loading rate of a repository. If the stress magnitudes are low, the ultimate goal is to make a design where the stress concentrations are kept to a minimum. The compressional stresses in the wall of the openings should be as low as possible and the regions of tensile stress should be avoided, so called "harmonic hole" (Amadei and Stephansson, 1997). On the contrary, if the stress magnitudes are high and close to the strength of the rock mass, the depth wise location, orientation and shape become crucial for a safe construction with long-term performance. The "harmonic hole" concept is not recommended when the in-situ stress magnitudes are high (e.g. Hoek and Brown, 1980). Instead the shape should be selected so that zones of high stresses are concentrated in sharp corners and that the zones have the smallest possible extension (Stephansson, 1997).

Generally, in-situ stress measuring techniques consist of disrupting the rock. The response associated with the disturbance, and often also the process of the disturbance itself, is measured (strain, displacement or hydraulic pressure record) and analyzed by making several assumptions about the rock's constitutive behavior. Over the past 30 years, numerous techniques have been developed and improved. These may be divided into six main groups: hydraulic methods, relief methods, jacking methods, strain recovery methods, borehole breakout methods, and others (Amadei and Stephansson, 1997). Hydraulic stress measurements measure the state of stress in boreholes using fluid pressure to open, generate, propagate and reopen fractures in rock. The direction of the in-situ stresses is using hydraulic methods inferred by inversion techniques or by observing or measuring the orientation of hydraulically induced fractures. The hydraulic methods may be divided into three subgroups: hydraulic fracturing measurements (HF), sleeve fracturing, and hydraulic test in pre-existing fractures (HTPF).

At Äspö the in-situ rock stress measurements consists of hydraulic fracturing stress measurements (HF), hydraulic tests in pre-existing fractures (HTPF) (Bjarnason et al., 1989; Ljunggren and Klasson, 1997; Ekman, 1997; Ekman et al., 1997) and overcoring stress measurements (Bjarnason et al., 1989; Lee et al., 1993; Lee et al., 1994; Litterbach et al., 1994; Ljunggren and Klasson, 1996; Nilsson et al., 1997; Ljunggren and Bergsten, 1998; Klasson et al., 2000). Totally, the in-situ rock stress data consist of 80 HF, 5 HTPF and 109 overcoring stress measurements.

The results of the in-situ hydraulic stress measurements at Äspö indicate a non-linear stress distribution versus depth and the magnitudes seems strongly influenced by discontinuities (Bjarnason et al., 1989; Leijon, 1995; Hansson et al., 1995; Ljunggren and Klasson, 1997; Ekman, 1997; Ekman et al., 1997), see also Figures 2-1 to 2-6. The discontinuity in KAS02 occurs below 600 m depth; in KAS03 between 575 and 750 m depth; and in KLX02 between 700 and 1100 m depth. The orientation of the maximum horizontal stress as determined from the hydraulic fracturing stress measurements is scattered and, especially at great depths in KLX02, a rotation versus depth have been interpreted by Ljunggren and Klasson (1997). Further, the hydraulic and overcoring stress measurements indicate different states of stress, especially concerning the magnitudes. Generally, the overcoring stress measurements indicate larger or even much larger magnitudes compared to the hydraulic stress measurements. The orientation of the maximum horizontal stress is though rather consistent in both methods, NW-SE.

The discrepancies between the hydraulic and overcoring measurements at Äspö have been investigated by Ljunggren et al. (1998), based on statistical analyses of the Äspö stress data (Andersson, 1996 and 1997), and a comparison of the Äspö stress data with the data in the Fennoscandian Rock Stress Data Base (FRSDB) (Ljunggren and Persson, 1995). The results indicate that the variance of the stresses at Äspö differs significantly between the methods. To some extent, this could be explained by depth-dependency, but the remaining variance is large for the two methods and presumably Gaussian distributed. However, in average, the difference is quite small (Ljunggren et al., 1998).

The present study aims at improving the existing interpretation of the in-situ stress field in the Äspö region. This report is the first of a series in which the inversion method developed by Cornet and Valette (1984) is applied. We will in this report deal with the hydraulic stress measurements (HF and HTPF) conducted in three surface drilled deep boreholes in the Äspö region (KAS02, KAS03 and KLX02, Table 1-1 and Fig. 1-1), southeastern Sweden. The second report will deal with the overcoring stress measurements, and the third report will deal with a possible integration of these two. Hopefully, also other stress indicators will be included at a later stage, e.g. borehole breakouts, drilling induced tensile fracture, focal mechanisms, slips on pre-existing faults, see Ch. 8. This approach will hopefully lead to a stepwise improvement of the existing interpretation of the in-situ stress field in the Äspö region, as more data successively are included in the inversion technique.

We will also attempt to find possible explanations for the non-linear stress field in the investigated boreholes based on structural geology maps, fracture frequency plots, core and borehole geophysical logs, hydraulic interference tests, seismic data and radar measurements.

Table 1-1. Orientations, coordinates and number of hydraulic stress measurements performed in boreholes KAS02, KAS03 and KLX02 (RT38-RH00-system).

Borehole	Dip/ Dip dir.	X (m)	Y (m)	Z (m)	HF	HTPF
KAS02	84° N42°W	6367795.2	1551420.7	7.7	20	2
KAS03	83° N34°W	6368215.4	1551005.8	8.8	15	6
KLX02	85° N3°W	6366768.6	1549224.2	18.3	28	10

2 ANALYSIS OF EXISTING HYDRAULIC STRESS DATA

2.1 GENERAL

The hydraulic stress data have been collected in three surface drilled boreholes, KAS02 and KAS03, on the island of Äspö, and KLX02, on the mainland immediately west of Äspö. The hydraulic measurements were conducted during different stress measurement campaigns. The measurements in KAS02 and KAS03 were conducted by Renco Co., in July 1988 and in April 1989, respectively (Bjarnason et al., 1989). The measurements in borehole KLX02 were performed by Vattenfall Hydropower Co. in 1996 (Ljunggren and Klasson, 1997). Stress measurements down to 756 m depth was conducted during several periods in 1996 and the deeper measurements (870-1 337 m) in October 1996.

The orientations of induced fractures of the deeper measurements in borehole KLX02 were determined by BIPS (Borehole Image Processing System) equipment during the spring 1997 (Ljunggren and Klasson, 1997). A re-interpretation of the existing BIPS-pictures has been performed in this study and is, together with the results from the hydraulic stress measurements, presented in Table A-1 in Appendix.

The applied inversion analysis is based on existing hydraulic stress data, which have been extracted and re-evaluated from several reports (Bjarnason et al., 1989; Ljunggren and Klasson, 1997; Ekman, 1997; Ekman et al., 1997), and will only be discussed briefly in this study. Figures 2-1 to 2-6 presents fracture normal stresses in boreholes KAS02, KAS03 and KLX02 assuming that the data obey Gaussian distribution. These may be used as a first estimation of the minimum horizontal stress when upper and lower boundaries for the normal stresses are included.

As can be seen, all boreholes indicate sections with different states of stress. In all boreholes three stress regimes may be distinguished. Consequently, the in-situ stress data have to be separated in different sub-sets in order to solve the stress versus depth using the integrated stress analysis method. However, this procedure has great consequences regarding the choice of model and the resolution of the unknowns in the model, see further Ch. 3.5. In this report, attempts to solve the state of stress in each of these sections using both the first and second shut-in pressure from the hydraulic fracturing data are conducted. The orientation of maximum horizontal stress in the deeper section of borehole KLX02, Figure 2-6, based on a report by Ljunggren and Klasson (1997), will be further discussed in Ch. 5.4 and 6.4.

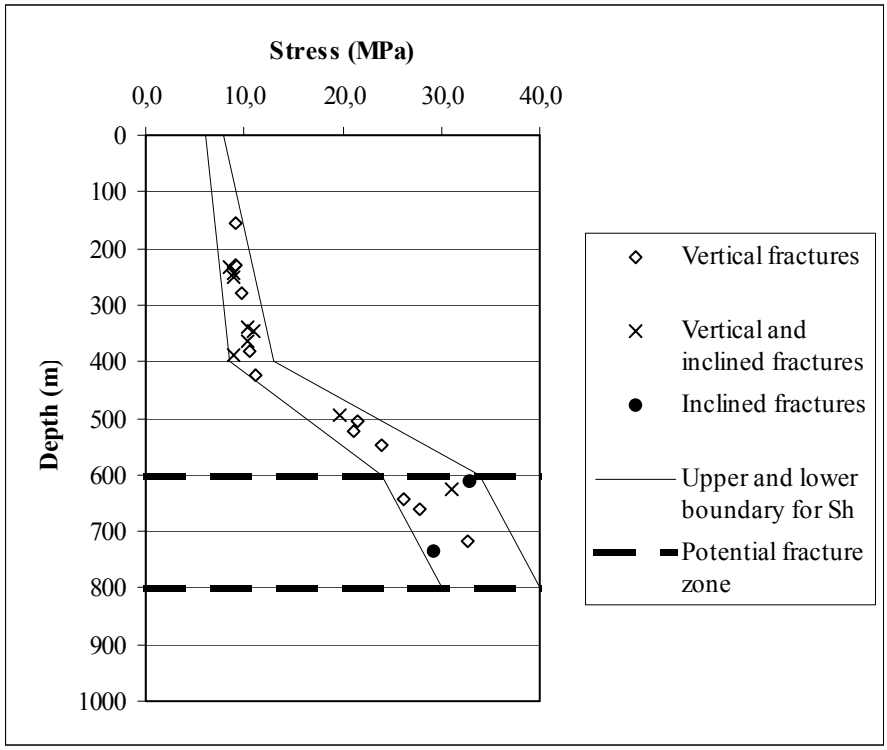

Figure 2-1. *Normal stress determined from second shut-in pressure in hydraulic fracturing stress measurements versus depth in borehole KAS02.*

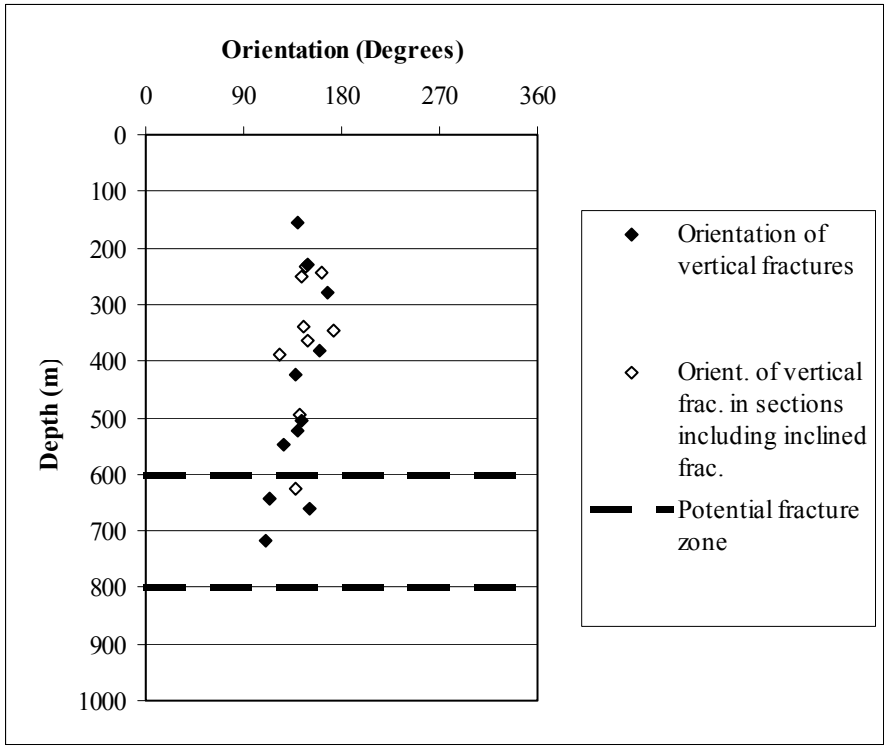

Figure 2-2. *Orientation of maximum horizontal stress versus depth from hydraulic fracturing stress measurements in borehole KAS02.*

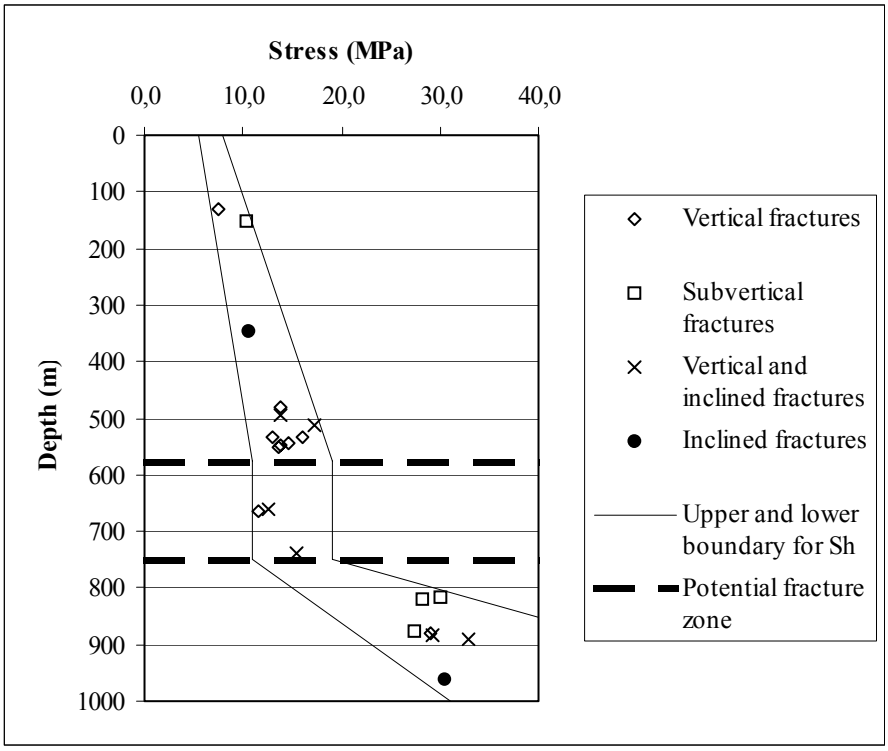

Figure 2-3. *Normal stress determined from second shut-in pressure in hydraulic fracturing stress measurements versus depth in borehole KAS03.*

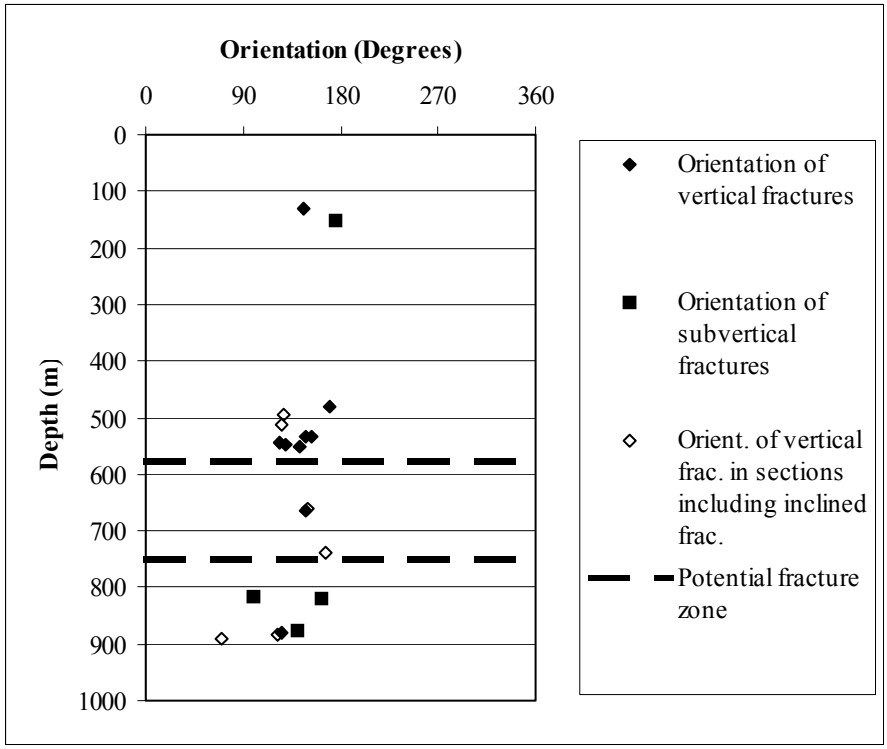

Figure 2-4. *Orientation of maximum horizontal stress versus depth from hydraulic fracturing stress measurements in borehole KAS03.*

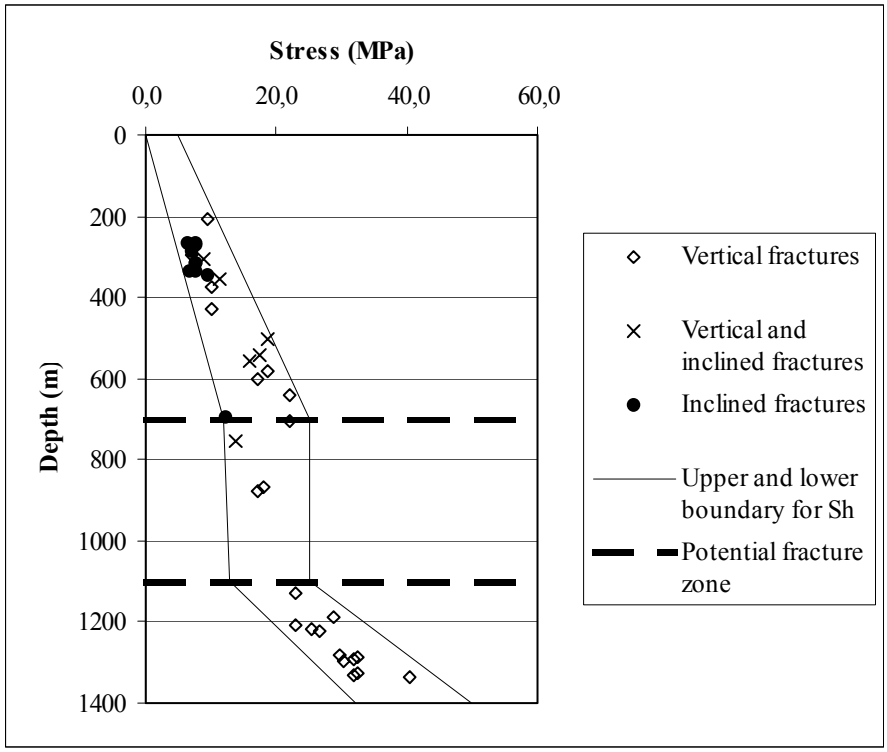

Figure 2-5. *Normal stress determined from second shut-in pressure in hydraulic fracturing stress measurements versus depth in borehole KLX02.*

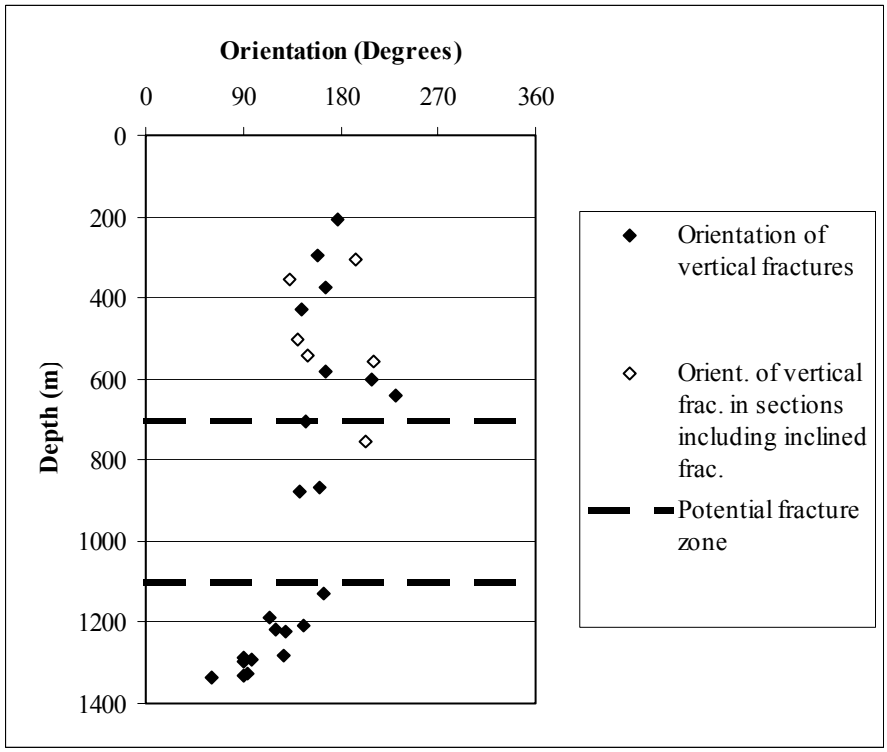

Figure 2-6. *Orientation of maximum horizontal stress versus depth from hydraulic fracturing stress measurements in borehole KLX02 (Ljunggren and Klasson, 1997).*

2.2 HYDRAULIC FRACTURING STRESS MEASUREMENTS

The hydraulic fracturing stress measurement (HF) involves subsequent pressurization of a sealed-off section in a borehole until the borehole wall fractures. During these measurements, the pressure versus time is recorded (Fig. 2-7). The pressure required to initiate hydrofractures, is called the breakdown pressure P_b. The succeeding re-pressurizations resulting in reopening pressures P_r, are usually defined as the points, during each pressurization cycle, where the pressure-time curve begins to deviate from linearity. When the hydraulic system is sealed or shut-in, two mechanisms are controlling the observed pressure drop in the test section: (i) the movement of the fluid in the system is stopped, causing the frictional losses to vanish (difference between propagation pressure and instantaneous shut-in pressure, P_s); and (ii) the excess fluid in the system, which is a function of the system compressibility, further propagates the fracture and depletes into the rock mass (difference between P_s and fracture closure pressure). This yields the instantaneous shut-in pressure, P_s, on the pressure time curve. At that instant, the pressure in the test section is equal to the magnitude of the minimum horizontal stress. The shut-in pressure, P_s, is usually determined using graphical methods, e.g. inflection point method (Gronseth and Kry, 1983), maximum curvature method (Hardy, 1973; Hayashi and Sakurai, 1989), the tangent intersection method (Enever and Chopra, 1986). The latter is the most commonly applied method, and has been used for the hydraulic measurements in the Äspö region. It is noteworthy, that the tangent intersection method gives the lowest shut-in pressure of these three methods (Klasson, 1989). With these notations, the maximum horizontal stress is determined by Eq. (2-1) (Hubbert and Willis, 1957; Bredehoeft et al., 1976).

As can be seen in Equation (2-1), the maximum horizontal stress is a function of the minimum horizontal stress, re-opening pressure and pore pressure (Fig. 2-7). The re-opening pressure is in turn a function of the breakdown pressure and tensile strength, T, of the rock: $P_r = P_b - T$. The initial pore pressure, P_0, in the formation is depicted in Figure 2-7 and is normally included in the theoretical evaluation of stresses.

$$\sigma_H = 3\sigma_h - P_r - \beta P_0 \qquad (2\text{-}1)$$

where σ_H = maximum horizontal stress
σ_h = minimum horizontal stress (P_s)
P_r = reopening pressure
P_0 = pore pressure
β = factor that varies between 0 and 1

In the integrated stress analysis method, all measurements are assumed to obey Gaussian distribution, which means that another slightly different method is used (Fig. 2-7). The fracture is assumed completely open when the system is shut-in and completely closed when the pressure decline has reach its asymptotic value. These assumptions define an interval with a central value, σ_n, and have a width of $\pm$ 3 standard deviations for a 99% confidence interval. A question then arises concerning which of the normal stresses that should be chosen, the shut-in after the breakdown or the shut-ins after the subsequent re-openings. The criteria to follow is that the fracture should be large enough to extend beyond the zone of stress concentration around the borehole, i.e.

fracture radius > 3 times the borehole radius (Ratigan, 1992). However, it has also been shown that the fracture propagation is very complex and non-linear (e.g. Shen, 1993), which implies that too large fracture planes should be avoided to minimize the uncertainties related to the assumption of planar fractures. Furthermore, as the fracture is allowed to propagate during each pumping cycle in the hydraulic fracturing stress measurements, it may connect with other fractures in the rock mass. This will change the hydraulic response in the test section and may result in an erroneous interpretation of the fracture normal stress. A rough calculation, based on known pumping flow rate and compressibility of the equipment and under the assumption that the fracture propagates for pressures exceeding the re-opening pressure, implies that the induced fracture is larger than 3 times the borehole radius already at the first pumping cycle. This result is confirmed by a modeling study by Rutqvist et al. (2000), which showed, using the same equipment that the radius of the induced fracture is of the magnitude 1 m after the first breakdown. Consequently, the normal stress determined from the first pumping cycle seems preferable. However, there is a drawback when using this approach. As can be seen in Figure 2-7, the 99% confidence interval for the normal stress after the breakdown is larger compared to the interval after the re-opening cycles. Therefore, in the inversion analysis the shut-in pressures for both the first and second pumping cycle have been used.

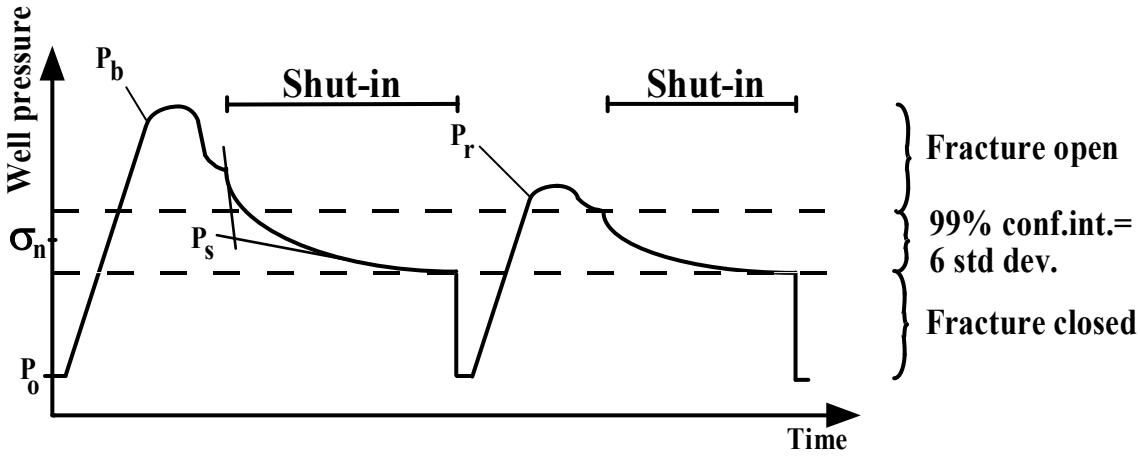

Figure 2-7. *Pressure - time record from hydraulic fracturing measurement and determination of normal stress and standard deviation for the second pump cycle.*

Also the fracture orientation data has been assumed to follow Gaussian distribution, which may be expressed by expected value and standard deviation. Figure 2-8 describes the procedure for an inclined fracture.

The orientations of the fractures have been determined with an impression packer equipped with a single-shot magnetic compass (Bjarnason and Torikka, 1989). Exceptions are the deep fracturing measurements in KLX02, below 870 m, which were determined using the BIPS-camera (Ljunggren and Klasson, 1997).

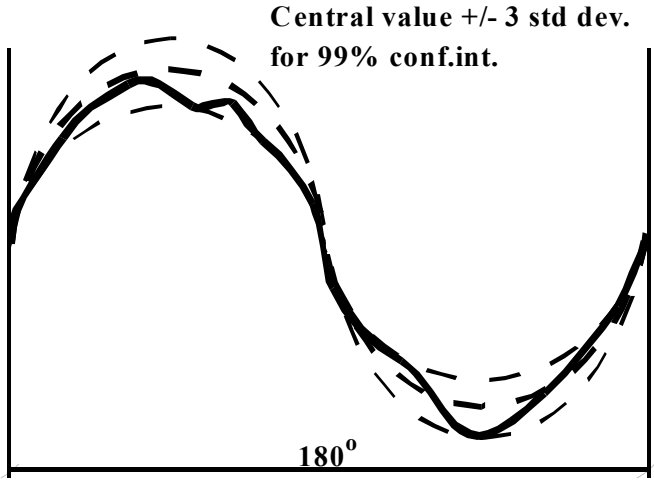

Figure 2-8. *Determination of fracture orientation and standard deviation of an inclined fracture on an imprint from the hydraulic fracturing measurements.*

2.3 HYDRAULIC TEST OF PRE-EXISTING FRACTURES

The HTPF measurements at Äspö mainly consist of unsuccessful hydraulic fracturing measurements, i.e. with the HF-type pumping test. Subsequently, these have been interpreted in the same manner as the HF measurements.

Some "true" HTPF measurements have though been conducted in KLX02 using a hydraulic jacking pumping test (Fig. 2-9). The purpose is to determine the well pressure that exactly balances the fracture normal stress. The hydraulic jacking test is conducted as a series of constant injection tests with step-wise increasing pressure. A steady injection flow should be attained at each pressure level, before proceeding to the next level. The distinctive features of the pressure curve in Figure 2-9 are two slightly non-linear slopes connected with a plateau part. This transition is used for determination of fracture normal stress. Generally, it is assumed that the fracture remains closed for pressures less than the fracture normal stress. For pressures above the fracture normal stress, the fracture opens and the flow rate increases. However, Rutqvist (1995) showed that the reopening of the fracture plane is gradual, and that it depends on the fracture normal stiffness and effective stress inside the fracture near the borehole. Hydraulic jacking tests are for that reason conducted in cycles, i.e. with a step-wise increase of well pressure to maximum flow rate (mechanical unloading), followed by step-wise decrease of well pressure (mechanical loading), until back-flow is obtained. Back flow occurs when the injection flow is too small to keep the fracture open. As the fracture closes and squeezes to a smaller volume, the flow is reversed, causing a temporary flow increase on the flow chart. The results are plotted on graphs for well pressure versus well flow at the end of each pressure level (Fig. 2-10). A similar approach, as for the HF measurements, is used to determine the normal stress and it's standard deviation.

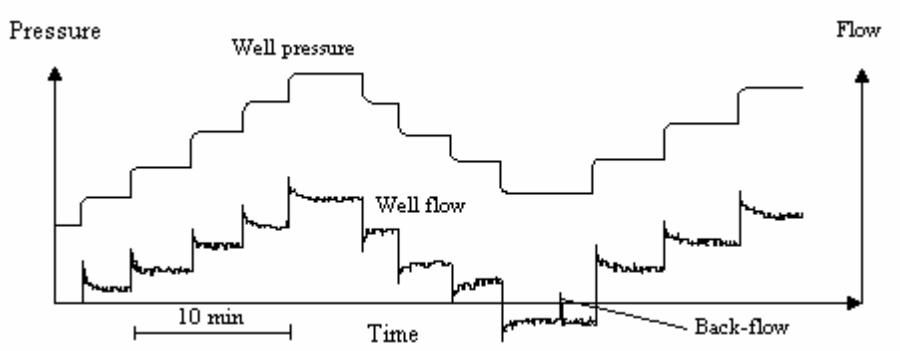

Figure 2-9. *Pressure and flow versus time record from hydraulic jacking test (after Ekman, 1997).*

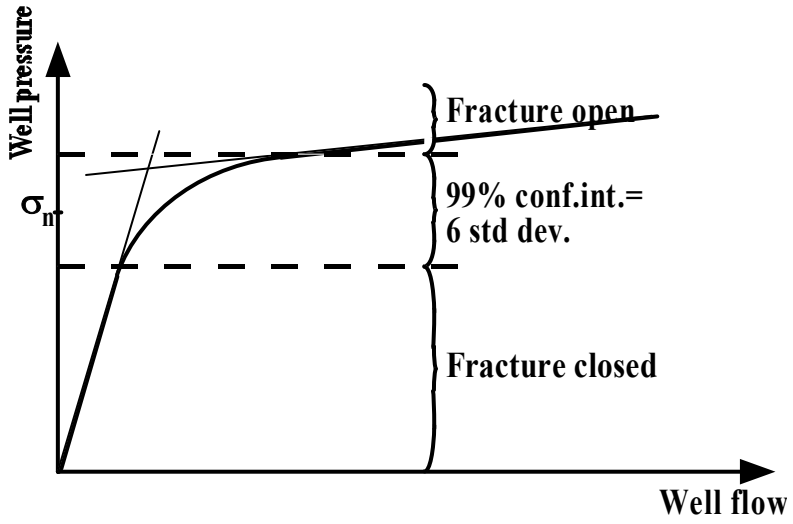

Figure 2-10. *Pressure versus flow and determination of normal stress and standard deviation of normal stress for a hydraulic jacking test.*

2.4 UNCERTAINTIES IN EXISTING STRESS DATA

The significant uncertainties in the analysis of existing stress data mainly involve:

(i) The determination of fracture normal stress during HF measurements
(ii) The determination of fracture plane orientation
(iii) The occurrence of multiple fractures and chevron notches

Furthermore, the hydraulic fracturing method itself includes uncertainties that should be kept in mind during the comparison with inversion results. The main uncertainties are:

(iv) The uncertainties involved in the pore pressure
(v) The definition of reopening pressure during HF measurements
(vi) The assumption that the borehole direction coincides with the direction of the vertical stress component and is equal to the weight of the overburden
(vii) The effect of non-vertical induced fractures and scattered orientations

The uncertainties listed are commented below:

(i) The majority of the stress measurements at Äspö are hydraulic fracturing measurements, which means that the normal high flow rate pumping test has been used. However, this pumping procedure does not give as well defined fracture normal stress as compared to the low flow rate hydraulic jacking tests, which in turn effects the resolution of the unknown parameters during inversion. This introduces a source of uncertainty in the analysis.

(ii) The induced fractures from the hydraulic fracturing measurements are assumed planar and parallel to the orientation of maximum horizontal stress. However, in many instances, especially in crystalline and metamorphic rocks, vertical fractures are not exactly parallel to each other but make an angle with the mean fracture orientation. This implies that the determination of fracture orientation may suffer from subjectivity. However, assuming that the fractures follow a Gaussian distribution, as in the integrated stress determination method, this may be dealt with using confidence intervals.

The fracture orientations of the deeper measurements (870-1 337 m) in borehole KLX02, were determined with the BIPS-camera. The analysis proved to be very difficult and the determination of fracture orientations are consequently associated with great uncertainties. Therefore, no inversion attempts were made in the deeper levels of borehole KLX02.

(iii) We have observed imprints that include both vertically induced and pre-existing fractures (Table 2-1). This is probably due to the chosen high flow rate pumping procedure. It is likely that the pre-existing fracture was sealed in the beginning of the test and opened simultaneously as the induced fractures. This reasoning is strengthened by the fact that the induced fractures in these sections often have a much smaller extent compared to sections with only an induced fracture. Furthermore, the orientations of the induced fractures in these sections are often diverted as compared to the average trend. This implies that the pre-existing fracture disturbs the stress field in the section. Consequently, the following pumping test involved both the induced and the pre-existing fracture/fractures. However, most likely, the pre-existing fracture dominates the hydraulic response in the section due to larger aperture and extent. In the inversion analysis, different fracture alternatives subsequently had to be tested (see Ch. 5).

Some induced fractures from the hydraulic fracturing measurements in the Äspö region include so-called chevron notches (Fig. 2-11 and Table 2-2). These may indicate three things: (i) that the vertical stress is inclined with respect to the borehole axis; (ii) that the stress field is disturbed by local heterogeneities in the rock mass; or (iii) that the induced fracture turns from vertical to horizontal as it propagates away from the borehole. The latter implies that the shut-in pressure may only represent the vertical stress and not the minimum horizontal stress. Thus, the maximum horizontal stress remains undetermined (Zoback et al., 1977; Evans et al., 1989). The notches in KAS02 and KAS03 proved to be difficult to classify and only one fracture, at 883.3 m depth in KAS03, was classified as being due to a local heterogeneity.

Table 2-1. Results from impression packer.

Borehole	Depth	Fracture impression results
KAS02	232.9	Induced and pre-existing fractures
	243.1	Induced and pre-existing fracture
	250.2	Induced and pre-existing fractures
	339.4	Two sets of sub-vertical fractures
	346.0	Induced and pre-existing fracture
	363.7	Induced and pre-existing fractures
	389.8	Two sets of sub-vertical fractures
	494.9	Induced and pre-existing fracture
	610.7	Two pre-existing fractures
	624.8	Induced and pre-existing fracture
	734.0	Two pre-existing fractures
KAS03	346.6	Three pre-existing fractures
	493.6	Induced and pre-existing fracture
	513.9	Induced and pre-existing fracture
	662.5	Induced and pre-existing fracture
	736.8	Induced and pre-existing fracture
	883.3	Induced and pre-existing fractures
	891.2	Induced and pre-existing fracture
KLX02	305.8	Induced and pre-existing fracture
	314.5	Three pre-existing fractures
	336.6	Two pre-existing fractures
	337.2	Three pre-existing fractures
	346.7	Two pre-existing fractures
	504.1	Induced and pre-existing fractures
	540.5	Induced and pre-existing fractures
	555.7	Induced and pre-existing fractures
	641.8	Two pre-existing fractures
	753.9	Induced and pre-existing fractures

In borehole KLX02, the chevron notch at 352.7 m depth is judged to be due to either (i) or (iii), as there is no reason to believe that local heterogeneities are present at this depth. The chevron notch at 704.8 m depth may be affected by the intersection of SFZ04 and SFZ07, however, a firm conclusion cannot be made.

Table 2-2. Evaluation of chevron notches.

Borehole, dip/dip direction	Depth	Occurrence of chevron notches
KAS02, 85°/N30°W	228.8	Indication
	243.1	Indication
KAS03, 82°/N30°W	546.6	Weak indication
	549.6	Indication
	736.8	Indication
	883.3	Strong indication
KLX02, 85°/N20°E	352.7	Strong indication
	704.8	Weak indication

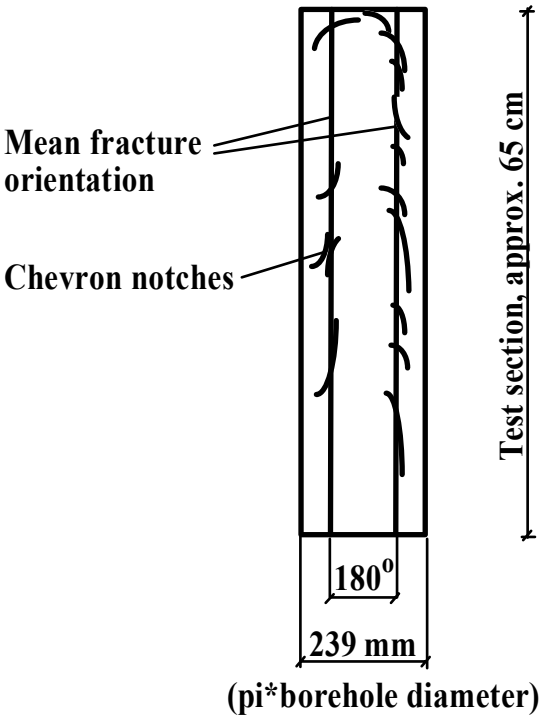

Figure 2-11. *Example of imprint including chevron notches at 352.7 m depth in borehole KLX02.*

(iv) Depending on whether the rock is considered porous or non-porous and whether fluids are penetrating or non-penetrating, three different relationships are used to determine the maximum horizontal stress for HF tests. Equations (2), (3) and (4) are used for: (i) porous material with fluid penetration, (ii) porous material with non-penetrating fluid, and (iii) non-porous media without pore pressure (Schmitt and Zoback, 1989).

$$P_B = \left(T + 3\sigma_h - \sigma_H - 2\eta P_0\right) / 2\left(1 - \eta\right) \quad (2\text{-}2)$$

$$P_B = T + 3\sigma_h - \sigma_H - P_0 \quad (2\text{-}3)$$

$$P_B = T + 3\sigma_h - \sigma_H \quad (2\text{-}4)$$

where η = poroelastic coefficient, $\eta = \alpha(1-2\nu)/2(1-\nu)$
α = Biot coefficient, $\beta = 1-K_s/K$
K_s = bulk modulus of the rock incl. mineral grains, pores and microcracks
K = bulk modulus of the mineral grain skeleton of the rock
ν = Poisson's ratio
P_B = breakdown pressure
P_o = pore pressure
T = tensile strength

Note that for stiff, low-porosity rocks $K \approx K_s$ and $\alpha \approx 0$. The major drawback with Equation (2-2) is that it is difficult in practice to determine α and ν.

Schmitt and Zoback (1989) found major differences when calculating the maximum horizontal stress using these formulas, especially for low-compressibility rocks at great depths (for which the Biot coefficient is small). For the samples tested, Equation (2-4) gives the largest value, Equation (2-3) the intermediate, and Equation (2-2) the smallest value on σ_H. Schmitt and Zoback (1989) therefore proposed a modified effective stress equation for extensional failure:

$$\sigma = S - \beta P_0 \tag{2-5}$$

where S is the total stress and β is a coefficient that varies between 0 and 1. With these notations, Equation (2-2) and (2-3) becomes:

$$P_B = \left(T + 3\sigma_h - \sigma_H - 2\eta P_0\right) / 2\left(1 + \beta - \eta\right) \tag{2-6}$$

$$P_B = T + 3\sigma_h - \sigma_H - \beta P_0 \tag{2-7}$$

Schmitt and Zoback (1992) later showed in a laboratory HF study, using thin-walled hollow granite cylinders, that fast flow rate pump tests result in increased apparent tensile strength and Young's modulus. This implies that the pore pressure diminishes because the pore pressure perturbation cannot reach equilibrium over the time scale of a fast flow rate pump test. The increase of tensile strength is a result of assuming that the initial pore pressure is uniformly maintained for the duration of the test. If the material strength is calculated under this assumption, the apparent strength will increase. This phenomena is denominated dilatancy hardening. The increase of Young's modulus, could be explained by elastic microcrack dilatancy, caused by the nonlinear stress-strain behavior in the tested rock samples. The elastic dilatancy is proposed since the increase in Young's modulus takes place before the sample is damaged, in contrast to the irreversible dilatancy hardening. To a small extent, the pore pressure drop could be explained by diffusion into the rock mass, however, the remainder mechanism could not be explained. Schmitt and Zoback (1992) proposed that the remainder effect could be due to elastic microcrack dilatancy or an irreversible production of new porosity. The consequence of this pore pressure drop is that the evaluated maximum horizontal stress may be exaggerated.

The introduction of the modified effective stress law implies that pore pressure effect can be neglected in low-permeability, hard granitic rocks (Equation (2-4)), although uncertainties are involved with this assumption. If the assumption is incorrect, the evaluated maximum horizontal stress is exaggerated. Moreover, none of the approaches mentioned above consider effects of fracture size in relation to borehole size or pressurization rate, although this has been reported in literature (Amadei and Stephansson, 1997).

A further complication about pore pressure effects in HF measurements is due to the fact that pore pressure is difficult to determine; in some cases fluid penetrates from the borehole into the pores of the rock, whereas in others very high fluid pressures leads to migration of fluid from the rock towards the borehole (Jaeger and Cock, 1969). Furthermore, pore pressure variations are known to occur in the vicinity of fault zones (e.g. Cornet and Jianmin, 1995).

(v) The reopening pressure is determined by subsequent re-pressurizations of the test section during a hydraulic fracturing stress measurement cycle, and it is commonly used for determining the magnitude of the maximum horizontal stress. However, several authors have found uncertainties in the interpretation of the reopening pressure (e.g. Cornet and Valette, 1984; Cornet, 1993a; Rutqvist, 1997; Ito et al., 1999; Rutqvist et al., 2000).

The reopening pressure is known to be dependent on the injection flow rate. The induced fracture has often a residual aperture after initiation as a result of shearing of the fracture plane or dislocation of individual rock grains preventing a complete closure of the fracture surfaces. When a residual aperture exists and the fluid injection rate is low, fluid will penetrate the fracture prior to reopening. This penetration results in an additional stress component on the internal surfaces of the crack, which reduces the magnitude of the reopening pressure. The size of the fluid injection rate makes it possible to account for the problem of fluid penetration in fractures with residual aperture: fluid cannot penetrate into the fracture if a high fluid injection rate is used (i.e. classical theory valid); whereas the fluid penetration can be accounted for if a low fluid injection rate is used (Ito et al., 1999). For low fluid injection rates, Ito et al. (1999) suggested that fluid penetration into fractures with residual aperture reduces the reopening pressure (P_r) by a factor of two (if the pore pressure effect is neglected) according to:

$$P_r = \frac{1}{2}\left(3\sigma_h - \sigma_H\right) \qquad (2\text{-}8)$$

Furthermore, Ito et al. (1999) identified an error in the reopening pressure determination that is related to the compliance of the equipment, which is an even more important source of uncertainty. Ito et al. (1999) showed that the discrepancies between true and apparent (i.e. detected) reopening pressure increases with increasing equipment compliance. A simulation with one pair of 1 m high axial fractures with a 2 μm residual hydraulic aperture in a 100 mm borehole, indicated that the system compliance must be less than $5 \cdot 10^{-7}$ m^3/MPa to estimate the true reopening pressure better than 10 %, assuming a low fluid injection rate ($<10^{-4}$ m^3/s). This very low value is attainable only for small diameter boreholes at shallow depths; thus it hardly applies to conventional hydrofracturing equipment. Ito et al. (1999) concluded that for measurements at great depth, a down hole flow meter is essential.

Ito et al. (1999) also suggested an explanation to why the apparent reopening pressure is often close to the minimum horizontal stress. They suggested that when the open fracture length, L, is less than a few borehole radii, the borehole pressure, P, increases linearly as if the fracture remained closed. At this stage, the change in pressurized fluid volume due to crack opening, dV_c/dP, is fairly small compared to the system compliance, C. As L exceeds a few borehole radii, which occurs as P approaches S_h regardless of stress state, then both the change of length and volume versus pressure, dL/dP and dV_c/dP, undergo rather abrupt increases. The combined effect produces a relatively marked deviation from linearity of the pressure versus time record. As this phenomenon occurs regardless of the magnitude of S_H, it may explain why the reopening pressure is often close to S_h.

A recent modeling study (Rutqvist et al., 2000) showed that the induced fracture disturbs the assumption of a linear elastic, homogeneous and isotropic medium, Fig. 2-12. The disturbance is attributed to the normal stiffness and the aperture of the induced fracture.

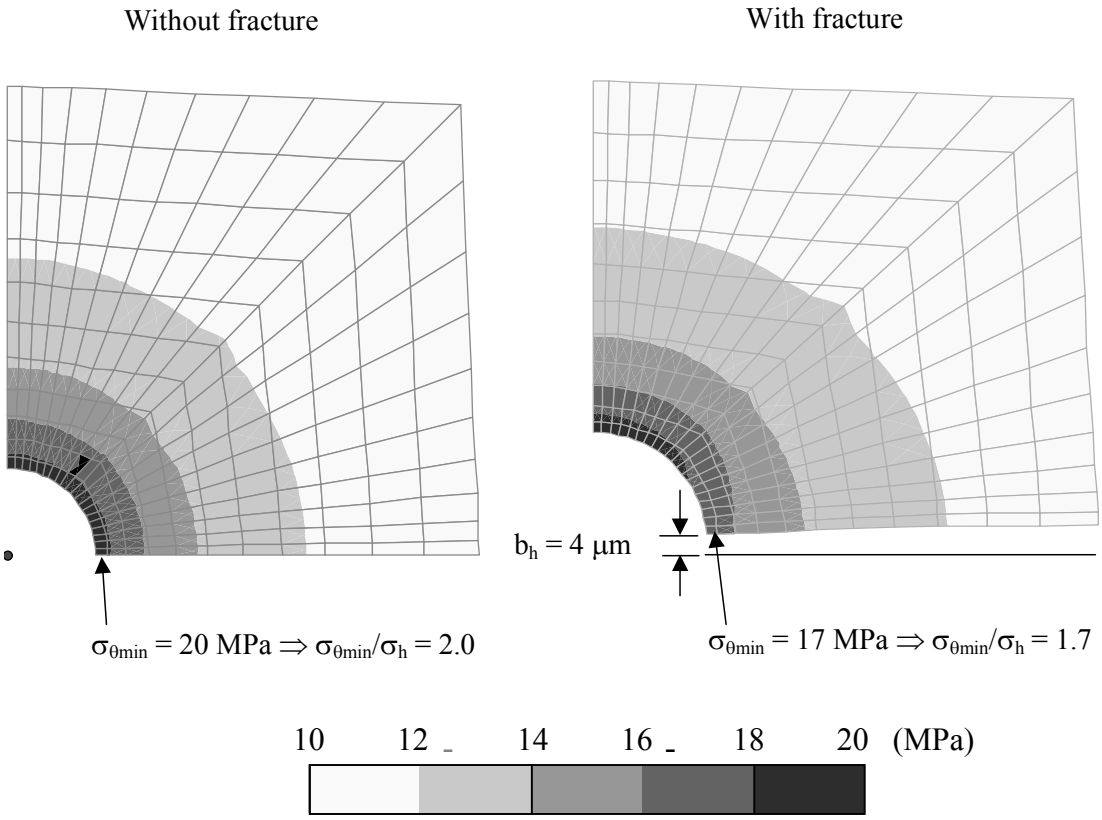

Figure 2-12. *Tangential stress as a result of modeling (a) without fracture and (b) with fracture. The remote stresses are isotropic at 10 MPa, and the fluid pressure is zero (Rutqvist et al., 2000).*

Further, Rutqvist et al. (2000) showed that the fracture reopening is gradual and starts much before the reopening pressure detected in the pressure versus flow charts, thus can therefore be denoted an apparent reopening pressure. With realistic equipment compliance, the study implies that the reopening pressure is most likely to be equal to the minimum horizontal stress and independent of the maximum horizontal stress. This result was also found by Ratigan (1992), for fractures with a radius larger than one borehole radius. The results imply that the maximum horizontal stress is set equal to two times the minimum horizontal stress with the classical formula. The stress ratio S_H/S_h of the hydraulic stress measurements at Äspö is close to two (1.8).

Conclusively, further research concerning the validity of the classical hydraulic fracturing theory using the reopening pressure is desirable.

(vi) The hydraulic fracturing stress measurement theory assumes that the borehole axis is vertical and oriented perpendicular to the horizontal in-situ stress components. Furthermore, the vertical stress component is assumed to be equal to the weight of the overburden. When these assumptions are fulfilled, the resulting induced fracture plane is, in theory, represented on the impression packer imprint by two straight vertical

fractures, 180° apart. However, the induced fractures are seldom perfectly linear, nor 180° opposed (Lee and Haimson, 1989). This implies that interpretation of the fracture orientation may suffer from subjectivity.

(vii) The induced fractures from the HF measurements are assumed to be vertical and parallel to the orientation on maximum horizontal stress. However, this is not always true, especially in crystalline and metamorphic rocks. If the fractures are assumed to be vertical and parallel to the orientation of maximum horizontal stress, the evaluated stresses will be exaggerated. Some of the induced fractures in the Äspö area are not perfectly vertical and the orientations of the fractures are scattered. This implies that the minimum horizontal stress and especially the maximum horizontal stress have been exaggerated.

Consider the HF measurements in KAS03 (Fig. 2-4 and Table A-1 in appendix), where the orientations of the induced fractures are in the range 100°-176°, with an average of 145° (N55°W). If the average is assumed to be the "true" orientation of maximum horizontal stress an offset angle can be calculated for each point (Table 2-3). The table shows that 11 measurement points have an offset of more than 15°. Furthermore, a number of fractures in KAS03 are not perfectly vertical, but more sub-vertical in dip. For example, the HF measurement at 820 m depth has an offset of 16° in dip and 24° in strike (if the maximum horizontal stress is assumed to be oriented N55°W).

Table 2-3. Analysis of fracture strike assuming that the average orientation of the induced fractures, N145°W, is the true orientation of maximum horizontal stress. Data from Bjarnasson et al. (1989).

Offset angle	Number of points
> 35°	1
34°-30°	1
29°-25°	1
24°-20°	4
19°-15°	4
14°-10°	0
9°-5°	4
< 4°	4

If we assume further, that the stress field at this depth is σ_h = 20 MPa, σ_H = 40 MPa, and σ_v = 22 MPa, the effects of the offset angles on the minimum horizontal stress are:

$\sigma_{h,dip}$ = 20.2 MPa, for 16° offset in dip
$\sigma_{h,strike}$ = 23.3 MPa, for 24° offset in strike
$\sigma_{h,combined}$ ≈ 23.4 MPa, for offset in both dip and strike

Thus, the assumptions of a perfectly vertical fracture and that the fracture is parallel to the orientation of maximum horizontal stress have great influence on the magnitude of minimum horizontal stress. At 820 m depth, the error is 3.4 MPa for minimum horizontal stress, which results in an error in the order of 7 MPa for the maximum

horizontal stress. Consequently, great care should be taken when analyzing HF measurements using inclined fractures and fractures with scattered orientation.

3 THE INTEGRATED STRESS ANALYSIS METHOD

The following chapter describes the parameterization of the stress field, the inverse problem and the solution of the inverse problem based to a large extent on Cornet (1993a); Cornet and Valette (1984); and Tarantola and Valette (1982). The method provides a measure of the resolution of the unknown parameters, which is presented in Ch. 3.4. Finally, the choice of model and the uncertainties involved with the choice of model are described.

1.1 PARAMETERIZATION OF THE REGIONAL STRESS FIELD

The measured rock volume is discretizised into sub-volumes in which the stress field is approximated by its first order linear expansion. The stress at a point X^m of the m^{th} measurement is given by

$$\sigma\left(X^m\right) = \sigma(X) + \left(x^m - x\right)\alpha^{[x]} + \left(y^m - y\right)\alpha^{[y]} + \left(z^m - z\right)\alpha^{[z]} \qquad (3\text{-}1)$$

where $\sigma(X^m)$ is the stress tensor in the point X^m (with co-ordinates x^m, y^m, z^m), $\sigma(X)$ is the stress tensor in the point X (with co-ordinates x, y, z), according to Equation (10), and $\alpha^{[1]}$, $\alpha^{[2]}$ and $\alpha^{[3]}$ are second-order symmetrical tensors characterizing the stress gradient in the x-, y- and z-directions according to Equation (3-3).

$$\sigma(X) = \begin{bmatrix} \sigma_x & \tau_{xy} & \tau_{xz} \\ \tau_{yx} & \sigma_y & \tau_{yz} \\ \tau_{zx} & \tau_{zy} & \sigma_z \end{bmatrix} \qquad (3\text{-}2)$$

$$\alpha^{[i]} = \begin{bmatrix} \frac{\partial \sigma_x}{\partial x_i} & \frac{\partial \tau_{xy}}{\partial x_i} & \frac{\partial \tau_{xz}}{\partial x_i} \\ \frac{\partial \tau_{yx}}{\partial x_i} & \frac{\partial \sigma_y}{\partial x_i} & \frac{\partial \tau_{yz}}{\partial x_i} \\ \frac{\partial \tau_{zx}}{\partial x_i} & \frac{\partial \tau_{zy}}{\partial x_i} & \frac{\partial \sigma_z}{\partial x_i} \end{bmatrix} \qquad (3\text{-}3)$$

Equation (3-1) satisfies the following equilibrium constraints:

$$div\left(\sigma\left(X^m\right)\right) - \rho(X) b_i = 0 \tag{3-4}$$

where $\rho(X)$ is the density of the rock mass in the point X; b_i is the gravitational acceleration ($b_i = g\delta_{i3}$; $\delta_{i3} = 0$ for $i \neq 3$; $\delta_{i3} = 1$ for $i = 3$). Equation (3-4) can be rewritten according to

$$\frac{\partial \sigma_x^m}{\partial x} + \frac{\partial \tau_{yx}^m}{\partial y} + \frac{\partial \tau_{zx}^m}{\partial z} = 0 \tag{3-5}$$

$$\frac{\partial \tau_{xy}^m}{\partial x} + \frac{\partial \sigma_y^m}{\partial y} + \frac{\partial \tau_{zy}^m}{\partial z} = 0 \tag{3-6}$$

$$\frac{\partial \tau_{xz}^m}{\partial x} + \frac{\partial \tau_{yz}^m}{\partial y} + \frac{\partial \sigma_z^m}{\partial z} - \rho\left(x^m, y^m, z^m\right) b_i = 0 \tag{3-7}$$

or in terms of $\alpha^{[i]}$ as

$$\alpha_x^{[x]} + \alpha_{yx}^{[y]} + \alpha_{zx}^{[z]} = 0 \tag{3-8}$$

$$\alpha_{xy}^{[x]} + \alpha_y^{[y]} + \alpha_{zy}^{[z]} = 0 \tag{3-9}$$

$$\alpha_{xz}^{[x]} + \alpha_{yz}^{[y]} + \alpha_z^{[z]} - \rho\left(x^m, y^m, z^m\right) b_i = 0 \tag{3-10}$$

Accordingly, the first order approximation of the stress field requires the determination of 22 parameters (6 are associated with $\sigma(X)$; 18 are associated with $\alpha^{[x]}$, $\alpha^{[y]}$ and $\alpha^{[z]}$; and finally one associated with the density of the rock $\rho(x^m, y^m, z^m)$ minus the three equilibrium equations). A number of simplifying assumptions may be formulated which helps reduce the number of unknowns:

Simplifying assumption [1]. The lateral stress variations may be neglected so that $\alpha^{[x]}$ and $\alpha^{[y]}$ are zero. This reduces the number of unknown parameters to 10 since Equations (3-8) and (3-9) imply that $\alpha_{zx}^{[z]} = \alpha_{zy}^{[z]} = 0$. The equilibrium condition implies that the vertical direction must be a principal direction for $\alpha^{[z]}$ when the stress varies linearly with depth.

Simplifying assumption [2]. The vertical direction is assumed to be a principal direction throughout the volume. When assumption [1] does not hold, assumption [2] implies that $\sigma_{xz}(X) = \sigma_{yz}(X) = \alpha_{xz}^{[i]} = \alpha_{zx}^{[i]} = \alpha_{yz}^{[i]} = \alpha_{zy}^{[i]} = 0$. This leaves 14 parameters. When assumption [1] and [2] are combined, the number of unknowns is reduced to 8.

Simplifying assumption [3]. When the vertical stress is a principal stress, the parameter $\alpha_z^{[z]}$ is equal to the rock mass density and may be evaluated by direct measurements on cores (the rock mass density is assumed to be identical to the rock matrix density). When assumption [1], [2] and [3] are combined, the number of unknowns is reduced to 7.

Simplifying assumption [4]. The volume in which the regional stress field is computed is small enough for neglecting the rotations of principal stress directions ($\alpha_{xy}^{[i]} = \alpha_{yx}^{[i]} = 0$). This implies that the directions of $\alpha^{[i]}$ are the same as those of $\sigma(X^m)$. This reduces the number of unknowns to 6 when all the previous simplifying assumptions hold.

Simplifying assumption [5]. The stress field is assumed to be continuous up to ground surface. When the vertical direction is principal and when X^m is chosen to be at ground surface then $\sigma_z(X^m) = 0$. The stress tensor $\sigma(X^m)$ is defined of only three components, the two horizontal principal stresses and the orientation of one of them (when $\sigma(z=0)$ the stress tensor is called S).

Simplifying assumption [6]. The volume in which the regional stress field is computed is small enough for neglecting the gradient of the horizontal stresses, i.e. the number of unknowns is equal to three when previous assumptions hold.

Thus, in best of cases, disregarding simplifying assumption [6], the regional stress field is characterized by five parameters, and Equation (3-1) reduces to

$$\sigma\left(X^m\right) = S + z^m \alpha^{[z]} \tag{3-11}$$

where S and $\alpha^{[z]}$ are second order symmetrical tensors with one of the eigenvectors oriented in the vertical direction. Equation (3-11) can be combined with the normal stress equation:

$$\sigma\left(X^m\right) n^m n^m = \sigma_{normal}^m \tag{3-12}$$

with

$$n^m = \begin{bmatrix} n_{x_1} \\ n_{x_2} \\ n_{x_3} \end{bmatrix} = \begin{bmatrix} \cos\phi^m \sin\theta^m \\ \sin\phi^m \sin\theta^m \\ \cos\theta^m \end{bmatrix} \tag{3-13}$$

where ϕ^m is the azimuth of the normal to the m^{th} fracture plane and θ^m the inclination of the normal of the m^{th} fracture plane with respect to the vertical direction.

Equations (3-11) and (3-12) then yield

$$\sigma^{m}_{normal} - Sn^{m}n^{m} - z^{m}\alpha^{[z]}n^{m}n^{m} = 0 \qquad (3\text{-}14)$$

S may be represented by two eigenvalues, S_1 and S_2, where λ is the orientation of the S_1 eigenvector (defined with respect to North, positive to the East). $\alpha^{[3]}$ may be represented by three eigenvalues, α_1, α_2 and α_3, where η is the orientation of the α_1 eigenvector with respect to the S_1 eigenvector. This implies that the angle ϕ^i is reduced by λ for S_1 and S_2 and by $(\lambda+\eta)$ for α_1, α_2 and α_3. Equation (3-14) can then be expressed as:

$$\sigma^{m}_{normal} - \alpha_3 z^{m}\, cos^{2}\,\theta^{m} - \qquad (3\text{-}15)$$

$$\frac{1}{2} sin^{2}\,\theta^{m} \begin{Bmatrix} S_1 + S_2 + (\alpha_1 + \alpha_2)z^{m} + (S_1 - S_2)cos\,2(\phi^{m} - \lambda) \\ + (\alpha_1 - \alpha_2)z^{m}\, cos\,2(\phi^{m} - (\lambda + \eta)) \end{Bmatrix}$$

3.2 THE INVERSE PROBLEM

The inversion will be performed using a method developed by Cornet and Valette (1984), based on the least squares criterion (Tarantola and Valette, 1982). In this method, all measurements are assumed to obey Gaussian distribution so that they may be described by their expected value, and their variance and covariance's with other measurements. Furthermore, *a priori* knowledge of the unknowns is assumed to exist that can be formulated in terms of expected value, variance and covariance's. In practice, large error bars are placed on assumed central values for the unknowns. The solution to Equation (3-15) is defined by the minimum of the sum given by

$$\sum_{k=1}^{N} \left\{ \left[\frac{(\phi - \phi_0)}{\varepsilon_0^{\phi}} \right]_k^2 + \left[\frac{(\theta - \theta_0)}{\varepsilon_0^{\theta}} \right]_k^2 + \left[\frac{(\sigma_{normal} - \sigma_{normal0})}{\varepsilon_0^{\sigma_{normal}}} \right]_k^2 + \left[\frac{(z - z_0)}{\varepsilon_0^{z}} \right]_k^2 \right.$$

$$+ \left(\frac{S_1 - S_{10}}{\varepsilon_0^{S_1}} \right)^2 + \left(\frac{S_2 - S_{20}}{\varepsilon_0^{S_2}} \right)^2 + \left(\frac{\lambda - \lambda_0}{\varepsilon_0^{\lambda}} \right)^2 \qquad (3\text{-}16)$$

$$\left. + \left(\frac{\alpha_1 - \alpha_{10}}{\varepsilon_0^{\alpha_1}} \right)^2 + \left(\frac{\alpha_2 - \alpha_{20}}{\varepsilon_0^{\alpha_2}} \right)^2 + \left(\frac{\alpha_3 - \alpha_{30}}{\varepsilon_0^{\alpha_3}} \right)^2 + \left(\frac{\eta - \eta_0}{\varepsilon_0^{\eta}} \right)^2 \right\}$$

Equation (3-16) exhibits 4N+7 = 1 components for N measurements for a seven-parameter model.

3.3 THE SOLUTION OF THE INVERSE PROBLEM

Let π_0 be a vector of *a priori* values according to

$$\pi_0 = col\begin{bmatrix}(\phi_0,\theta_0,\sigma_{normal0},z_0)^1,...,(\phi_0,\theta_0,\sigma_{normal0},z_0)^N,\\ S_{10},S_{20},\lambda_0,\alpha_{10},\alpha_{20},\alpha_{30},\eta_0\end{bmatrix} \tag{3-17}$$

with *a priori* standard deviations ε_0^{ϕ}, ε_0^{θ}, $\varepsilon_0^{\sigma normal}$, ε_0^{z}, ε_0^{S1}, ε_0^{S2},ε_0^{λ}, $\varepsilon_0^{\alpha 1}$, $\varepsilon_0^{\alpha 2}$, $\varepsilon_0^{\alpha 3}$ and ε_0^{η}. C_0 is the corresponding *a priori* covariance matrix. It is diagonal because measurements and unknowns are supposed to be independent (Cornet and Valette, 1984). Corresponding *a posteriori* vector π is of the form

$$\pi = col\begin{bmatrix}(\phi,\theta,\sigma_{normal},z)^1,...,(\phi,\theta,\sigma_{normal},z)^N,\\ S_1,S_2,\lambda\ ,\alpha_1,\alpha_2,\alpha_3,\eta\end{bmatrix} \tag{3-18}$$

A vector function $f(\pi)$ may be introduced in which the m^{th} component is defined by

$$f^m(\pi) = \sigma^m_{normal} - \alpha_3 z^m \cos^2\theta^m -$$

$$\frac{1}{2}\sin^2\theta^m\begin{Bmatrix}S_1+S_2+(\alpha_1+\alpha_2)z^m+(S_1-S_2)\cos 2(\phi^m-\lambda)\\ +(\alpha_1-\alpha_2)z^m\cos 2(\phi^m-(\lambda+\eta))\end{Bmatrix}=0 \tag{3-19}$$

With these notations, the solution of the inverse problem is defined by the minimum of

$$(\pi-\pi_0)^T C_0^{-1}(\pi-\pi_0) \tag{3-20}$$

which belongs to the set of solutions of

$$f(\pi)=0 \tag{3-21}$$

The components of π are referred to as computed values or *a posteriori* values. If a point π satisfies Equations (3-20) and (3-21), it also contains local minimum, saddle points, local maximum, etc. Tarantola and Valette (1982) showed that the system with Equations (3-20) and (3-21) is obtained by the iterative algorithm

$$\pi_{n+1} = \pi_0 + C_0 F_n^T\left(F_n C_0 F_n^T\right)^{-1}\left[F_n(\pi_n-\pi_0)-f(\pi_n)\right] \tag{3-22}$$

where F is a matrix of partial derivatives of f(π) valued at point π. Accordingly, the components of F are

$$\left(F_n\right)_{mj} = \left(\frac{\partial f^m}{\partial \pi_j}\right)_{\pi=\pi_n} \tag{3-23}$$

where f^m is the m^{th} component of f(π) and π_j is the j^{th} component of π, so that, from Equation (3-23)

$$\frac{\partial f^m}{\partial z^m} = -\alpha_3 \cos^2\theta^m - \frac{1}{2}\sin^2\theta^m\left\{\left(\alpha_1+\alpha_2\right)+\left(\alpha_1-\alpha_2\right)\cos 2\left[\phi^m-\left(\lambda+\eta\right)\right]\right\} \tag{3-24}$$

$$\frac{\partial f^m}{\partial \phi^m} = \sin^2\theta^m\left\{\left(\alpha_1-\alpha_2\right)z^m \sin 2\left[\phi^m-\left(\lambda+\eta\right)\right]+\left(S_1-S_2\right)\sin 2\left(\phi^m-\lambda\right)\right\} \tag{3-25}$$

$$\frac{\partial f^m}{\partial \theta^m} = \frac{1}{2}\sin 2\theta^m\begin{Bmatrix} z^m\left[2\alpha_3-\left(\alpha_1+\alpha_2\right)-\left(\alpha_1-\alpha_2\right)\cos 2\left(\phi^m-\left(\lambda+\eta\right)\right)\right] \\ -\left(S_1+S_2\right)-\left(S_1-S_2\right)\cos 2\left(\phi^m-\lambda\right) \end{Bmatrix} \tag{3-26}$$

$$\frac{\partial f^m}{\partial \sigma^m_{normal}} = 1 \tag{3-27}$$

$$\frac{\partial f^m}{\partial S_1} = -\frac{1}{2}\sin^2\theta^m\left[1+\cos 2\left(\phi^m-\lambda\right)\right] \tag{3-28}$$

$$\frac{\partial f^m}{\partial S_2} = -\frac{1}{2}\sin^2\theta^m\left[1-\cos 2\left(\phi^m-\lambda\right)\right] \tag{3-29}$$

$$\frac{\partial f^m}{\partial \lambda} = -\sin^2\theta^m\left\{\left(\alpha_1-\alpha_2\right)z^m \sin 2\left[\phi^m-\left(\lambda+\eta\right)\right]+\left(S_1-S_2\right)\sin 2\left(\phi^m-\lambda\right)\right\} \tag{3-30}$$

$$\frac{\partial f^m}{\partial \alpha_1} = -\frac{1}{2}\sin^2\theta^m z^m\left[1+\cos 2\left(\phi^m-\left(\lambda+\eta\right)\right)\right] \tag{3-31}$$

$$\frac{\partial f^m}{\partial \alpha_2} = -\frac{1}{2}\sin^2\theta^m z^m\left[1-\cos 2\left(\phi^m-\left(\lambda+\eta\right)\right)\right] \tag{3-32}$$

$$\frac{\partial f^m}{\partial \alpha_3} = -z^m \cos^2 \theta^m \tag{3-33}$$

$$\frac{\partial f^m}{\partial \eta} = -(\alpha_1 - \alpha_2) z^m \sin^2 \theta^m \sin 2\left[\phi^m - (\lambda + \eta)\right] \tag{3-34}$$

The derivatives of f^m with respect to ϕ^k,θ^k, σ^k and z^k are null for $m \neq k$. The iterative procedure is stopped when $f(\pi_n)$ is sufficiently close to zero. The procedure is repeated with different *a priori* values for the unknown parameters to verify that the final solution does not depend on the start value.

Tarantola and Valette (1982) has showed that the stationary point π obtained from the iterative process in Equation (3-22) corresponds to a strict local minimum of f if and only if $C_0^{-1} L_\pi Q_\pi$ is not negative. Q_π is the linear projector defined by

$$Q_\pi = 1 - C_0 F_\pi^T \left(F_\pi C_0 F_\pi^T\right)^{-1} F_\pi \tag{3-35}$$

and L_π is the operator defined by

$$L_\pi(V) \equiv V - Q_\pi C_0 \left[K_\pi(V)\right]^T \left(F_\pi C_0 F_\pi^T\right)^{-1} F_\pi (\pi - \pi_0) \tag{3-36}$$

where V is any vector and K_π is the second order partial derivative operator of $f(\pi)$ taken at point π.

3.4 RESOLUTION AND PRESENTATION OF RESULTS

The *a posteriori* variance and covariance's associated with the unknowns provide a measure of the quality with which the unknowns have been resolved. If the *a posteriori* variance is small, the value has been well resolved; if it is nearly equal to the *a priori* variance the corresponding unknown has not been resolved. In any case, as stated by Tarantola and Valette (1982), a good estimate of the resolution of a parameter is obtained by the ratio

I = [*a posteriori* variance of a parameter]/[*a priori* variance of a parameter]

This ratio, named indetermination estimator, verifies $0 \leq I \leq 1$. For a well-resolved parameter, $I \approx 0$; for a poorly resolved parameter, $I \approx 1$.

When the problem is linear ($\eta \neq 0$), it can be shown that the *a posteriori* covariance matrix is given by

$$C = QC_0 \tag{3-37}$$

When the problem is non-linear, expression of the *a posteriori* covariance matrix can still be computed but its value depends on the final value π_{n+1}. However, when both $(\pi-\pi_0)^T C_0^{-1}(\pi-\pi_0)$ and $\|K_\pi\|$ are small, the linear approximation Equation (3-37) yields a satisfactory result (Cornet and Valette, 1984).

3.5 CHOICE OF MODEL

In this study, the analysis are mostly based on six- and seven-parameter models, which fulfil assumptions [1],[2],[3], and [5] respectively [1],[2] and [5] according to (see also pages 27-28):

[1]. The lateral stress variation is neglected. The vertical direction is a principal direction for $\alpha^{[z]}$ when the stress varies linearly with depth.
[2]. The vertical direction is a principal direction throughout the volume.
[3]. The parameter $\alpha_z^{[z]}$ is the rock mass density and is evaluated by measurements on cores (the rock mass density is assumed identical to the rock matrix density).
[5]. The stress field is continuous up to ground surface.

The six-parameter model can be expressed according to

$$\sigma\left(X^m\right) = \begin{bmatrix} \sigma_x & \tau_{xy} & 0 \\ \tau_{yx} & \sigma_y & 0 \\ 0 & 0 & 0 \end{bmatrix} + z^m \begin{bmatrix} \frac{\partial \sigma_x}{\partial z} & \frac{\partial \tau_{xy}}{\partial z} & 0 \\ \frac{\partial \tau_{yx}}{\partial z} & \frac{\partial \sigma_y}{\partial z} & 0 \\ 0 & 0 & \gamma \end{bmatrix} \tag{3-38}$$

The seven-parameter also has the density, γ, as an unknown parameter. The six-parameter model in graphical form with eigenvalues is shown in Figure 3-1.

However, as described in the introduction, the in-situ stress data have to be divided into subsets due to strong non-linear stress distribution versus depth caused by discontinuities. This implies that a much smaller amount of data is available at each depth interval, thus a model with a smaller number of unknowns has to be used. Following assumptions have been made when the six- or seven-parameter models did not give satisfactory results, thus resulting in a five- and three-parameter model:

[4]. The volume in which the regional stress field is computed is small enough for neglecting the rotations of principal stress directions, i.e. the number of unknowns are equal to five when previous assumptions hold.

[6]. The volume in which the regional stress field is computed is small enough for neglecting the gradient of the horizontal stresses, i.e. the number of unknowns are equal to three when previous assumptions hold.

The weight of the overburden, γ, has been determined from density measurements on cores. The density of crystalline rocks is highly dependent upon the mineral composition. The density of the acid variant of Småland granite and the more basic Äspö diorite has been determined to 2.65-2.75 tonnes/m^3. However, more basic rock types with high mafic mineral content and low SiO_2-content have a high density (> 3.0 tonnes/m^3). These high density rock types observed in Äspö have been assigned to the Greenstone group, including diorites-gabbros (Rhén et al., 1997).

The γ-value used in the six-parameter inversion program has been set to 2.65 tonnes/m^3. However, analysis with different γ-values was also performed as well as attempts to determine the rock mass density in-situ using the seven-parameter model.

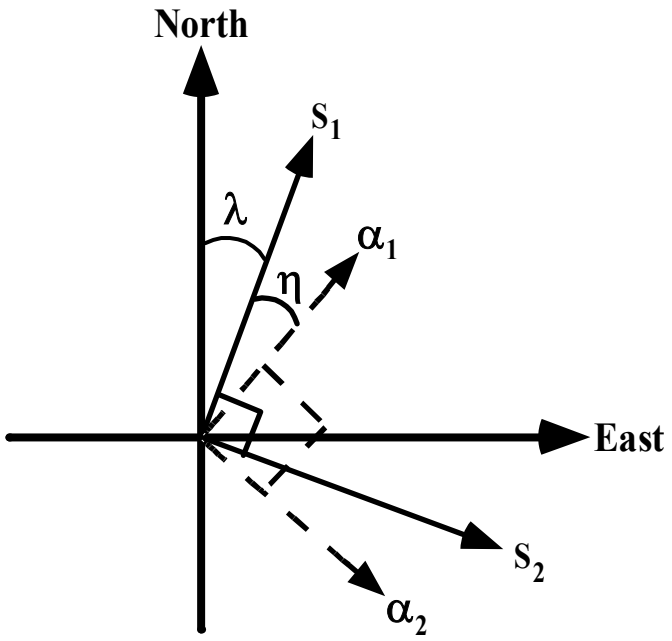

Figure 3-1. *The six-parameter model in graphical form expressed with eigenvalues and eigenvectors.*

3.6 UNCERTAINTIES IN CHOICE OF MODEL

The state of stress in rock is usually described within the context of continuum mechanics. However, a rock mass is not continuous or homogeneous but contains discontinuities with different mechanical properties. The stress tensor in a continuous material is therefore dependent on scale and is only valid between well-defined geological boundaries where it is consistent with the homogenization criterion. Cornet (1993b) defined the main model related errors:

{1} The area concerned by each measurement and the number of measurements are not consistent with the homogenizing criterion.

{2} The stress field does not follow the pattern assumed by the model.

The first model related error is taken care of by dividing the data set into subsets with a reasonably linear stress field, i.e. one data set above, one data set below and, one data set within the potential sub-horizontal discontinuity. In boreholes KAS02 and KLX02, the data set above the discontinuity had to be divided once more. However, this means that in some sections a very small number of measurement points are available. In order to solve the state of stress in these sections a simpler model must be chosen. This in turn may lead to the situation posed in model related error {2}. Consequently, it is important to have a good idea of site specific structural geology and limitations in the applied theory and parameterization of the rock mass.

Other possible model related errors are:

{3} The assumption that data and estimated model parameters follow Gaussian distribution.

{4} Convergence and non-uniqueness of a non-linear least square problem.

{5} Topographical effect on the state of stress.

The basic premise of an inverse method is that the data and model parameters are related. That is, when estimating model parameters on the basis of measured data, the solution tends to map errors in the data to the estimated model parameters. If the data follow Gaussian distribution and the theory is linear it can be shown that the estimated model parameters will tend to follow Gaussian distribution as long as the noise in the data comes from several sources of comparable size (*the central limit theorem*). On the other hand, if the theory is non-linear, the final distribution is not Gaussian. However, if the theory is not too non-linear, it may be approximated as being Gaussian (e.g. Menke, 1984).

Once a solution is obtained, there exist a number of methods to test its validity, for example to compare the *a posteriori*/*a priori* data, compare the *a posteriori*/*a priori* standard deviation of the unknown parameters, calculate the standard deviation of stress versus depth, check that the covariance matrix is diagonal etc. All are based on the assumption that a "true" solution is obtained, which is not necessarily correct. Valette (1982) showed that the stationary point π obtained from the iterative process in Equation (30) corresponds at least to a local minimum, i.e. not necessarily the global minimum. Consequently, even if an inverse problem is known to have a unique solution, there is no guarantee that the iterative method will converge to that solution. We have attempted to overcome this drawback by testing different *a priori* values of the unknowns to verify that the solution does not depend on the initial guess.

The Äspö region is characterized by a slightly undulated topography. Consequently, topographical effects have been neglected.

4 CALIBRATION OF MODEL

The six- and seven parameter models was validated and calibrated using published data. Totally, six calibrations were performed on sites located in Sweden and France. The Swedish data have been published by Ljunggren and Raillard (1987) and the French data by Cornet and Burlet (1992). Cornet and Burlet (1992) used a seven parameter model where also the vertical gradient or the weight of the overburden, α_3, was assumed to be an unknown parameter. Ljunggren and Raillard (1987) used a six-parameter model.

4.1 SWEDEN

4.1.1 Gideå

The Gideå site, located about 480 km North of Stockholm, Sweden, is one of the selected test sites for investigating a future deep disposal of Swedish high-level nuclear waste. Ljunggren and Raillard (1987) performed HTPF and conventional hydraulic fracturing measurements in one borehole at depths between 90 and 270 m depth (10 measurement points). A comparison between the six-parameter models is presented in Table 4-1 and Figure 4-1. Unfortunately, no comparison concerning the orientation of the horizontal stresses could be performed for this site. The rock mass density, α_3, is equal to 0.0265 MPa/m.

Table 4-1. Comparison of models at the Gideå site, Sweden.

Model	**S_1** [MPa]	**S_2** [MPa]	**α_1** [MPa/m]	**α_2** [MPa/m]	**λ** [°N]	**η** [°]
This study	4.82	-3.98	0.0150	0.0839	25	6
Ljunggren and Raillard, 1987	4.89	-2.47	0.0146	0.0710	26	4

Table 4-1 shows that there are some discrepancies concerning the values for S_1 and α_1. The S_2-value is slightly larger compared to the published value but is compensated with a larger stress gradient α_2. The comparison of horizontal stresses versus depth gives a satisfactory fit. However, the maximum horizontal stress according to Ljunggren and Raillard (1987) is smaller for the depth interval, especially between 175-250 m depth.

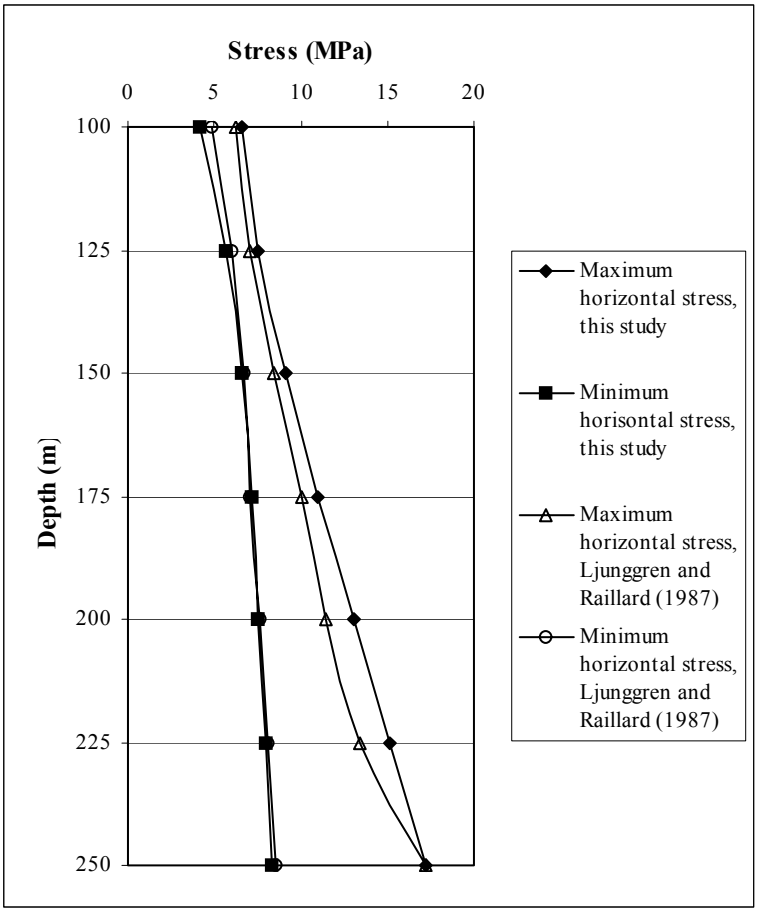

Figure 4-1. *Comparison of maximum and minimum horizontal stress versus depth for the Gideå site, Sweden.*

4.2 FRANCE

4.2.1 Chassoles

The Chassoles site is located approximately 60 km South of Clermont Ferrand, in the Massif Central of southern France. Cornet and Burlet (1992) performed 14 HTPF and conventional hydraulic fracturing measurements in a single borehole at depths between 340 and 820 m depth. A comparison between the models is presented in Table 4-2 and Figures 4-2 and 4-3.

Table 4-2 shows that the horizontal stresses versus depth and orientation of maximum horizontal stress versus depth agree well with the result by Cornet and Burlet (1992).

Table 4-2. Comparison of models at the Chassoles site, France.

Model	S_1 [MPa]	S_2 [MPa]	α_1 [MPa/m]	α_2 [MPa/m]	λ [°N]	η [°]	α_3 [MPa/m]
This study	9.63	1.04	0.0001	0.0206	-100	-6	0.0225
Cornet and Burlet, 1992	9.50	2.40	0.0010	0.0180	-96	-9	0.0220

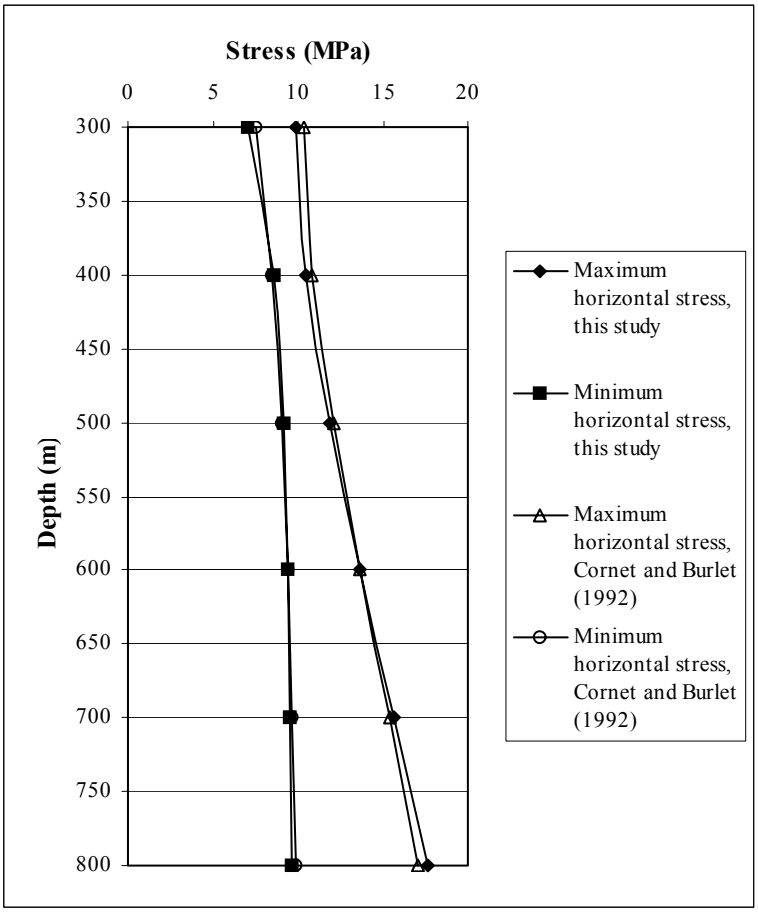

Figure 4-2. *Comparison of maximum and minimum horizontal stress versus depth for the Chassoles site, France.*

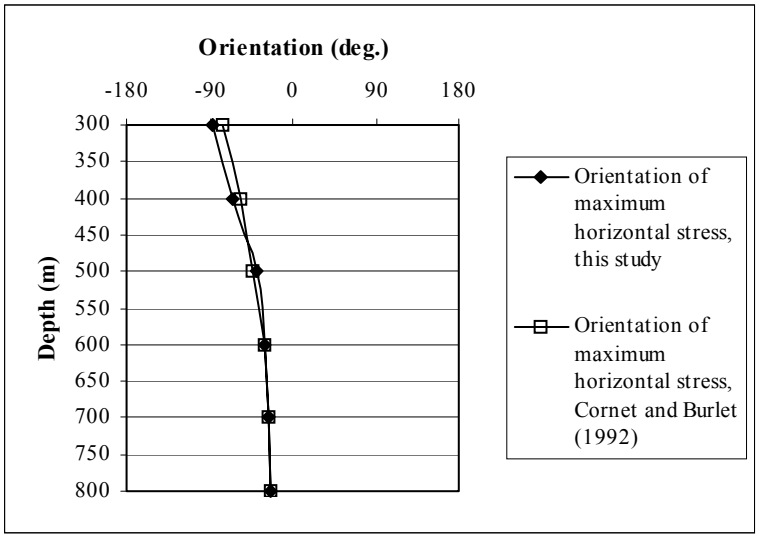

Figure 4-3. *Comparison of orientation of maximum horizontal stress versus depth for the Chassoles site, France.*

4.2.2 Le Mayet de Montagne

The Le Mayet de Montagne site is located 25 km Southeast of Vichy, in central France. Cornet and Burlet (1992) conducted 18 HTPF measurements in a number of boreholes at depths between 60 and 730 m depth. A comparison between the models is presented in Table 4-3 and Figures 4-4 and 4-5.

As can be seen in Table 4-3, S_1 and S_2 are switched, and λ are approximately 90° offset and η approximately 180° offset. However, this is explained by the definition of the model, Figure 3.1, and is a geometric phenomenon with no significance for the calculated stresses and orientations versus depth. A comparison of the horizontal stresses versus depth and orientation of maximum horizontal stress versus depth are in accordance with the Cornet and Burlet (1992) results.

Table 4-3. Comparison of models at the Le Mayet de Montagne site, France.

Model	S_1 [MPa]	S_2 [MPa]	α_1 [MPa/m]	α_2 [MPa/m]	λ [°N]	η [°]	α_3 [MPa/m]
This study	0.14	5.32	0.0236	0.0075	115	194	0.0243
Cornet and Burlet, 1992	5.1	0.30	0.0083	0.0239	30	19	0.0242

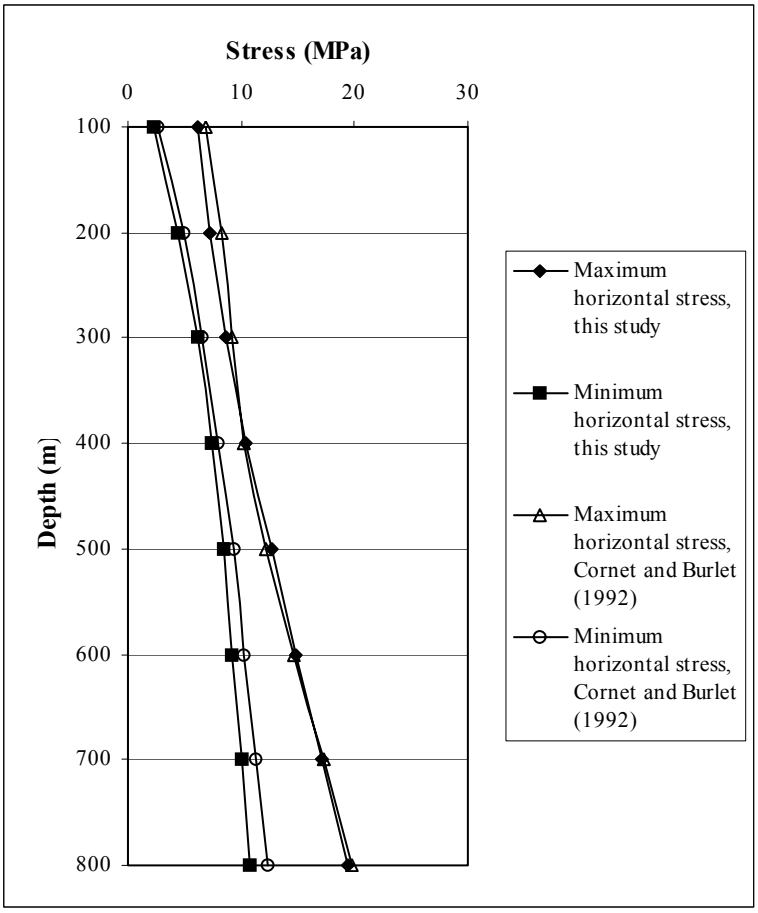

Figure 4-4. *Comparison of maximum and minimum horizontal stress versus depth for the Le Mayet de Montagne site, France.*

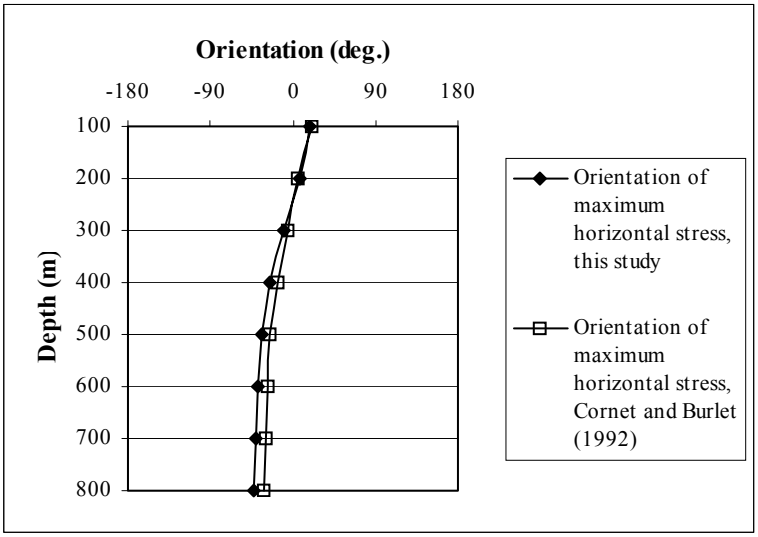

Figure 4-5. *Comparison of orientation of maximum horizontal stress versus depth for the Le Mayet de Montagne site, France.*

4.2.3 Echassières

The Echassières site is located about 40 km West of Vichy, in central France. Cornet and Burlet (1992) performed HTPF and hydraulic fracturing measurements in a 950 m deep borehole. The results from measurements between 121 and 649 m depth are shown in Tables 4-4 and 4-5 and Figures 4-6 and 4-7.

The horizontal stresses versus depth and orientation of maximum horizontal stress versus depth are in accordance with the Cornet and Burlet (1992) results.

Table 4-4. Comparison of models for the upper section at the Echassières site, France.

Model	S_1 [MPa]	S_2 [MPa]	α_1 [MPa/m]	α_2 [MPa/m]	λ [°N]	η [°]	α_3 [MPa/m]
This study	2.20	2.28	0.0119	0.0083	191	0	0.0150
Cornet and Burlet, 1992	1.9	2.2	0.0129	0.009	192	0	0.0150

Table 4-5. Comparison of models for the lower section at the Echassières site, France.

Model	S_1 [MPa]	S_2 [MPa]	α_1 [MPa/m]	α_2 [MPa/m]	λ [°N]	η [°]	α_3 [MPa/m]
This study	22.67	5.25	0.0296	0.0068	146	0	0.0240
Cornet and Burlet, 1992	23.3	3.7	0.0280	0.0100	146	0	0.0240

4.2.4 Auriat

The Auriat site is located near the village of Auriat approximately 30 km East of Limoges, in western France. Cornet and Burlet (1992) performed 12 HTPF measurements in two boreholes at depths between 120 and 980 m depth. A comparison between the models is presented in Table 4-6 and Figures 4-8 and 4-9.

The comparison of horizontal stresses versus depth and orientation of maximum horizontal stress versus depth are in accordance with the Cornet and Burlet (1992) publication.

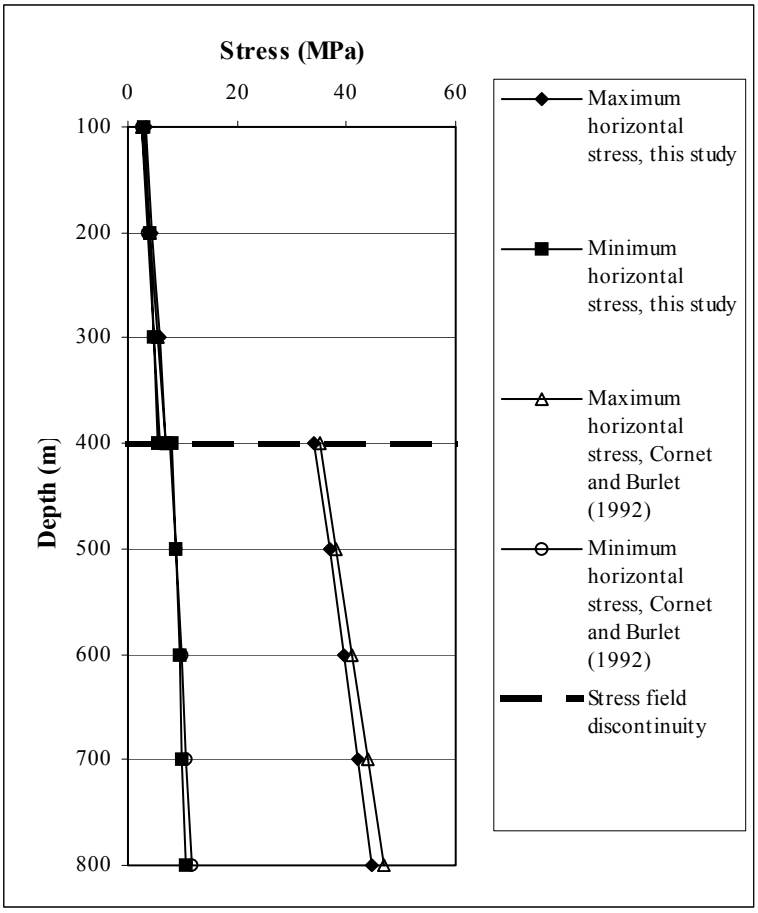

Figure 4-6. *Comparison of maximum and minimum horizontal stress versus depth for the Echassières site, France.*

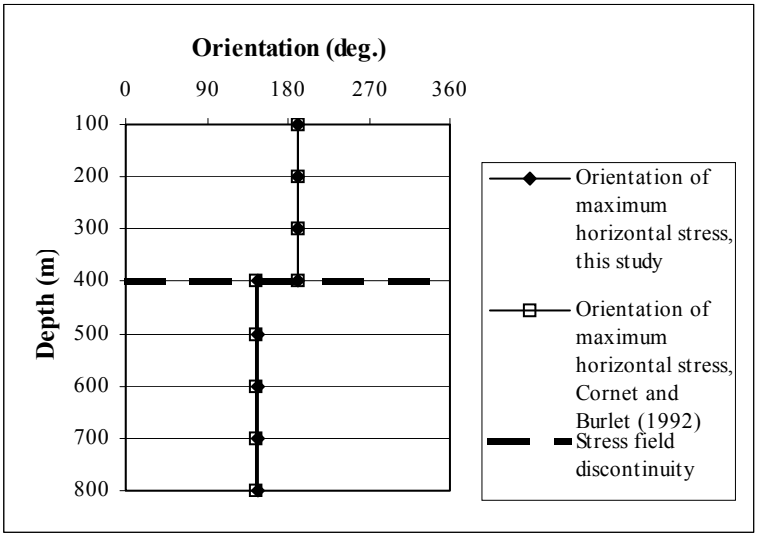

Figure 4-7. *Comparison of orientation of maximum horizontal stress versus depth for the Echassières site, France.*

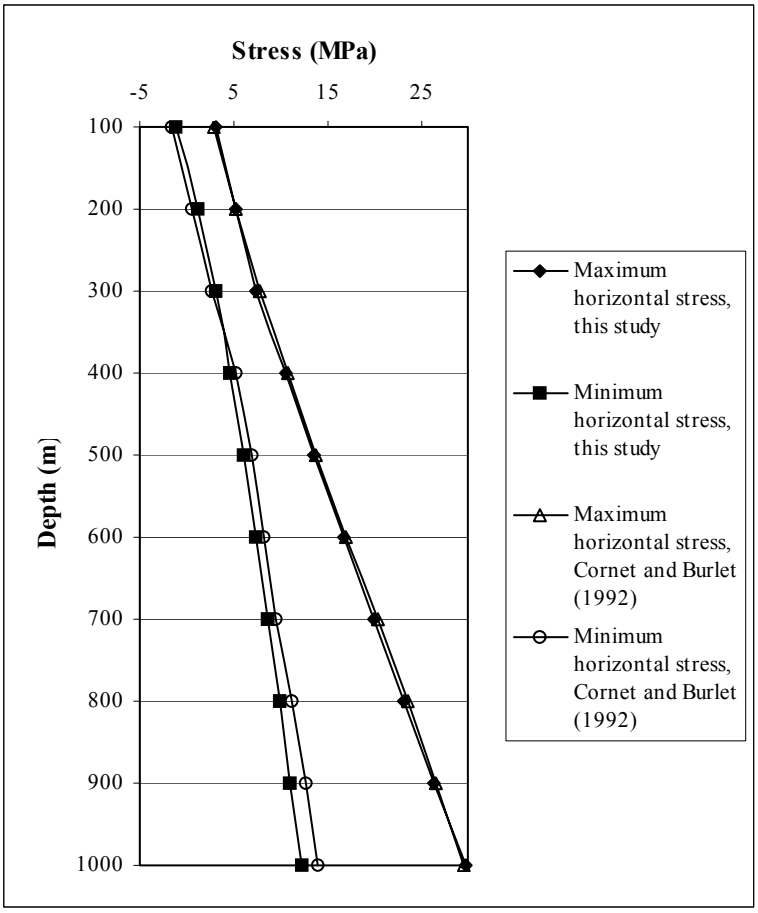

Figure 4-8. *Comparison of maximum and minimum horizontal stress versus depth for the Auriat site, France.*

Table 4-6. Comparison of models at the Auriat site, France.

Model	S_1 [MPa]	S_2 [MPa]	α_1 [MPa/m]	α_2 [MPa/m]	λ [°N]	η [°]	α_3 [MPa/m]
This study	1.5	-4.0	0.0327	0.0119	88	-113	0.0260
Cornet and Burlet, 1992	-3.9	1.2	0.0319	0.0113	1	-26	0.0264

4.2.5 Lodève

The Lodève site is located at Merifons in the small Lodève basin, 50 km West of Montpellier, in southern France. Cornet and Burlet (1992) performed 15 HTPF measurements in one 1000 m deep borehole. A comparison between the models is presented in Table 4-6 and Figures 4-10 and 4-11. The comparison of horizontal stresses versus depth and orientation of maximum horizontal stress versus depth are in accordance with the results by Cornet and Burlet (1992).

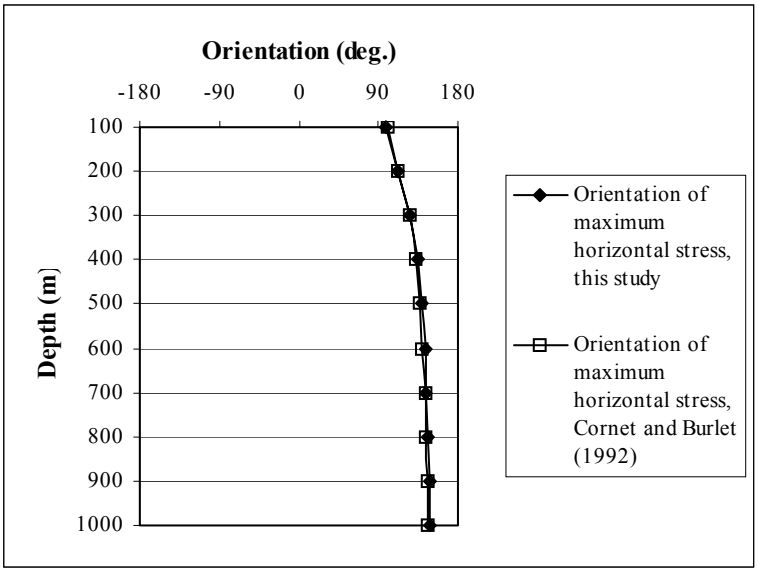

Figure 4-9. *Comparison of orientation of maximum horizontal stress versus depth for the Auriat site, France.*

Table 4-6. Comparison of models at the Lodève site, France.

Model	S_1 [MPa]	S_2 [MPa]	α_1 [MPa/m]	α_2 [MPa/m]	λ [°N]	η [°]	α_3 [MPa/m]
This study	3.97	-5.00	0.0119	0.0180	69	-2	0.0344
Cornet and Burlet, 1992	-4.8	3.7	0.0180	0.0012	-24	-16	0.0330

4.3 SUMMARY OF RESULTS FROM THE CALIBRATION

The calibrations of the six- and seven-parameter models are successful. In average, the discrepancies of σ_H, σ_h, and orientation of σ_H are 0.61 MPa, 0.56 MPa, and 2.8°, respectively. Consequently, we conclude that the horizontal stresses versus depth and also the orientation of maximum horizontal stress are in accordance with the published data. The parameters S_1 and S_2 and also α_1 and α_2 are though often switched and orientations are offset about 90° compared to the published data. However, this is explained by the definition of the model, Figure 3.1, and is a geometric phenomenon with no significance for the calculated stresses and orientations versus depth.

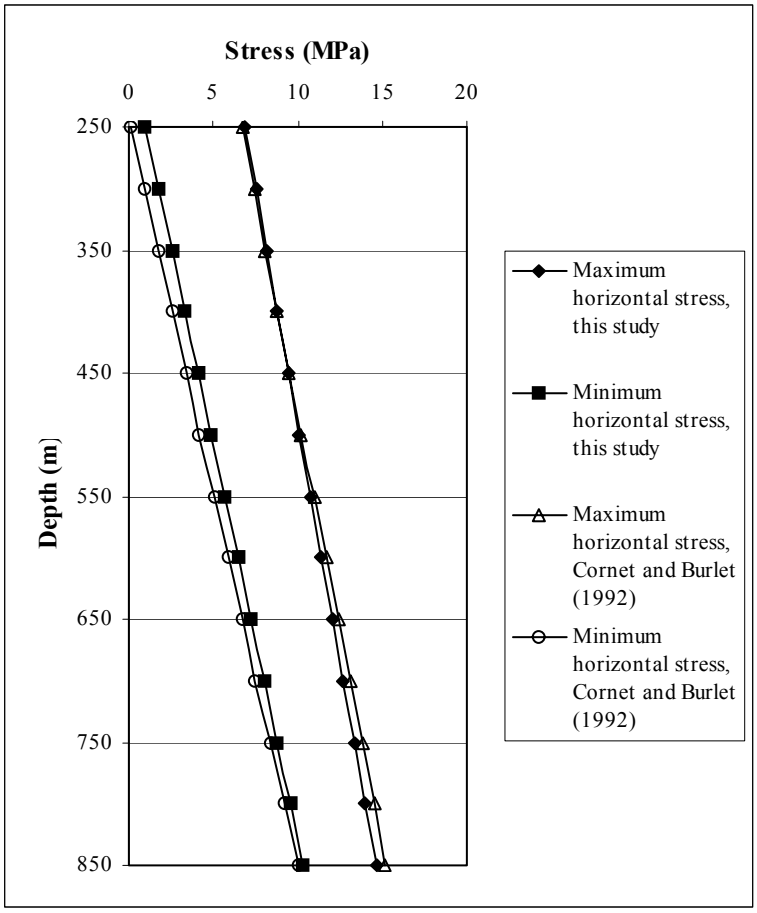

Figure 4-10. *Comparison of maximum and minimum horizontal stress versus depth for the Lodève site, France.*

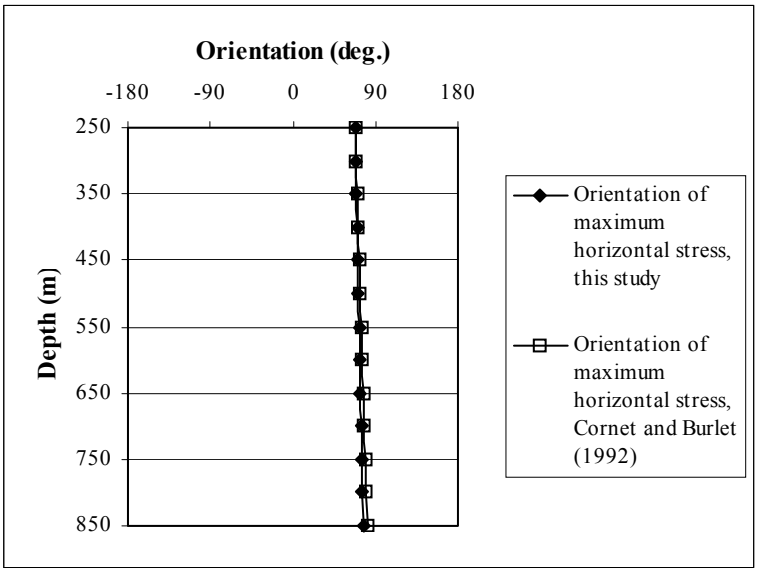

Figure 4-11. *Comparison of orientation of maximum horizontal stress versus depth for the Lodève site, France.*

5 RESULTS FROM THE ÄSPÖ AREA

5.1 GENERAL

The analysis of the Äspö area has been performed on each borehole with the aim to determine the stress versus depth. However, the regional stress field is disturbed by discontinuities (Bjarnason et al., 1989; Leijon, 1995; Hansson et al., 1995; Ljunggren and Klasson, 1997; Ekman, 1997; Ekman et al., 1997) and the measurement points in each borehole have therefore been divided into smaller groups, see Figures 1-2 to 1-7. The analysis has been performed using mainly the six- and seven-parameter models. In some sections, where only a few measurement points were available, a three-parameter model was used. Furthermore, since most stress measurements have been conducted using the high flow rate hydraulic fracturing test, two separate analysis have been attempted using the first and the second shut-in pressure from the hydraulic fracturing measurements respectively. The *a priori* guess of the unknowns are listed below:

$S_1 = S_2 = 0$ MPa
$\alpha_1 = \alpha_2 = 0.015$ MPa/m
λ = mean orientation of hydrofractures
$\eta = 0°$
$\varepsilon_S = 30$ MPa
$\varepsilon_\alpha = 0.025$ MPa/m
$\varepsilon_\lambda = 120°$
$\varepsilon_\eta = 120°$

Once a solution was found, the procedure was repeated with different *a priori* values of the unknown parameters to verify that the final solution did not depend on the initial start value of the unknowns and that the least square solution corresponds to at least a local minimum.

5.2 RESULTS FROM BOREHOLE KAS02

Borehole KAS02 includes 22 successful stress measurements as reported by Bjarnason et al. (1989). Of these, 11 included two or three fractures in the test section, see Table A-1 in Appendix. The measurement points were divided into three groups, 150-450 m, 490-550 m and 620-740 m. This means that the upper data set includes 432 different fracture combinations (2^4*3^3), the middle section 2 combinations (2^1), and the lower section 8 fracture combinations (2^3). However, during analysis it was obvious that all combinations for the upper section did not have to be tested. In total, 48 combinations were tested for the upper section.

5.2.1 Analysis using first shut-in

The analysis of the upper section in KAS02, 150-450 m, included 12 measurement points. The result using the 7-parameter model and the first shut-in pressure are presented in Figures 5-1 and 5-2, and the density of the rock mass was determined to α_3 = 0.0264 MPa/m.

The resolution (I = *a posteriori* variance/*a priori* variance) of the unknowns is acceptable. The standard deviations versus depth are presented in Table 5-1. The inversion result of the measurement points is presented in Table 5-2. The best solution of the six-parameter model was found after 51 iterations according to the following (values at 300 m depth)

S_1 = 9.97 MPa	ε_{S1} = 4.0 MPa	I = 0.018
S_2 = 5.64 MPa	ε_{S1} = 0.4 MPa	I = 0.002
α_1 = 0.0092 MPa/m	$\varepsilon_{\alpha 1}$ = 0.008 MPa/m	I = 0.102
α_2 = 0.0182 MPa/m	$\varepsilon_{\alpha 2}$ = 0.017 MPa/m	I = 0.462
λ = N156°E	ε_{λ} = 46°	I = 0.147
η = -31°	ε_{η} = 11°	I = 0.008

Table 5-1. Standard deviation versus depth using the first shut-in pressure between 150 and 450 m depth in KAS02.

Depth (m)	$\varepsilon^{\sigma H}$ (MPa)	$\varepsilon^{\sigma h}$ (MPa)	$\varepsilon^{\text{Orientation } \sigma H}$ (degrees)
150	5.2	0.6	26
250	4.4	0.4	16
350	3.7	0.5	11
450	3.3	1.1	25

Table 5-2. Results from hydraulic tests in KAS02 using the first shut-in pressure between 150 and 450 m depth.

Vertical depth	ϕ	ε_ϕ	ϕ_c	θ	ε_θ	θ_c	σ_n	$\varepsilon_{\sigma n}$	σ_{nc}
155.2	230	3	230.1	90	1	90.0	9.1	1.0	8.3
222.8	238	3	238.0	90	3	90.0	9.1	0.7	9.1
232.9	231	3	230.9	82	4	81.9	8.5	0.9	9.0
243.1	251	1	251.0	90	4	90.0	8.9	0.9	9.2
250.2	234	6	233.6	90	2	90.0	9.0	0.8	9.3
279.9	257	1	257.0	90	2	90.0	9.8	1.5	9.5
339.4	236	1	236.0	90	2	90.0	10.4	1.8	10.3
346.0	263	1	263.0	90	2	90.0	10.9	1.1	10.3
363.7	267	3	267.0	90	2	90.0	10.3	0.9	10.4
380.7	250	2	250.0	90	2	90.0	10.5	0.9	10.9
389.8	209	2	208.9	84	3	84.0	9.0	0.8	9.3
425.6	227	1	227.2	90	1	90.0	11.2	0.7	10.7

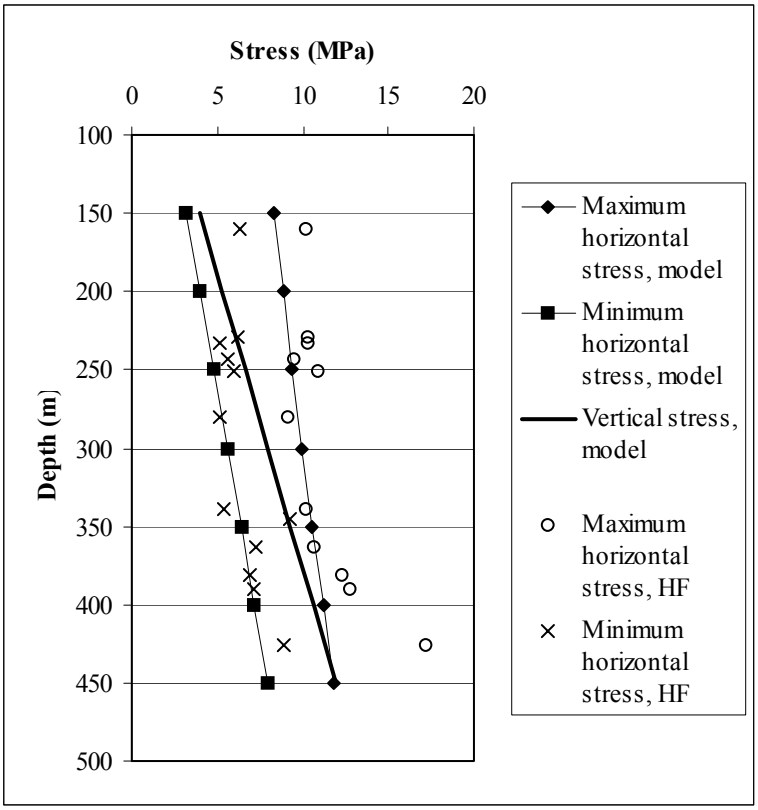

Figure 5-1. *Results from KAS02, 150-450 m depth using a seven-parameter model and first shut-in pressure.*

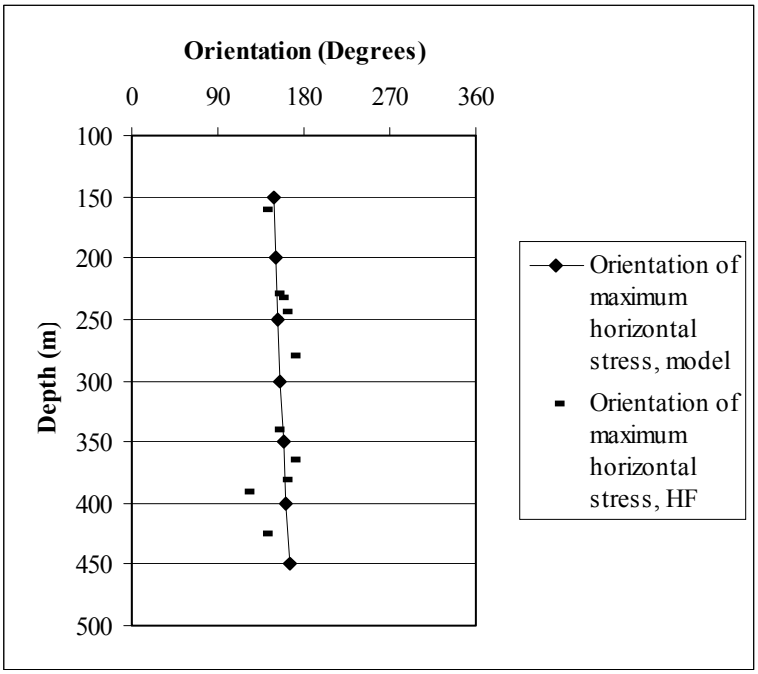

Figure 5-2. *Results from KAS02, 150-450 m depth using a seven-parameter model and first shut-in pressure.*

As indicated in Table 5-2, almost all fractures are vertical. This makes it very difficult to receive a good resolution of the unknown parameters and to reduce the standard deviations of the calculated stresses and their orientation. However, the calculated values for the orientation of the fractures are satisfactory and the fracture normal stresses are reasonable compared with the measured.

The analysis of the middle section in KAS02, 490-550 m, included only 4 measurement points. To solve the stress field a very simple model using three unknowns (S_1, S_2, λ) had to be chosen. The gradients α_1 and α_2 were chosen equal to the increase of the normal stress according to the measured data. The result using the 3-parameter model and the first shut-in pressure are presented in Figures 5-3 and 5-4 using a rock mass density of α_3 = 0.0265 MPa/m. The standard deviations versus depth are presented in Table 5-3. The inversion result of the measurement points is presented in Table 5-4. The solution of the three-parameter model was found after 7 iterations according to (at 525 m depth)

S_1 = 33.90 MPa	ε_{S1} = 5.3 MPa	I = 0.031
S_2 = 22.12 MPa	ε_{S1} = 1.0 MPa	I = 0.001
λ = N139°E	ε_{λ} = 16°	I = 0.018

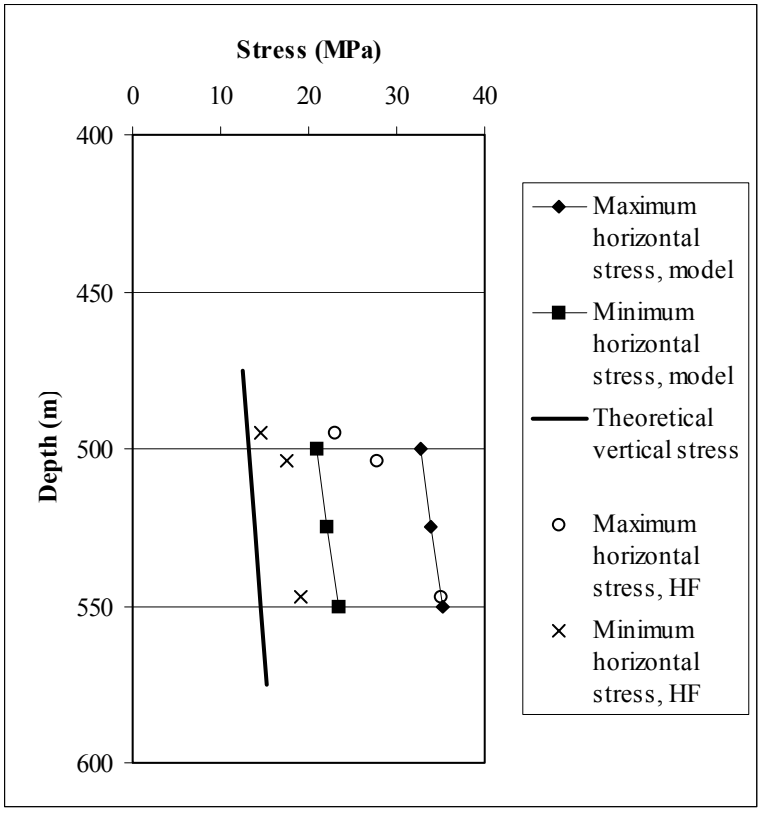

Figure 5-3. *Results from KAS02, 490-550 m depth using a three-parameter model and first shut-in pressure.*

Table 5-3. Standard deviation versus depth using the first shut-in pressure between 490 and 550 m depth in KAS02.

Depth (m)	$\varepsilon^{\sigma H}$ (MPa)	$\varepsilon^{\sigma h}$ (MPa)	$\varepsilon^{\text{Orientation } \sigma H}$ (degrees)
500	5.3	1.0	16
525	5.3	1.0	16
550	5.3	1.0	16

Table 5-4. Results from hydraulic tests in KAS02 using the first shut-in pressure between 490 and 550 m depth.

Vertical depth	ϕ	ε_ϕ	ϕ_c	θ	ε_θ	θ_c	σ_n	$\varepsilon_{\sigma n}$	σ_{nc}
494.9	158	1	158.0	36	1	36.0	19.6	1.4	19.4
504.1	234	1	234.0	90	1	90.0	21.5	1.4	21.2
521.8	230	1	230.0	90	1	90.0	21.2	2.1	21.9
547.0	216	1	216.0	90	1	90.0	23.9	1.5	23.9

As indicated in Table 5-4, most fractures are vertical. The calculated values for the orientation of the fractures are good and the fracture normal stresses are reasonable compared with the measured.

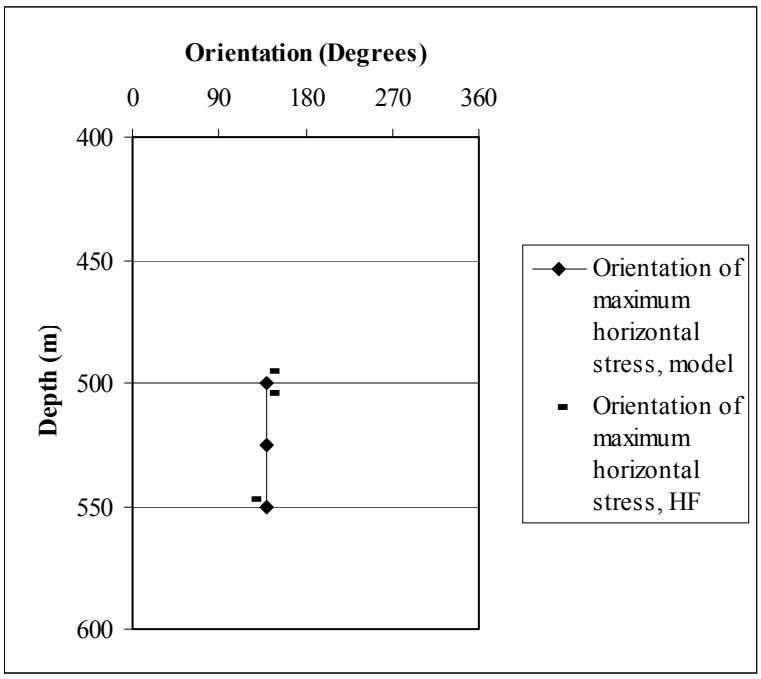

Figure 5-4. *Results from KAS02, 490-550 m depth using a three-parameter model and first shut-in pressure.*

The analysis of the lower section in KAS02, 620-740 m, included only 5 measurement points (of which one had to be excluded), thus the three-parameter model (S_1, S_2, λ) was

used. The result using the 3-parameter model and the first shut-in pressure are presented in Figures 5-5 and 5-6 using a rock mass density of α_3 = 0.0265 MPa/m.

The standard deviations versus depth are presented in Table 5-5. The inversion result of the measurement points is presented in Table 5-6. The solution of the three-parameter model was found after 5 iterations according to (at 670 m depth)

S_1 = 33.31 MPa	ε_{S1} = 3.0 MPa	I = 0.010
S_2 = 26.34 MPa	ε_{S1} = 1.0 MPa	I = 0.001
λ = N177°E	ε_{λ} = 10°	I = 0.007

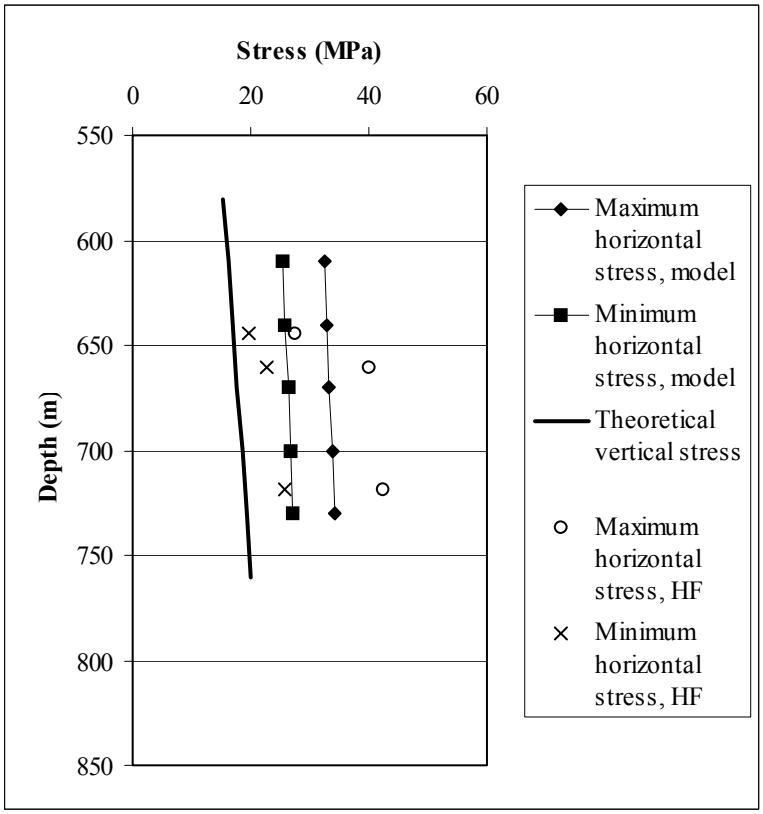

Figure 5-5. *Results from KAS02, 620-740 m depth using a three-parameter model and first shut-in pressure.*

Table 5-5. Standard deviation versus depth using the first shut-in pressure between 620 and 740 m depth in KAS02.

Depth (m)	$\varepsilon^{\sigma H}$ (MPa)	$\varepsilon^{\sigma h}$ (MPa)	$\varepsilon^{\text{Orientation } \sigma H}$ (degrees)
610	3.0	1.0	10
670	3.0	1.0	10
730	3.0	1.0	10

Table 5-6. Results from hydraulic tests in KAS02 using the first shut-in pressure between 620 and 740 m depth.

Vertical depth	ϕ	ε_ϕ	ϕ_c	θ	ε_θ	θ_c	σ_n	$\varepsilon_{\sigma n}$	σ_{nc}
624.8	19	2	19.0	77	1	77.0	31.1	1.1	30.9
660.7	240	1	240.0	90	1	90.0	27.8	2.0	27.7
718.5	200	1	200.0	90	2	90.0	32.6	1.6	33.0
734.0	160	2	160.0	56	3	56.0	29.2	1.1	29.2

The calculated values for the orientation of the fractures are good and the fracture normal stresses are reasonable compared with the measured.

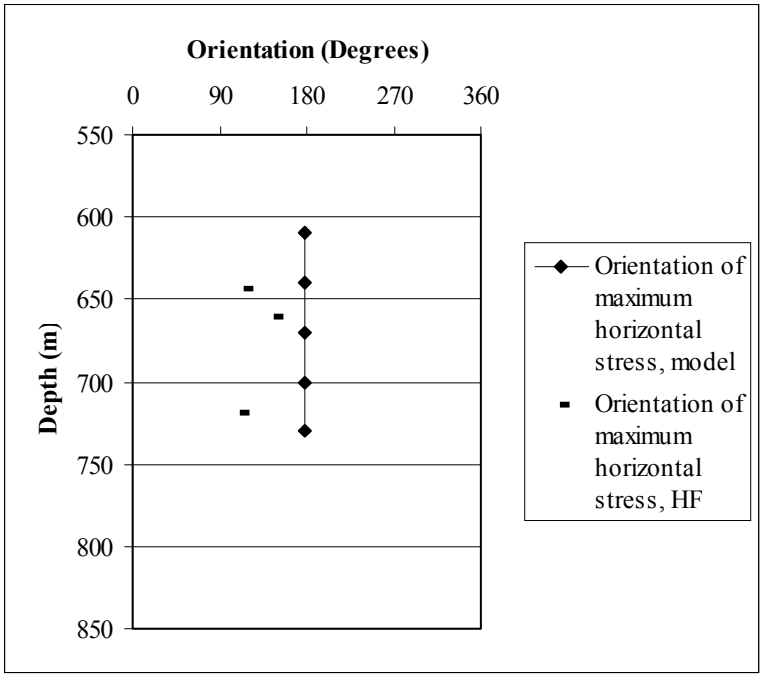

Figure 5-6. *Results from KAS02, 620-740 m depth using a three-parameter model and first shut-in pressure.*

5.2.2 Analysis using second shut-in

The analysis of the upper section in KAS02, 150-450 m using the second shut-in pressure, included 12 measurement points. The standard deviations of the normal stress data had to be slightly increased in order to receive a convergence. The result using the 7-parameter model and the first shut-in pressure are presented in Figures 5-7 and 5-8, and the density of the rock mass was determined to $\alpha_3 = 0.0264$ MPa/m.

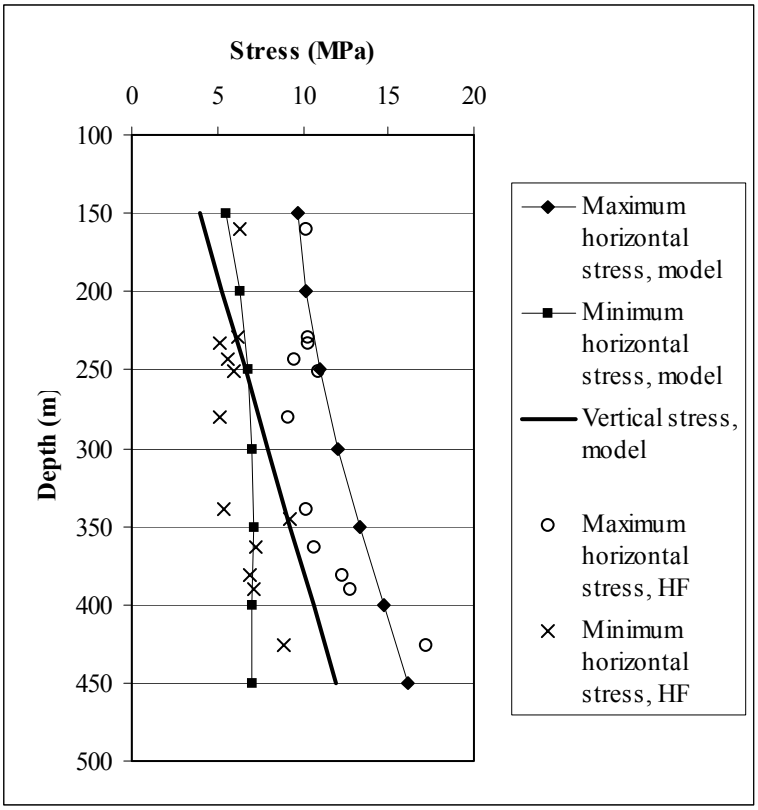

Figure 5-7. *Results from KAS02, 150-450 m depth using a seven-parameter model and second shut-in pressure.*

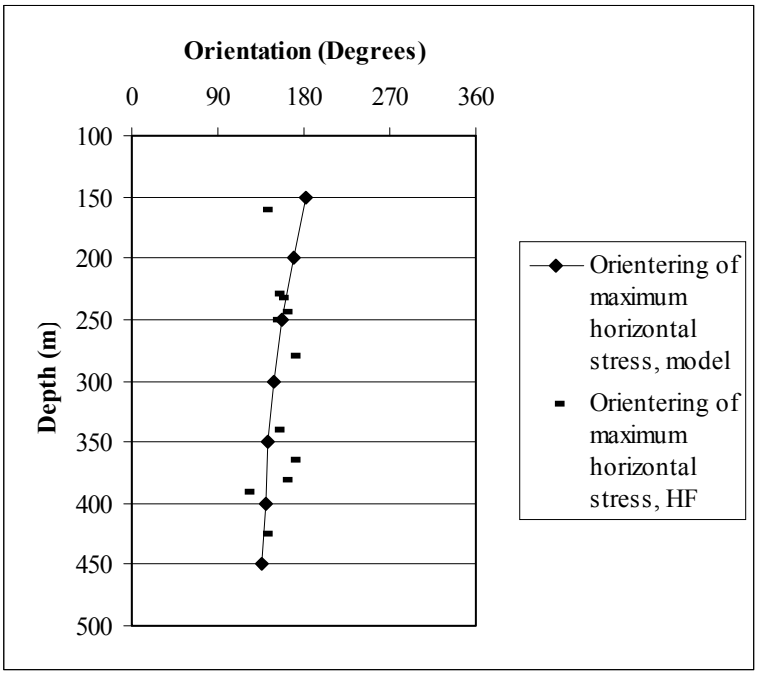

Figure 5-8. *Results from KAS02, 150-450 m depth using a seven-parameter model and second shut-in pressure.*

The standard deviations versus depth are presented in Table 5-7. The inversion result of the measurement points is presented in Table 5-8. The best solution of the six-parameter model was found after 51 iterations according to the following (at 300 m depth):

S_1 = 12.07 MPa	ε_{S1} = 3.1 MPa	I = 0.011
S_2 = 7.04 MPa	ε_{S1} = 0.3 MPa	I = 0.0001
α_1 = 0.0298 MPa/m	$\varepsilon_{\alpha 1}$ = 0.023 MPa/m	I = 0.846
α_2 = -0.0034 MPa/m	$\varepsilon_{\alpha 2}$ = 0.007 MPa/m	I = 0.078
λ = N149°E	ε_{λ} = 25°	I = 0.043
η = -24°	ε_{η} = 6°	I = 0.003

Table 5-7. Standard deviation versus depth using the second shut-in pressure between 150 and 450 m depth in KAS02.

Depth (m)	$\varepsilon^{\sigma H}$ (MPa)	$\varepsilon^{\sigma h}$ (MPa)	$\varepsilon^{\text{Orientation } \sigma H}$ (degrees)
150	5.2	1.9	41
250	4.1	0.3	10
350	2.5	0.4	4

Table 5-8. Results from hydraulic tests in KAS02 using the second shut-in pressure between 150 and 450 m depth.

Vertical depth	ϕ	ε_{ϕ}	ϕ_c	θ	ε_{θ}	θ_c	σ_n	$\varepsilon_{\sigma n}$	σ_{nc}
155.2	230	3	229.6	90	1	90.0	7.5	0.5	7.4
222.8	238	3	237.1	90	3	90.0	7.6	0.5	6.9
232.9	231	3	232.4	82	4	8179	6.2	0.5	7.1
243.1	251	1	251.0	90	4	90.0	6.8	0.5	6.8
250.2	234	6	232.5	90	2	90.0	7.4	0.5	7.1
279.9	257	1	256.9	90	2	90.0	6.4	0.7	7.3
339.4	236	1	236.0	90	2	90.0	7.0	0.6	7.1
346.0	263	1	263.1	90	2	90.0	9.0	0.6	8.6
363.7	267	3	266.9	90	2	90.0	9.1	0.8	9.2
380.7	250	2	250.1	90	2	90.0	7.9	0.5	7.9
389.8	209	2	208.9	84	3	84.0	8.1	0.5	8.1

Again, as indicated in Table 5-8, almost all fractures are vertical. However, the calculated values for the orientation of the fractures are satisfactory and the fracture normal stresses are reasonable compared with the measured.

The analysis of the middle section in KAS02, 490-550 m, included only 4 measurement points of which one had to be excluded. Again, the simple three-parameter model was used, which in this case mean no redundancy. The gradients α_1 and α_2 were chosen equal to the increase of the normal stress according to the measured data. The result using the 3-parameter model and the second shut-in pressure are presented in Figures 5-9 and 5-10 using a rock mass density of α_3 = 0.0265 MPa/m.

The standard deviations versus depth are presented in Table 5-9. The inversion result of the measurement points is presented in Table 5-10. The solution of the three-parameter model was found after 7 iterations according to (at 525 m depth)

S_1 = 27.9 MPa	ε_{S1} = 4.0 MPa	I = 0.018
S_2 = 19.5 MPa	ε_{S1} = 1.6 MPa	I = 0.003
λ = N158°E	ε_{λ} = 19°	I = 0.025

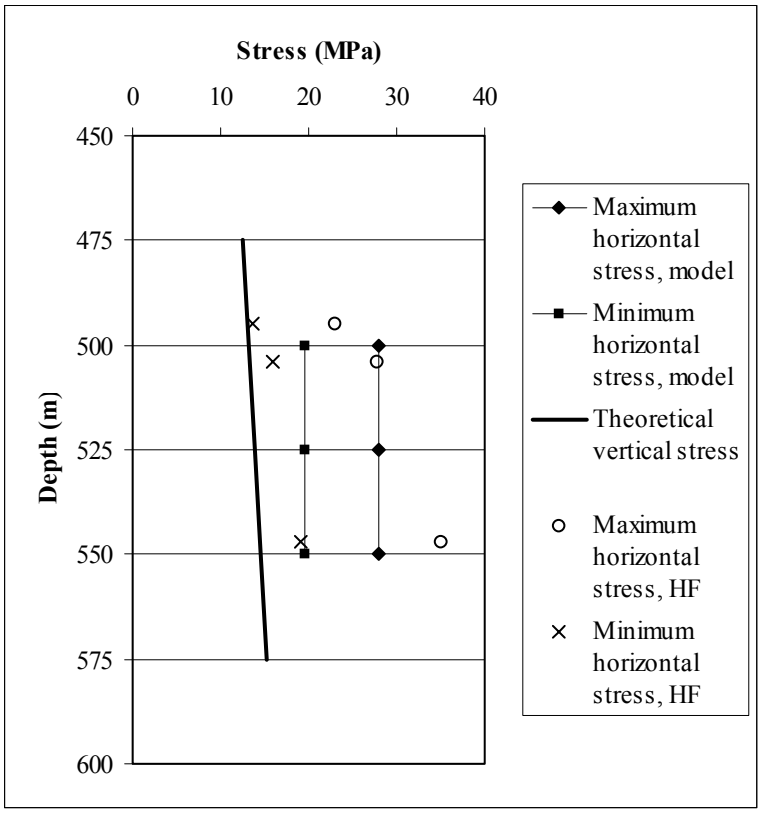

Figure 5-9. *Results from KAS02, 490-550 m depth using a three-parameter model and second shut-in pressure.*

Table 5-9. Standard deviation versus depth using the second shut-in pressure between 490 and 550 m depth in KAS02.

Depth (m)	$\varepsilon^{\sigma H}$ (MPa)	$\varepsilon^{\sigma h}$ (MPa)	$\varepsilon^{\text{Orientation } \sigma H}$ (degrees)
500	4.0	1.6	19
525	4.0	1.6	19
550	4.0	1.6	19

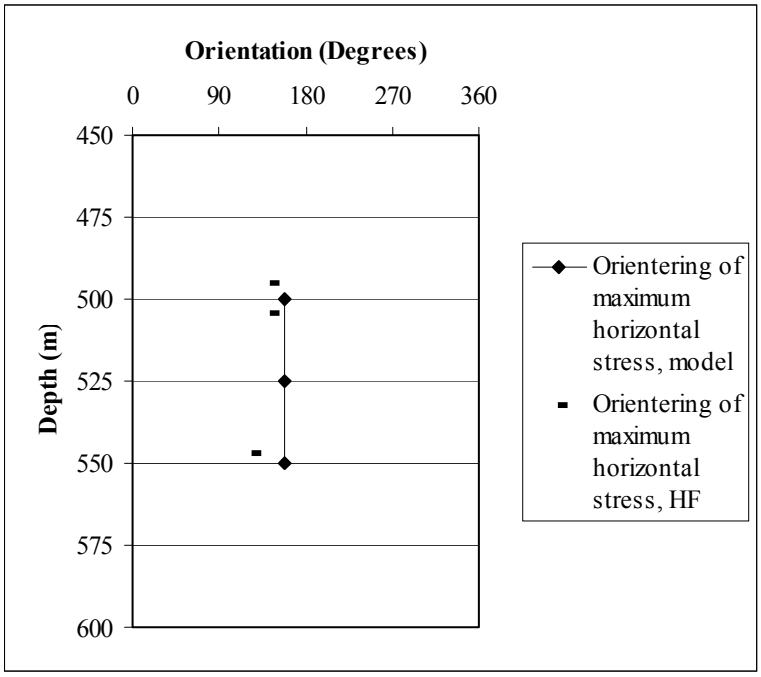

Figure 5-10. *Results from KAS02, 490-550 m depth using a three-parameter model and second shut-in pressure.*

Table 5-10. Results from hydraulic tests in KAS02 using the second shut-in pressure between 490 and 550 m depth.

Vertical depth	ϕ	ε_ϕ	ϕ_c	θ	ε_θ	θ_c	σ_n	$\varepsilon_{\sigma n}$	σ_{nc}
494.9	158	1	158.0	36	1	36.0	19.6	1.4	18.2
504.1	234	1	234.0	90	1	90.0	21.5	0.5	20.1
547.0	216	1	216.0	90	1	90.0	23.9	1.0	22.0

Table 5-10 indicates that most fractures are vertical. The calculated values for the orientation of the fractures are good but the fracture normal stresses fits poorly the measured.

The analysis of the lower section in KAS02, 620-740 m, included only 5 measurement points of which one had to be excluded, thus the three-parameter model (S_1, S_2, λ) was used. The result using the 3-parameter model and the second shut-in pressure are presented in Figures 5-11 and 5-12 using a rock mass density of $\alpha_3 = 0.0265$ MPa/m.

The standard deviations versus depth are presented in Table 5-11. The inversion result of the measurement points is presented in Table 5-12. The solution of the three-parameter model was found after 5 iterations according to (at 670 m depth)

$S_1 = 30.4$ MPa	$\varepsilon_{S1} = 2.2$ MPa	I = 0.005
$S_2 = 28.8$ MPa	$\varepsilon_{S1} = 1.2$ MPa	I = 0.002
λ = N144°E	$\varepsilon_\lambda = 65°$	I = 0.284

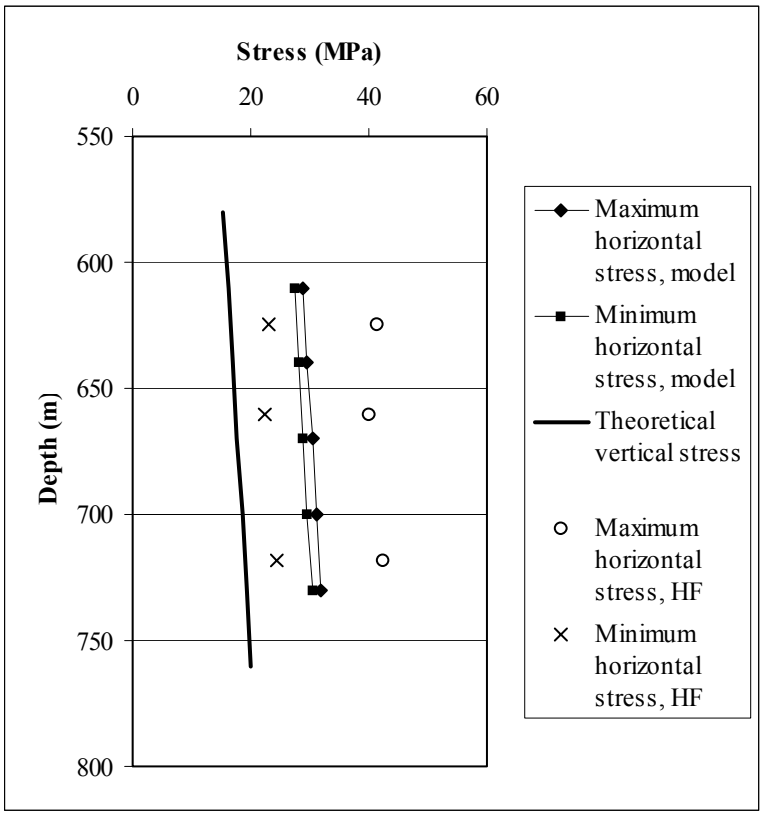

Figure 5-11. *Results from KAS02, 620-740 m depth using a three-parameter model and second shut-in pressure.*

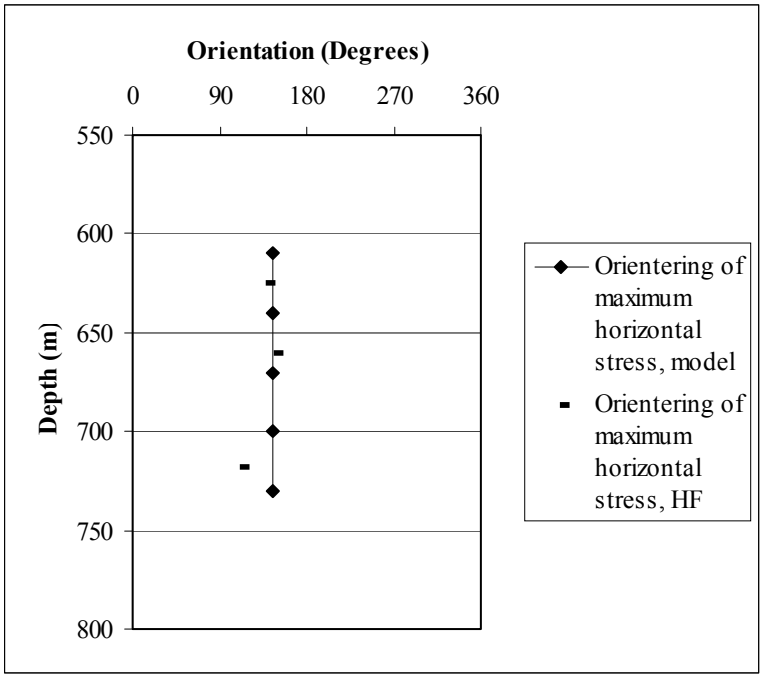

Figure 5-12. *Results from KAS02, 620-740 m depth using a three-parameter model and second shut-in pressure.*

Table 5-11. Standard deviation versus depth using the second shut-in pressure between 620 and 740 m depth in KAS02.

Depth (m)	$\varepsilon^{\sigma H}$ (MPa)	$\varepsilon^{\sigma h}$ (MPa)	$\varepsilon^{\text{Orientation } \sigma H}$ (degrees)
610	3.3	1.0	6
670	3.3	1.0	6
730	3.3	1.0	6

Table 5-12. Results from hydraulic tests in KAS02 using the second shut-in pressure between 620 and 740 m depth.

Vertical depth	ϕ	ε_ϕ	ϕ_c	θ	ε_θ	θ_c	σ_n	$\varepsilon_{\sigma n}$	σ_{nc}
624.8	227	2	227.0	90	1	90.0	28.8	1.5	27.7
660.7	240	1	240.0	90	1	90.0	27.5	2.0	28.6
718.5	200	1	200.2	90	2	90.0	30.2	1.2	30.5
734.0	160	2	160.0	56	3	56.3	28.2	1.0	28.0

The calculated values for the orientation of the fractures and their associated normal stress fits the measured values well.

5.3 RESULTS FROM BOREHOLE KAS03

Borehole KAS03 includes 21 successful stress measurements as reported by Bjarnason et al. (1989). Of these, 7 included two or three fractures in the test section, see Table A-2 in Appendix. The measurement points were divided into three groups of depth intervals 100-550 m, 650-750 m, and 820-900 m. The upper data set includes 12 fracture combinations (2^2*3^1), the middle set 4 (2^2), and the lower data set 6 fracture combinations (2^1*3^1). All fracture combinations were tested.

5.3.1 Analysis using first shut-in

The analysis of the upper section in KAS03, 100-550 m, included 11 measurement points. Only the fracture at 534.7 m depth had to be excluded. The results using first shut-in pressure are presented in Figures 5-13 and 5-14. The 6- and 7-parameter models gave very similar result and the density of the rock mass was determined α_3 = 0.0265 MPa/m. The standard deviation versus depth are presented in Table 5-13. The inversion result of the measurement points is presented in Table 5-14.

The resolution of the unknowns is reasonable except for the gradient of maximum horizontal stress. The best solution of the six-parameter model was found after 12 iterations according to (at 300 m depth):

S_1 = 15.80 MPa	ε_{S1} = 4.60 MPa	I = 0.024
S_2 = 10.02 MPa	ε_{S1} = 0.36 MPa	I = 0.000
α_1 = 0.0207 MPa/m	$\varepsilon_{\alpha 1}$ = 0.0228 MPa/m	I = 0.832
α_2 = 0.0126 MPa/m	$\varepsilon_{\alpha 2}$ = 0.0053 MPa/m	I = 0.045
λ = N143°E	ε_{λ} = 31°	I = 0.067
η = 31°	ε_{η} = 34°	I = 0.080

Table 5-13. Standard deviation versus depth using the first shut-in pressure between 100 and 550 m depth in KAS03.

Depth (m)	$\varepsilon^{\sigma H}$ (MPa)	$\varepsilon^{\sigma h}$ (MPa)	$\varepsilon^{\text{Orientation } \sigma H}$ (degrees)
100	6.6	1.5	25
200	4.4	1.2	52
300	2.7	1.1	66
400	5.3	1.9	112
500	7.1	3.0	144

Table 5-14. Results from hydraulic tests in KAS03 using the first shut-in pressure between 100 and 550 m depth.

Vertical depth	ϕ	ε_{ϕ}	ϕ_c	θ	ε_{θ}	θ_c	σ_n	$\varepsilon_{\sigma n}$	σ_{nc}
131.2	235	1	235.0	90	1	90.0	7.6	1.4	7.7
153.5	266	2	266.0	88	2	88.0	10.3	2.1	10.1
346.6	40	2	40.0	42	1	42.0	10.5	2.0	10.2
480.3	260	3	260.1	90	2	90.0	13.8	1.5	13.4
493.6	217	2	216.9	90	1	90.0	13.8	1.2	13.5
513.9	150	1	150.0	53	1	53.0	17.3	1.7	17.5
532.8	238	1	238.0	90	1	90.0	13.0	0.4	13.1
544.6	214	1	214.0	90	1	90.0	14.6	1.0	14.5
546.6	219	6	219.5	90	3	90.0	13.9	0.9	14.1
549.6	233	1	233.0	90	1	90.0	13.6	0.7	13.4

As indicated in Table 5-14, almost all fractures are vertical, implying difficulties to receive satisfactory resolution of unknowns and standard deviations of the calculated stresses. However, the calculated values for the orientation of the fractures and the fracture normal stresses are satisfactory compared with the measured.

When comparing the calculated magnitudes with the hydraulic fracturing data, both the minimum and maximum horizontal stress seems overestimated at small depth. However, this may be explained by the lack of measurements at shallow depth and that the large number of tests between 480 to 549 m depth restrain the solution. Attempts were made to exclude the shallow measurements, however, it did not improve the resolution of the unknowns nor change the state of stress in the specified depth interval.

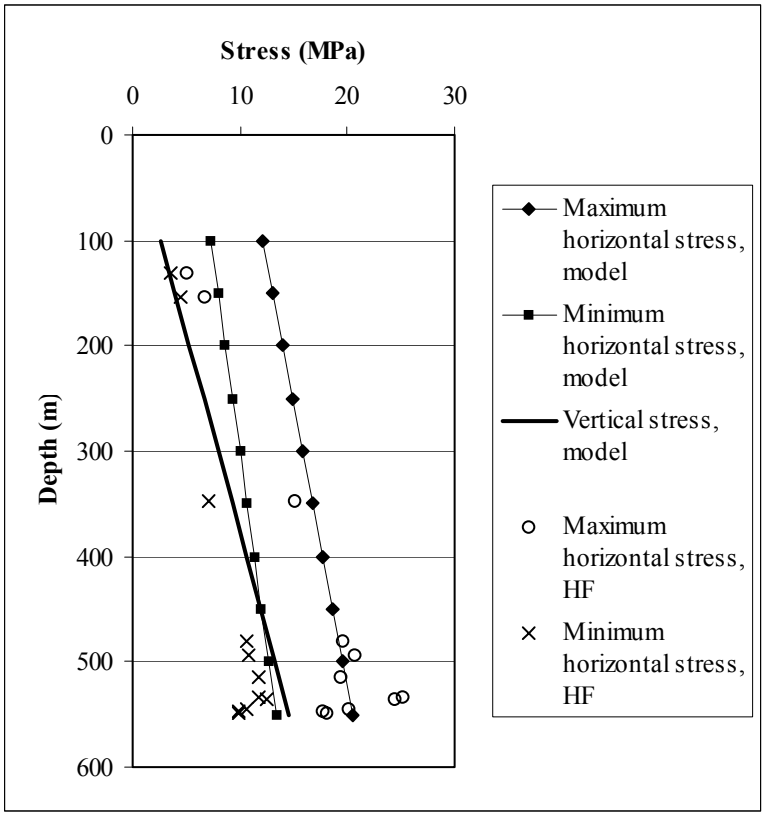

Figure 5-13. *Results from KAS03, 100-550 m depth using a seven-parameter model and first shut-in pressure.*

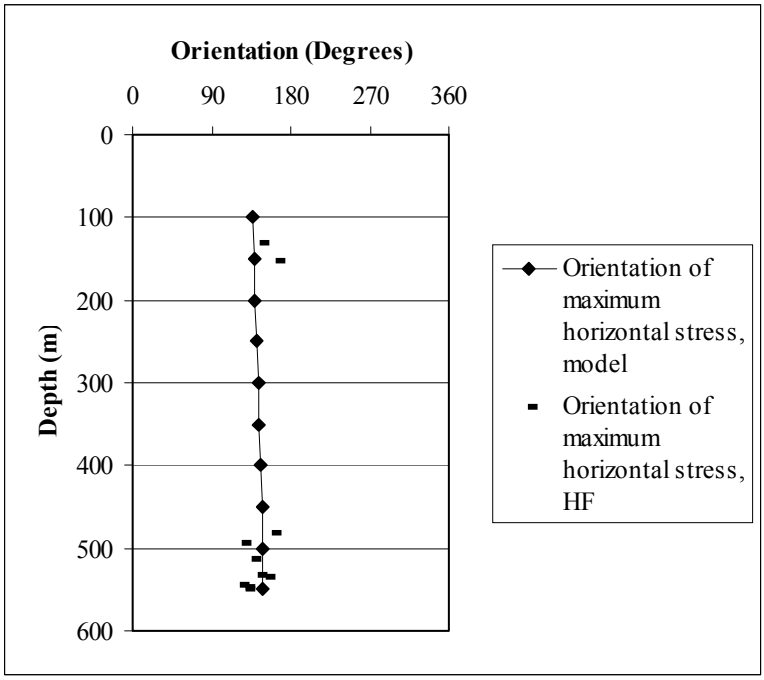

Figure 5-14. *Results from KAS03, 100-550 m depth using a seven-parameter model and first shut-in pressure.*

The analysis of the middle section in KAS03, depth interval 650-750 m, included 3 measurement points and a solution was not possible to achieve.

The lower section in KAS03, depth interval 820-900 m, included 6 measurement points. A three-parameter model was chosen for the analysis and the results using first shut-in pressure are presented in Figures 5-15 and 5-16. The gradients α_1 and α_2 were chosen equal to the increase of the normal stress according to the measured data and the density of the rock mass, α_3 = 0.0265 MPa/m. The standard deviation versus depth are presented in Table 5-15 and the inversion result in Table 5-16.

The best solution of the three-parameter model was found after 5 iterations according to (at 860 m depth)

S_1 = 38.9 MPa	ε_{S1} = 5.0 MPa	I = 0.028
S_2 = 28.9 MPa	ε_{S1} = 1.1 MPa	I = 0.001
λ = N130°E	ε_λ = 6°	I = 0.003

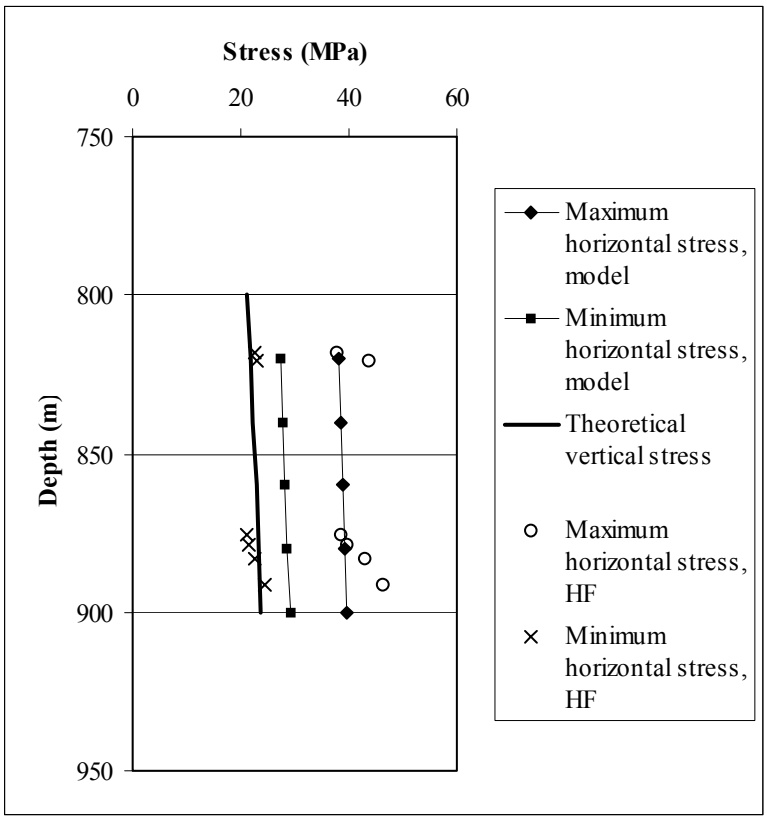

Figure 5-15. *Results from KAS03, 820-900 m depth using a three-parameter model and first shut-in pressure.*

Table 5-15. Standard deviation versus depth using the first shut-in pressure between 820 and 900 m depth in KAS03.

Depth (m)	$\varepsilon^{\sigma H}$ (MPa)	$\varepsilon^{\sigma h}$ (MPa)	$\varepsilon^{\text{Orientation } \sigma H}$ (degrees)
820	5.0	1.1	6
860	5.0	1.1	6
900	5.0	1.1	6

Table 5-16. Results from hydraulic tests in KAS03 using the first shut-in pressure between 820 and 900 m depth.

Vertical depth	ϕ	ε_ϕ	ϕ_c	θ	ε_θ	θ_c	σ_n	$\varepsilon_{\sigma n}$	σ_{nc}
818.0	190	2	190.0	85	3	85.0	30.0	1.5	30.0
820.4	253	2	252.8	74	2	73.9	29.2	1.6	30.0
875.4	230	2	229.9	75	2	74.9	27.4	1.8	28.6
878.4	216	4	216.0	90	3	90.0	29.0	1.9	28.7
883.3	212	6	211.8	90	2	90.0	29.2	1.5	28.9
891.2	251	2	251.3	90	5	75.1	32.2	1.7	31.3

The calculated values for the orientation of the fractures and their associated normal stress fits satisfactory the measured values.

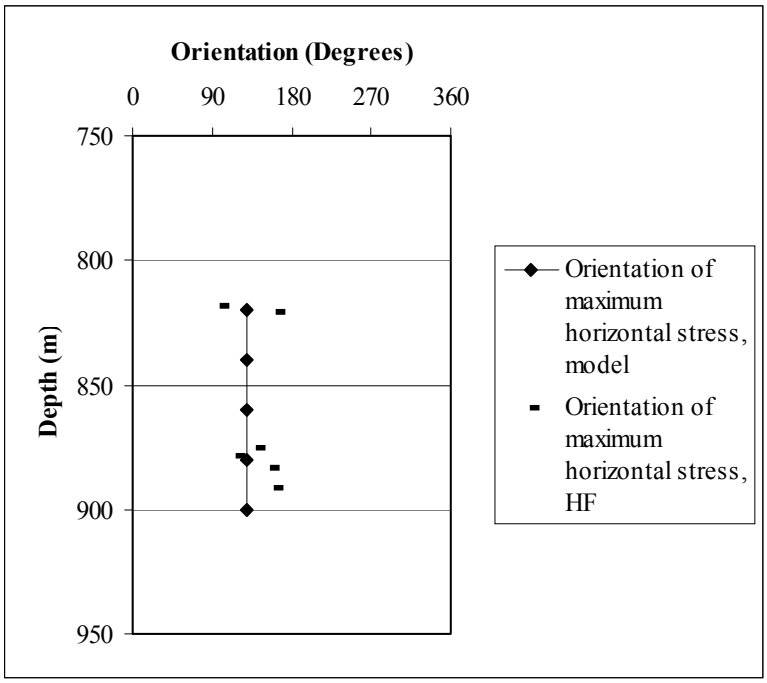

Figure 5-16. *Results from KAS03, 820-900 m depth using a three-parameter model and first shut-in pressure.*

5.3.2 Analysis using second shut-in

The analysis of the upper section in KAS03, 100-550 m, included 11 measurement points. The results using second shut-in pressure are presented in Figures 5-17 and 5-18. The 7-parameter model gave a very low rock mass density, α_3 = 0.0238 MPa/m, which is unrealistic for the rocks types at Äspö. Therefore, the 6-parameter model was used with a density of the rock mass α_3 = 0.0265 MPa/m. The standard deviation versus depth are presented in Table 5-17. The inversion result of the measurement points is presented in Table 5-18.

The resolution of the unknowns is reasonable except for the gradient of maximum horizontal stress. The best solution of the six-parameter model was found after 12 iterations according to (at 300 m depth)

S_1 = 11.42 MPa	ε_{S1} = 3.27 MPa	I = 0.011
S_2 = 8.27 MPa	ε_{S1} = 0.46 MPa	I = 0.0002
α_1 = 0.0216 MPa/m	$\varepsilon_{\alpha 1}$ = 0.0040 MPa/m	I = 0.026
α_2 = 0.0126 MPa/m	$\varepsilon_{\alpha 2}$ = 0.0135 MPa/m	I = 0.292
λ = N146°E	ε_{λ} = 18°	I = 0.023
η = 40°	ε_{η} = 66°	I = 0.303

Table 5-17. Standard deviation versus depth using the second shut-in pressure between 100 and 550 m depth in KAS03.

Depth (m)	$\varepsilon^{\sigma H}$ (MPa)	$\varepsilon^{\sigma h}$ (MPa)	$\varepsilon^{\text{Orientation } \sigma H}$ (degrees)
100	6.9	0.8	15
200	5.1	0.6	16
300	3.3	0.5	18
400	1.6	0.4	14
500	1.0	0.2	4

Table 5-18. Results from hydraulic tests in KAS03 using the second shut-in pressure between 100 and 550 m depth.

Vertical depth	ϕ	ε_ϕ	ϕ_c	θ	ε_θ	θ_c	σ_n	$\varepsilon_{\sigma n}$	σ_{nc}
131.2	235	1	235.0	90	1	90.0	5.3	0.8	5.3
153.5	266	2	266.0	88	2	88.0	6.0	0.6	5.9
346.6	29	2	29.0	15	1	15.0	8.1	1.1	9.2
480.3	260	3	259.1	90	2	90.0	12.1	0.5	12.5
493.6	188	2	188.0	81	2	81.0	12.5	0.4	12.5
513.9	150	1	150.0	53	1	53.0	14.4	1.1	14.4
532.8	238	1	238.0	90	1	90.0	12.5	0.1	12.5
543.7	244	1	24.2	90	1	90.0	13.4	0.4	12.8
544.6	214	1	214.0	90	1	90.0	12.5	0.4	12.3
546.6	219	6	219.5	90	3	90.0	11.7	0.6	12.3
549.6	233	1	233.0	90	1	90.0	12.3	0.4	12.6

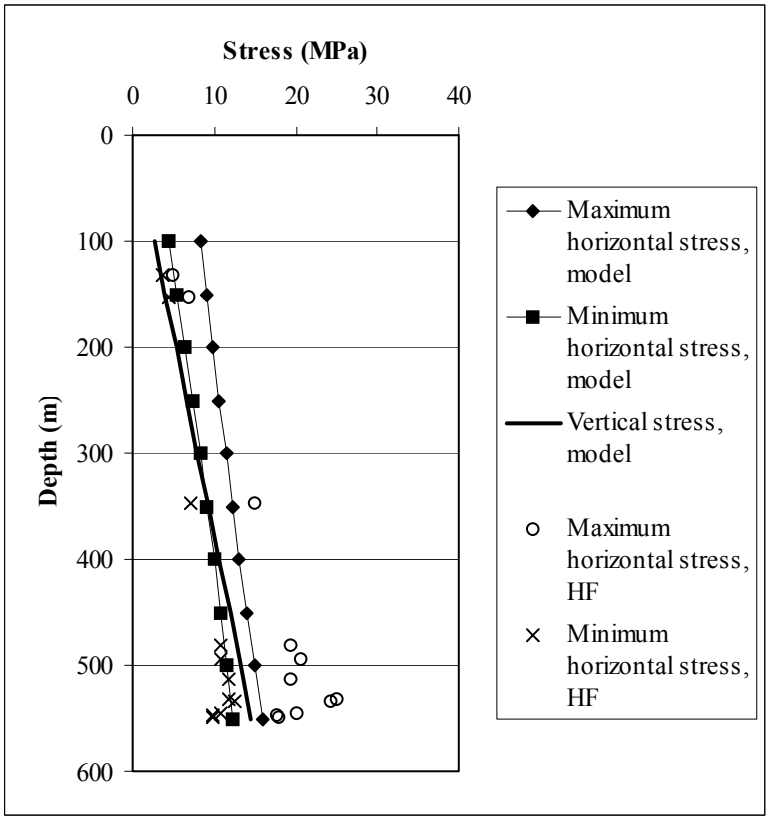

Figure 5-17. *Results from KAS03, 100-550 m depth using a seven-parameter model and second shut-in pressure.*

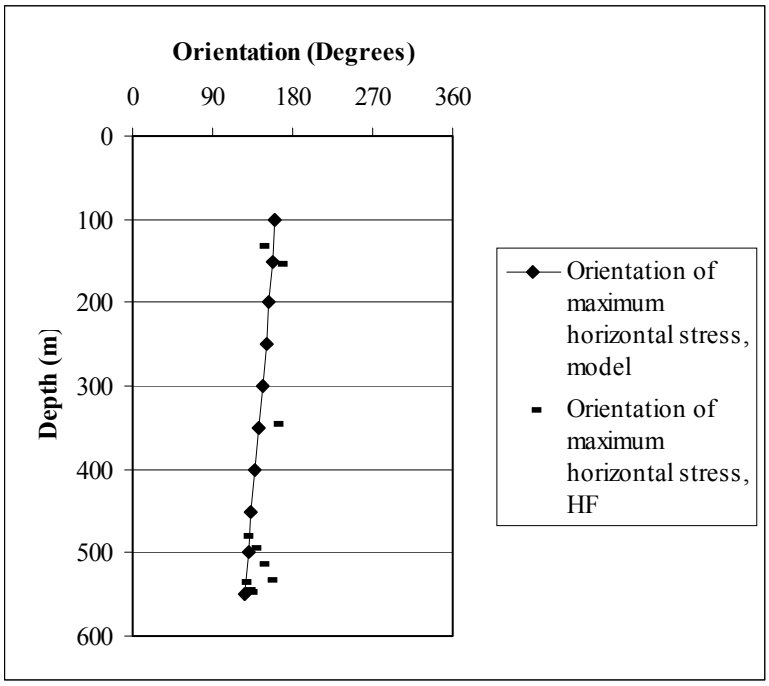

Figure 5-18. *Results from KAS03, 100-550 m depth using a seven-parameter model and second shut-in pressure.*

Table 5-18 shows that the calculated values for the orientation of the fractures and the fracture normal stresses are in good agreement with the measured. When comparing the calculated magnitudes with the hydraulic fracturing data, the maximum horizontal stress seem underestimated at larger depth.

The analysis using second shut-in pressure in borehole KAS03 failed for the middle section.

The lower section in KAS03, depth interval 820-900 m, included 6 measurement points of which one had to be excluded. A three-parameter model was chosen for the analysis and the results using second shut-in pressure are presented in Figures 5-19 and 5-20. The gradients α_1 and α_2 were chosen equal to the increase of the normal stress according to the measured data and the density of the rock mass, α_3 = 0.0265 MPa/m. The standard deviation versus depth are presented in Table 5-19 and the inversion result in Table 5-20.

The best solution of the three-parameter model was found after 5 iterations according to (at 860 m depth)

S_1 = 42.7 MPa	ε_{S1} = 6.8 MPa	I = 0.051
S_2 = 23.6 MPa	ε_{S1} = 0.7 MPa	I = 0.0005
λ = N136°E	ε_{λ} = 3°	I = 0.0006

Table 5-19. Standard deviation versus depth using the second shut-in pressure between 820 and 900 m depth in KAS03.

Depth (m)	$\varepsilon^{\sigma H}$ (MPa)	$\varepsilon^{\sigma h}$ (MPa)	$\varepsilon^{\text{Orientation } \sigma H}$ (degrees)
820	6.9	1.1	3
860	6.8	0.7	3
900	6.9	0.7	3

Table 5-20. Results from hydraulic tests in KAS03 using the second shut-in pressure between 820 and 900 m depth.

Vertical depth	ϕ	ε_ϕ	ϕ_c	θ	ε_θ	θ_c	σ_n	$\varepsilon_{\sigma n}$	σ_{nc}
820.4	253	2	252.9	74	2	74.0	26.4	0.5	26.4
875.4	230	2	23.0	75	2	75.0	23.8	0.7	23.8
878.4	216	4	216.2	90	3	90.0	24.5	0.5	24.5
883.3	212	6	210.2	90	2	90.0	25.5	0.2	25.5
891.2	251	2	251.3	90	5	75.0	27.4	0.5	27.4

The calculated values for the orientation of the fractures and their associated normal stress fits satisfactory the measured values.

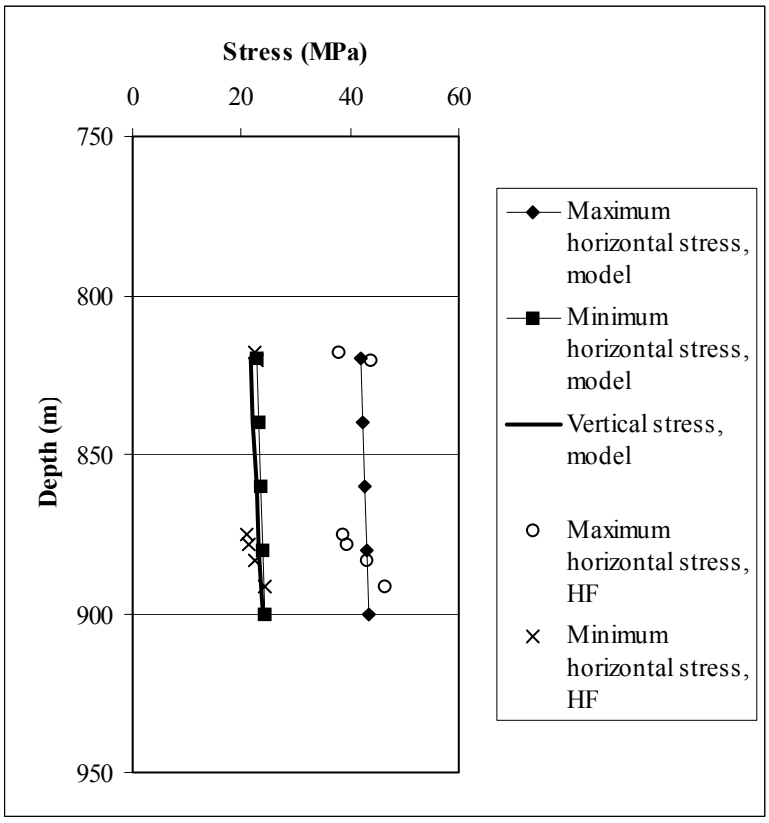

Figure 5-19. *Results from KAS03, 650-1000 m depth using a three-parameter model and second shut-in pressure.*

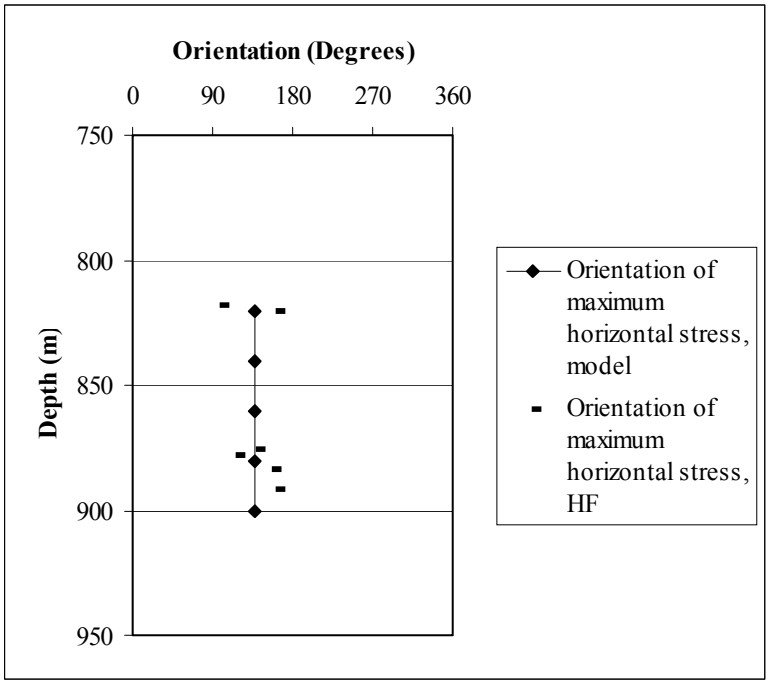

Figure 5-20. *Results from KAS03, 820-900 m depth using a three-parameter model and second shut-in pressure.*

5.4. RESULTS FROM BOREHOLE KLX02

Borehole KLX02 includes 42 successful stress measurements. In the deeper measurements, below 700 m depth, the fracture orientations were determined using the BIPS-camera. The analysis of BIPS-pictures proved to be very difficult and the determination of fracture orientations are consequently associated with great uncertainties. The state of stress in the deeper section of KLX02 will therefore be discussed only tentatively.

5.4.1 Analysis using first shut-in

The analysis of the upper section in borehole KLX02, 200-400 m, included 12 measurement points of which two had to be excluded. The results using first shut-in pressure are presented in Figures 5-21 to 5-22. The 7-parameter model gave very similar result and the density of the rock mass was determined to α_3 = 0.0262 MPa/m. The standard deviation versus depth are presented in Table 5-21. The inversion result of the measurement points is presented in Table 5-22.

The resolution of the unknowns is good. The best solution of the six-parameter model was found after 19 iterations according to (at 300 m depth)

S_1 = 12.29 MPa	ε_{S1} = 1.64 MPa	I = 0.003
S_2 = 6.82 MPa	ε_{S1} = 0.30 MPa	I = 0.000
α_1 = 0.0155 MPa/m	$\varepsilon_{\alpha 1}$ = 0.0147 MPa/m	I = 0.346
α_2 = 0.0207 MPa/m	$\varepsilon_{\alpha 2}$ = 0.0079 MPa/m	I = 0.100
λ = N136°E	ε_{λ} = 4°	I = 0.001
η = 14°	ε_{η} = 74°	I = 0.380

As can be seen in Table 5-22 all calculated values for orientation and fracture normal stress agree well with the measured value. Unfortunately, a comparison of the inversion result with the HF measurements is difficult due to unrepresentative HF result in this section.

Table 5-21. Standard deviation versus depth using the first shut-in pressure between 200 and 400 m depth in KLX02.

Depth (m)	$\varepsilon^{\sigma H}$ (MPa)	$\varepsilon^{\sigma h}$ (MPa)	$\varepsilon^{\text{Orientation } \sigma H}$ (degrees)
200	1.3	0.9	6
300	1.6	0.3	5
400	2.7	0.7	12

Table 5-22. Results from hydraulic tests in KLX02 using the first shut-in pressure between 200 and 400 m depth.

Vertical depth	ϕ	ε_ϕ	ϕ_c	θ	ε_θ	θ_c	σ_n	$\varepsilon_{\sigma n}$	σ_{nc}
206.4	267	1	267.0	90	1	90.0	8.6	0.8	8.5
265.4	259	2	259.0	66	2	66.0	7.6	0.3	7.6
266.0	230	5	229.9	65	3	65.0	6.3	0.4	6.3
272.5	356	2	356.0	44	2	44.0	7.9	1.5	8.3
288.2	210	3	210.0	8	1	8.0	7.5	0.9	7.6
305.8	91	1	91.0	62	1	62.0	8.9	1.5	9.2
314.5	31	1	31.0	61	2	61.0	7.8	0.5	7.7
315.2	26	1	26.0	60	1	60.0	7.8	0.5	7.9
337.2	234	3	234.0	50	1	50.0	8.2	0.2	8.2
346.7	198	2	198.0	56	1	56.0	9.1	2.7	9.0

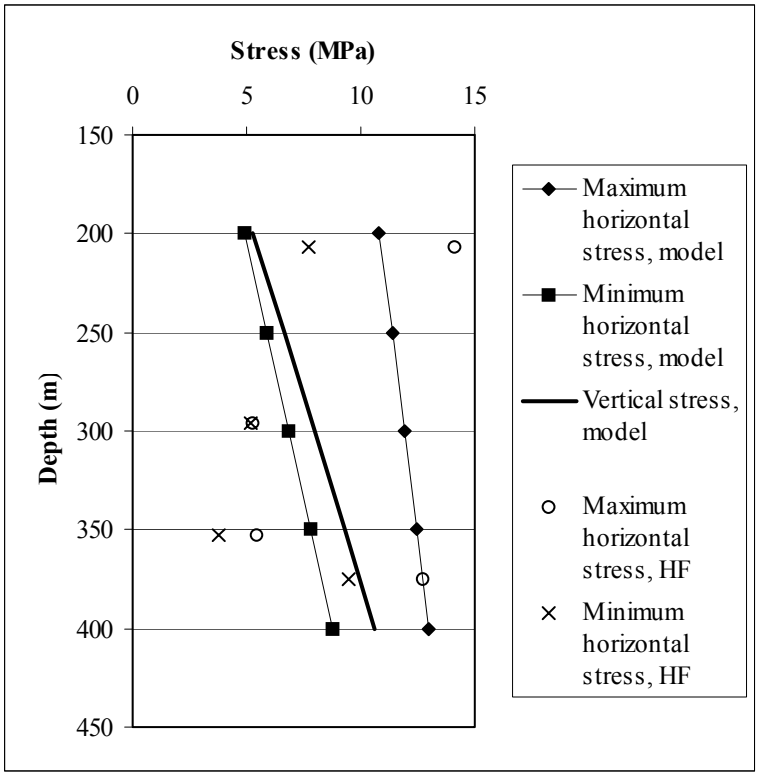

Figure 5-21. *Results from KLX02, 200-400 m depth using a seven-parameter model and first shut-in pressure.*

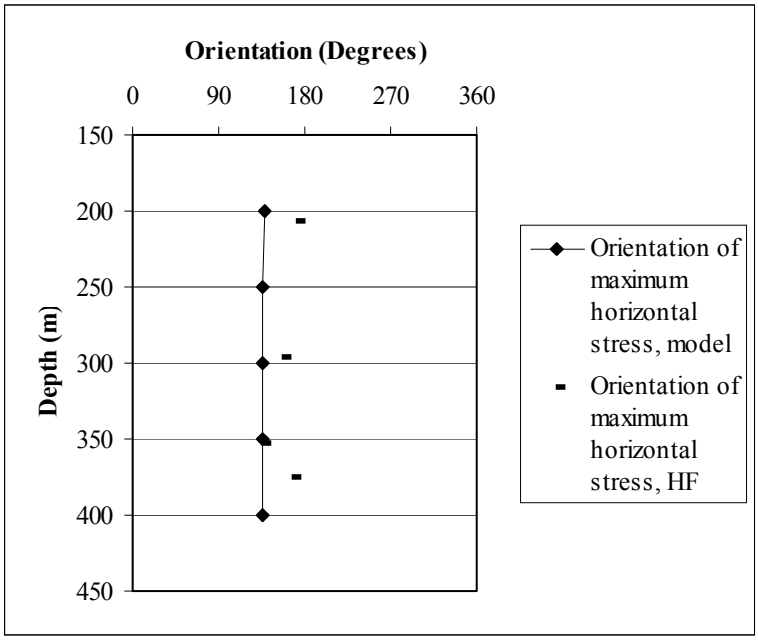

Figure 5-22. *Results from KLX02, 200-400 m depth using a seven-parameter model and first shut-in pressure.*

One inversion was also performed at 500-600 m depth, which involve 5 measurement points. The results using first shut-in pressure are presented in Figures 5-23 to 5-24. The 3-parameter model was used with a density of the rock mass equal to α_3 = 0.0265 MPa/m. The standard deviation versus depth are presented in Table 5-23 and the inversion result of the measurement points is presented in Table 5-24.

The best solution of the three-parameter model was found after 7 iterations according to (at 550 m depth):

S_1 = 18.16 MPa	ε_{S1} = 2.8 MPa	I = 0.009
S_2 = 15.04 MPa	ε_{S1} = 0.7 MPa	I = 0.001
λ = N154°W	ε_{λ} = 37°	I = 0.095

Table 5-23. Standard deviation versus depth using the first shut-in pressure between 500 and 600 m depth in KLX02.

Depth (m)	$\varepsilon^{\sigma H}$ (MPa)	$\varepsilon^{\sigma h}$ (MPa)	$\varepsilon^{\text{Orientation } \sigma H}$ (degrees)
500	2.9	0.8	37
550	2.9	0.8	37
600	2.9	0.8	37

Table 5-24 shows that the calculated values for orientation agree well and the calculated fracture normal stress agree satisfactory with the measured value.

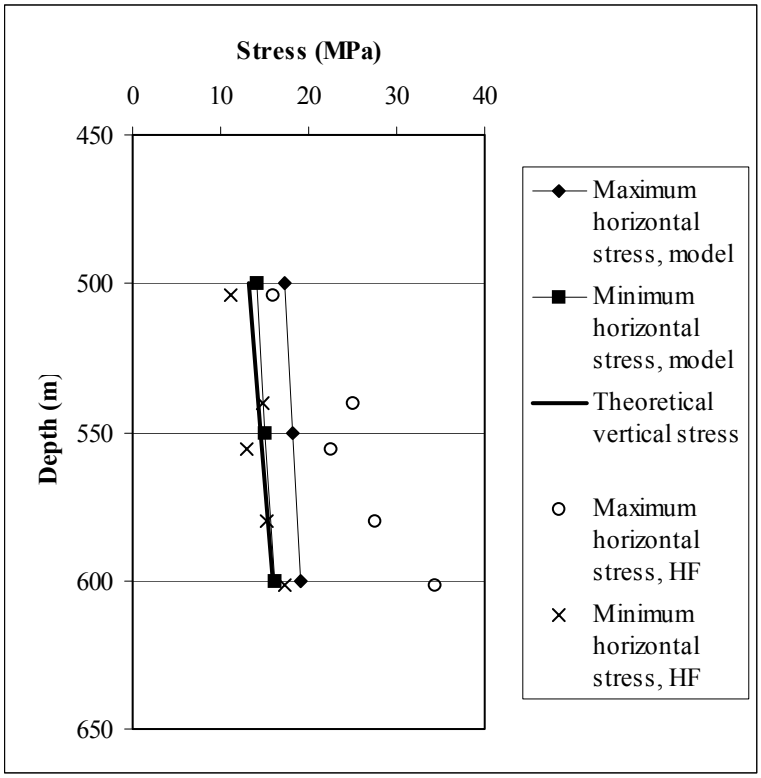

Figure 5-23. *Results from KLX02, 500-600 m depth using a three-parameter model and first shut-in pressure.*

Table 5-24. Results from hydraulic tests in KLX02 using the first shut-in pressure between 500 and 600 m depth.

Vertical depth	ϕ	ε_ϕ	ϕ_c	θ	ε_θ	θ_c	σ_n	$\varepsilon_{\sigma n}$	σ_{nc}
504.4	230	2	230.0	90	1	90.0	18.0	2.0	17.2
540.5	239	1	239.0	90	2	90.0	17.5	1.4	18.0
555.7	120	1	120.0	90	1	90.0	15.8	1.2	16.0
579.5	256	1	256.0	90	1	90.0	18.7	0.9	18.6
601.2	119	1	119.0	90	1	90.0	17.1	0.9	17.0

For the deeper measurement points, the fracture orientations were determined using BIPS-pictures. Due to mentioned uncertainties in this determination technique, inversion results will not be presented and the state of stress below 700 m depth will only be discussed, see Chap. 6.

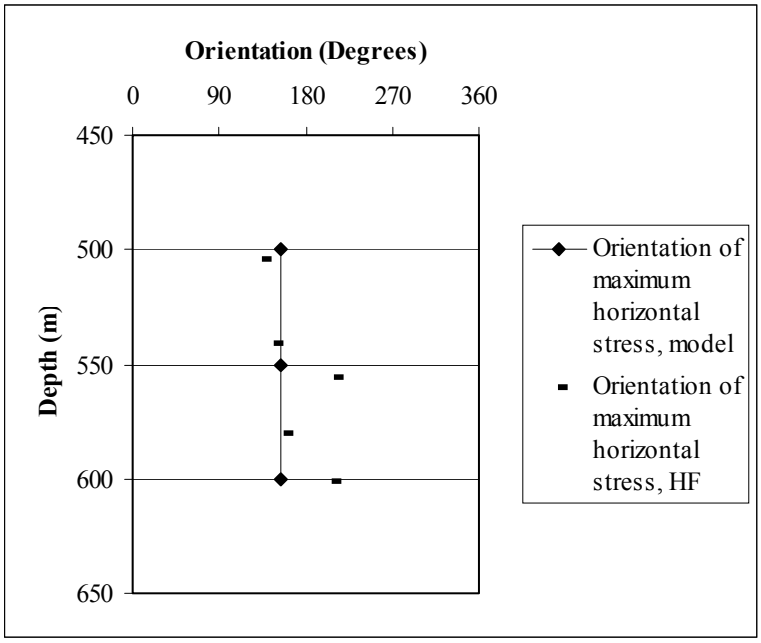

Figure 5-24. *Results from KLX02, 500-600 m depth using a three-parameter model and first shut-in pressure.*

5.4.2 Analysis using second shut-in

Attempts to determine the stress field using the second shut-in pressure in borehole KLX02 failed.

6 GENERAL GEOLOGY OF THE ÄSPÖ REGION AND IT'S INFLUENCE ON THE STRESS FIELD

6.1 GENERAL

The Äspö region is characterized by a slightly undulated topography of well-exposed rocks. The bedrock consists predominately of granitoides, i.e. granites and diorites, belonging to the vast Trans-Scandinavian Igneous Belt (Patchett et al., 1987). According to the established rock classification system at Äspö HRL, the rocks in the drill cores are divided into four main rock types: Småland (Ävrö) granite, Äspö diorite (a more mafic variety of Småland granite), greenestone, and aplite (fine-grained granite) (e.g. Wikberg et al., 1991; Kornfält and Wikman, 1994; Stanfors, 1995).

The hydraulic stress measurements performed in KAS02 and KAS03 on the island of Äspö and in KLX02 at Laxemar, on the mainland immediately west of the island of Äspö, are all significantly influenced by existing discontinuities (Bjarnason et al., 1989; Leijon, 1995; Ljunggren and Klasson, 1997; Ekman, 1997; Ekman et al., 1997), see Fig. 1-2 to 1-7. The discontinuities can redistribute the stress field, which results in non-linear and discontinuous magnitudes and scattered orientations of stresses versus depth. The stress field along all three boreholes can from top to bottom be described by an upper section of moderate increase in stress magnitudes versus depth, followed by a section with no or minor increase in stress magnitude. In the very deep borehole KLX02, the stress gradient is changed a second time, and this section is characterized by a small stress increase versus depth succeeded by another section of pronounced stress increase. Using the minimum horizontal stress from hydraulic fracturing measurements (Bjarnason et al., 1989; Ljunggren and Klasson, 1997; Ekman, 1997; Ekman et al., 1997) the discontinuities are indicated at slightly different depths in the three studied boreholes: a) KAS02 below 600 m depth, b) KAS03 between 575 and 750 m depth, and c) KLX02 between 700 and 1100 m depth (Figs. 6-1, 6-2 and 6-15).

In order to find possible explanations for the complex stress distribution, potential geological structures influencing the stress field were studied. The study is based on existing structural geological maps, fracture frequency plots, core and borehole geophysical logs, hydraulic interference tests, seismic data and radar measurements. Rock types, such as aplites (fine-grained granites), greenstones, and hybrids of these two, are known to often host a larger amount of small to intermediate fracture swarms than the other prevailing rock types in this area (e.g. Wikberg et al., 1991; Munier, 1995). Thus, these features were primarily chosen for a more thorough investigation.

The study is divided into three subsections: Ch. 6.2, discussing one (or several) potential sub-horizontal structure(s) below the island of Äspö; Ch. 6.3, one sub-vertical structure (the shear zone EW-1 crossing the island of Äspö); and Ch. 6.4, structures intersecting borehole KLX02 at Laxemar.

6.2 INFLUENCE OF ONE (OR SEVERAL) POTENTIAL SUB-HORIZONTAL ZONE(S) BELOW THE ISLAND OF ÄSPÖ ON THE STATE OF STRESS

6.2.1 Brief lithological description of the surface drilled boreholes KAS02-03, KAS06-08 and KAS16, Äspö island

KAS02

In KAS02 the bedrock is dominated by Småland granite down to 300 meters below ground level (mbgl). Below this depth, a medium-grained, weakly foliated diorite dominates (300-650, 710-750 and 720-860 mbgl). Substantial layers of aplites are found at 355-375, 650-710 and 860-905 mbgl (Fig. 6-1). Between 650 m and 680 m the aplite is strongly foliated. Two mylonitic zones have also been identified between 455-485 and 550-570 mbgl, both associated with a 1-2 m wide crush zone (Wikman et al., 1988; Stanfors, 1988; Nisca, 1988; Smellie and Laaksoharju, 1992). A major fracture zone is indicated from 802 m depth to the bottom of the borehole (920 m). The latter has by Smellie and Laaksoharju (1992) been interpreted as the intersection of the borehole with fracture zone NE-1 (6-7).

KAS03

In KAS03, the bedrock is more complex with a mixture of medium-grained granites, diorites and other granitoid variants (Fig. 6-2). However, a considerable section of aplites is located at 630-780 m depth. Mylonitic zones were identified at 390-420 m depth, with two 2 m wide mylonites at 397 m and 403 m depth. Another minor zone, approximately 1 m wide, is located at 456 m depth (Wikman et al., 1988; Stanfors, 1988; Sehlstedt and Triumf, 1988).

KAS06

The bedrock in KAS06 is dominated by Småland granite and smaller sections with aplites and greenstones (Fig. 6-3). A major section of greenstones is found at approx. 230-280 mbgl. Aplites occur from thin inclusions to substantial layers. Interestingly, the aplites seem to appear in sets; 100 mbgl, (200 mbgl,) 280 mbgl, 365 mbgl, and 460-535 mbgl. Increased fracturing occurs at 50-80 mbgl, 360 mbgl, 440-480 mbgl and 500-510 mbgl. From 440 to 505 mbgl the rock is tectonized and oxidized (Sehlstedt and Stråhle, 1989).

KAS07

Also the bedrock in KAS07 is dominated by Småland granite (Fig. 6-4). Major greenstone horizons appear at 15-25 mbgl, 190-215 mbgl, 375-385 mbgl, and 530-570 mbgl. Aplites are found as thin inclusions over the entire depth range with a larger section at 245-265 mbgl. Increased fracturing occurs at 0-20 mbgl, 50-60 mbgl, 100-120 mbgl, 240-265 mbgl, 380-450 mbgl, 530-570 mbgl, and 580-600 mbgl. From 400 to 600 mbgl the rock is tectonized and oxidized (Sehlstedt and Stråhle, 1989).

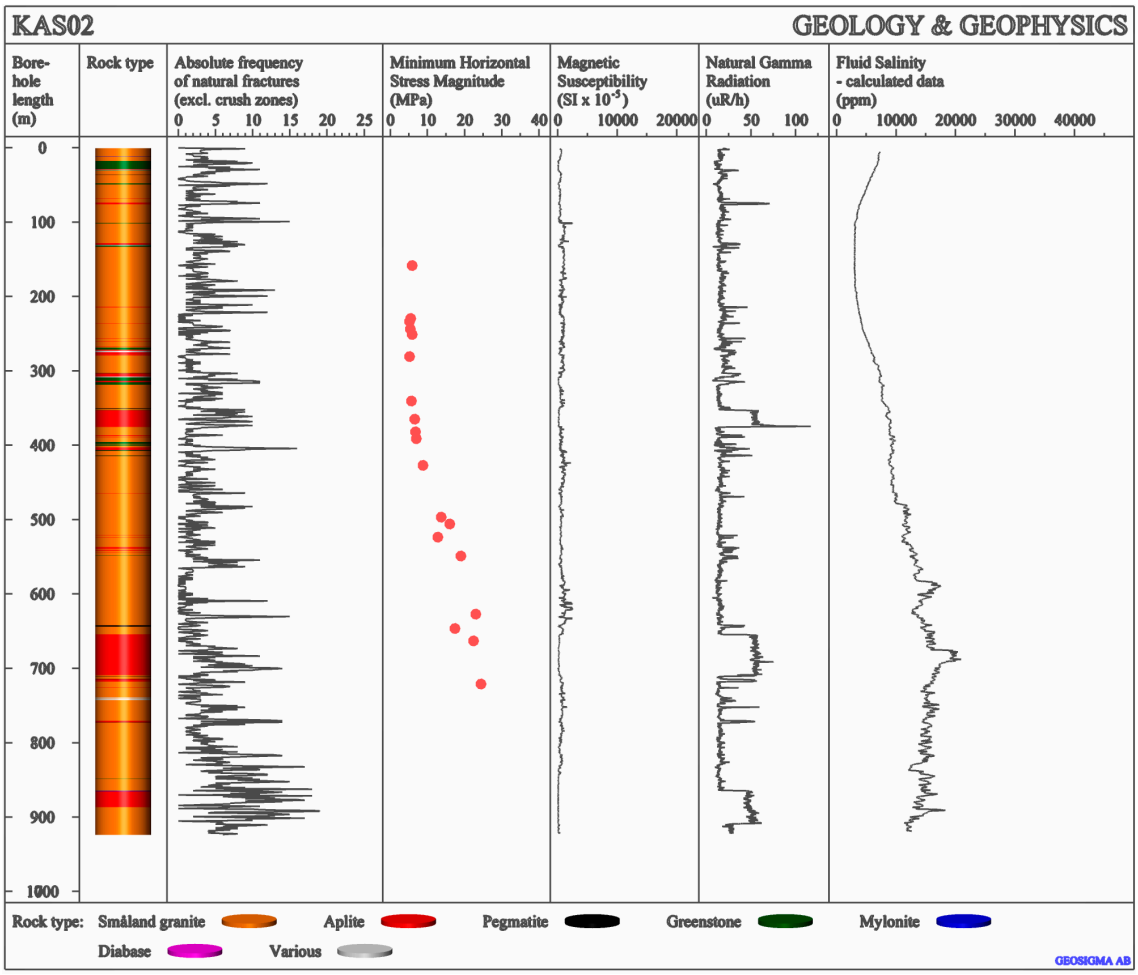

Figure 6-1. *The lithological and geophysical characteristics of borehole KAS02.*

KAS08

Like in KAS06 and KAS07, the bedrock in KAS08 is dominated by Småland granite (Fig. 6-5). A major mylonite section is found at 40-60 mbgl and a thin mylonite section at 545-550 mbgl. Greenstones sections appear at 90-130 mbgl, 230-235 mbgl, 380-390 mbgl, and 470-500 mbgl. Aplites occur as thin inclusions over the entire depth range with a larger section at 540-580 mbgl. Increased fracturing is found at 40-70 mbgl, 280-300 mbgl, 460-470 mbgl, and 540-600 mbgl. The rock is tectonized at 0-80 mbgl and 540-600 mbgl (Sehlstedt and Stråhle, 1989).

KAS16

Also in KAS16 the bedrock is dominated by Småland granite. Thin sections of greenstone appear along the entire depth range of the borehole. Aplite sections seem to occur in cycles: 0 mbgl, 60 mbgl, 180 mbgl, 320 mbgl, and 430 mbgl. The two latter are 45 respectively 58 m long in the direction of the borehole axis. The deeper aplite section 395-450 has been interpreted as a major fracture zone (Stanfors et al., 1997).

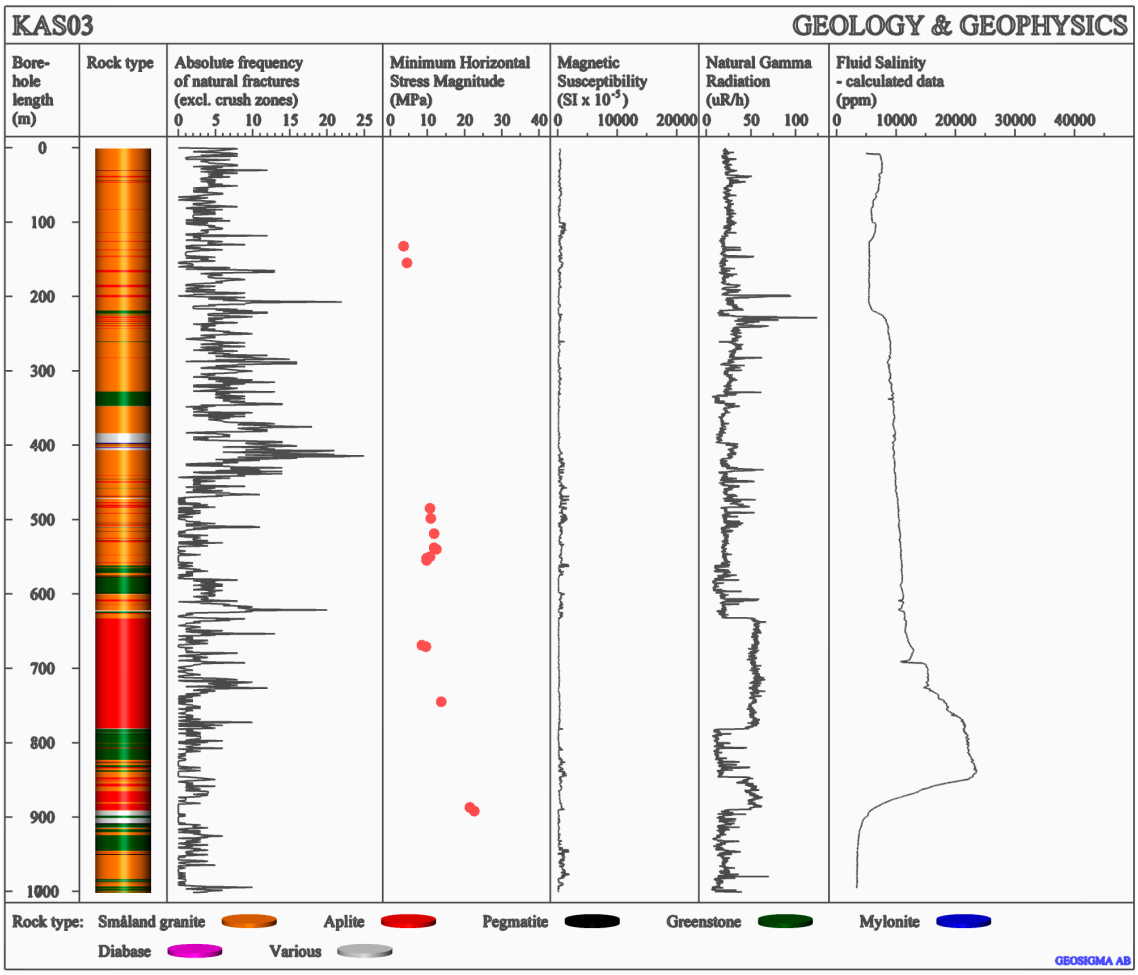

Figure 6-2. *The lithological and geophysical characteristics of borehole KAS03.*

6.2.2 Mapping of fractures and fracture zones

Prior to the excavation of the Äspö HRL, Talbot and Munier (1989) interpreted three gently dipping fracture zones (GDFs) striking N70°-80°E across Äspö and, possible, a fourth which strikes N120°E. Their strikes parallel the grain structures imposed by lithologies and foliations, but their dips are gentle, approx. 10-40° towards NNW and NNE. Talbot and Munier (1989) calculated, assuming a mean dip of 24°, a vertical thickness of 28-56 m and a center-line spacing of 90-133 m (Fig. 6-6). Note that this interpretation have been abandoned after the excavation.

The suggested occurrence of GDFs (Talbot and Munier, 1989) was later strengthened by Liedholm (1991a, 1991b), who found that the logarithmic hydraulic conductivity versus depth, based on 3 m packer tests from KAS02-08, appeared in cycles with a wave-length of 120-140 m. This seems to fit well with the wave-length of aplite sections, especially for KAS06 and KAS16.

The aplites in boreholes KAS06-08 are roughly located at 400-500 m depth and striking NE. If the GDFs dipping towards NNW suggested by Talbot and Munier (1989) are correctly assumed, the zone should be found at a similar depth in KAS16. Aplites

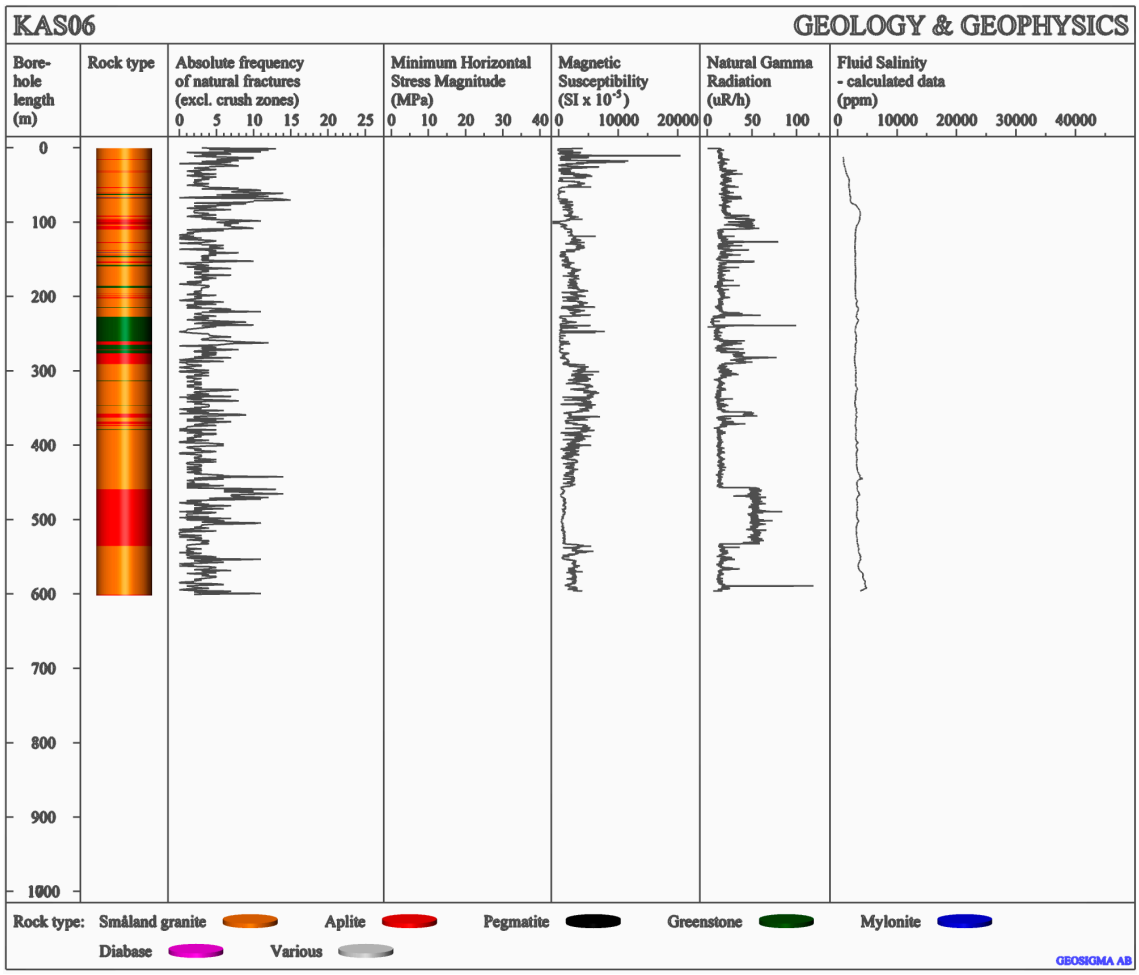

Figure 6-3. *The lithological and geophysical characteristics of borehole KAS06.*

appear according to the core log (Stanfors et al., 1997) at 280-330 m and 380-450 m depth. Thus, the latter seems to fit to the potential sub-horizontal zone.

The lower section of aplite in KAS16 has also been interpreted as the intersection with fracture zone NE-1 (Stanfors et al., 1997), Fig. 6-7. The hydraulic conductor at 500-600 mbgl in boreholes KAS07 and KAS08 has later been interpreted as due to the sub-vertical zone NE-1 (Rhén et al., 1997a). Possibly, the NE-1 zone also influences the borehole KAS02 below 700 m depth (Smellie and Laaksoharju, 1992).

The thorough geological sampling performed during the excavations of the HRL revealed that fracture zones in the Äspö area are more or less steeply dipping although with a wide variety of orientation and extent in space (Hermansson, 1995). Few gently dipping fracture zones (GDFs) are present in the rock mass. The predicted occurrence of GDFs at a 90-133 m spacing, according to Talbot and Munier (1989), were not found during excavation.

Hermansson (1995) suggested that the sub-horizontal fractures found in the HRL appear as fracture swarms rather than fracture zones, i.e. with substantially lower fracture intensity. Hermansson (1995) found four fracture swarms, which he combined into two groups and treated them as two larger swarms. Interestingly, these fracture swarms have

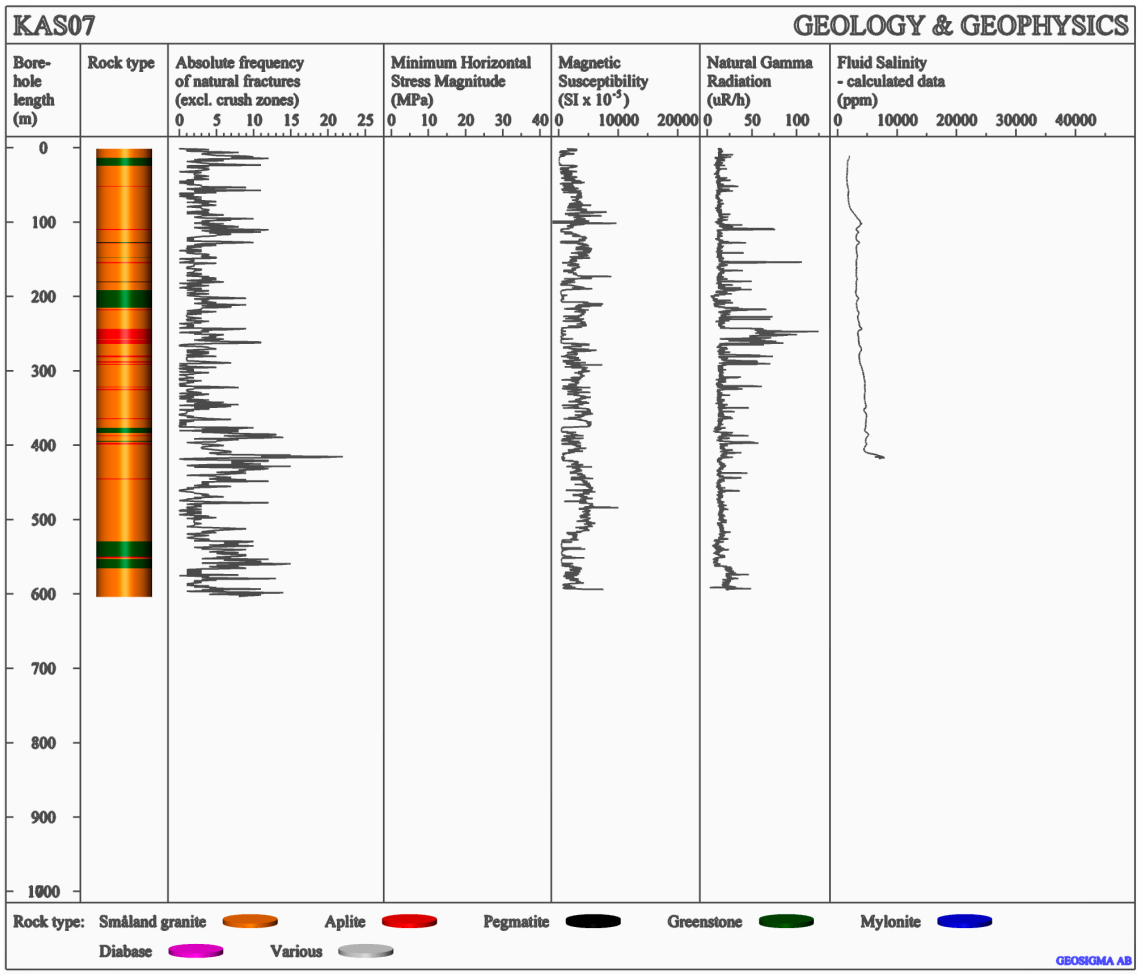

Figure 6-4. *The lithological and geophysical characteristics of borehole KAS07.*

a spacing of just less than 100 m, i.e. close to the predicted spacing by Talbot and Munier (1989). However, all observed fracture swarms dip SW to S (apart from one dipping NE) in opposition to Talbot's and Munier (1989) NNW dipping GDFs. Hermansson (1995) further concluded that the sub-horizontal fracture swarms or zones are not water bearing, except in rare cases when they crosscut steep structures. Tirén et al. (1996) suggested that these fracture zones/swarms, dipping SW-S and NNW, respectively, are two different fracture sets. The former is younger and characterized by a brittle failure mode and is often coated with chlorite and iron-oxyhydroxides. The latter are ductile shears (thrusts) and have a pronounced gneissosity with intercalated mylonitic bands, often containing epidote. The parallelism between these thrust planes and some sets of aplites is notable (Tirén et al., 1996).

Tirén et al. (1996) made an independent geological/structural interpretation of the Äspö area as a part of the study conducted by the Swedish Nuclear Power Inspectorate (SKI). They found relatively large bodies of aplites in the central part of the island. In the rest of Äspö the aplites most commonly appear as relatively thin dikes. The orientation of the dikes in the central part of the island (within the EW-1 zone) is mostly NE-SW with a steep dip. In the northwestern part, vertical dikes striking ENE-WSW dominate with subordinate vertical dikes striking N-S and NE-SW. In the southeastern part the situation is more complex. Vertical dikes strike N-S, NNE-SSW, ENE-WSW and NW-

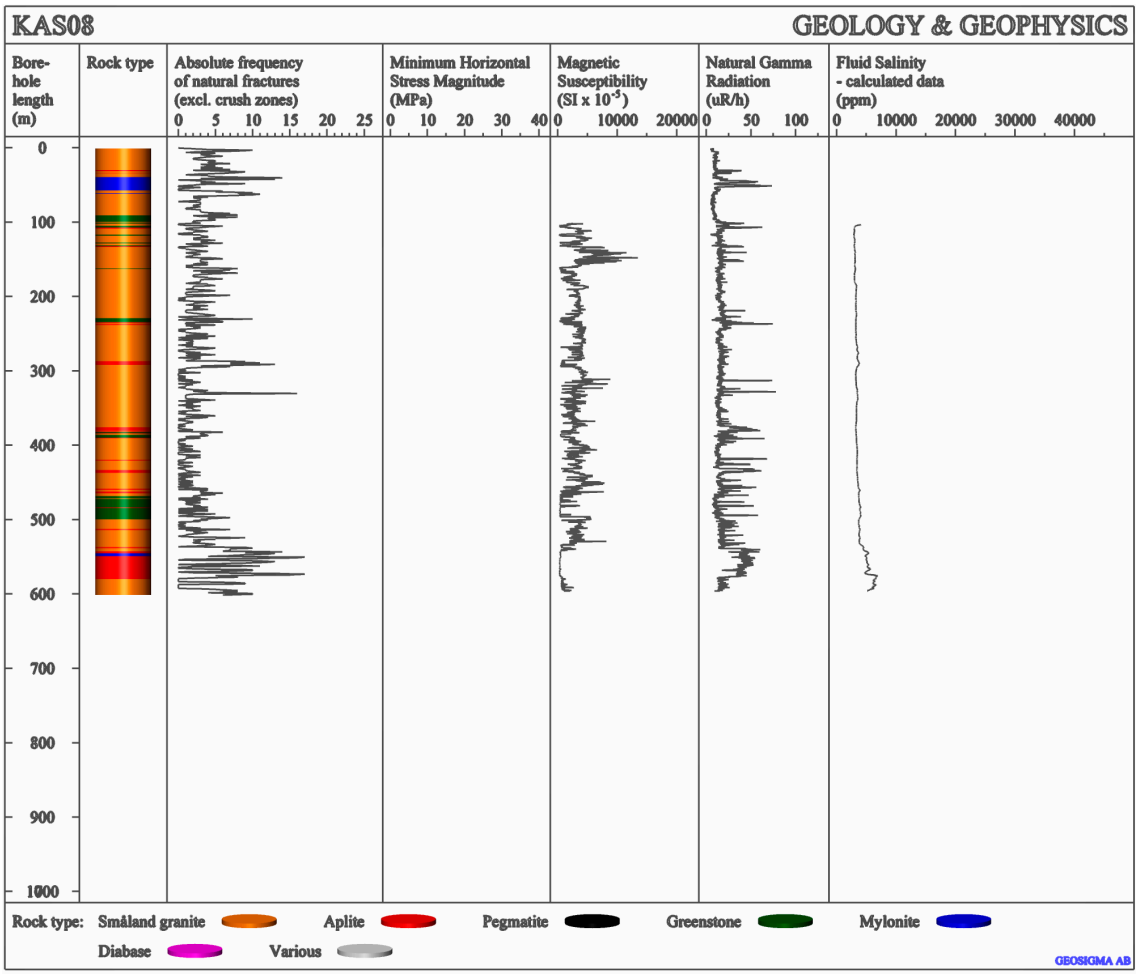

Figure 6-5. *The lithological and geophysical characteristics of borehole KAS08.*

SE and moderately inclined (approx. 45°) dikes dip northwards and southeastwards. The moderately dipping dikes strikes NNE-SSW and ENE-WSW.

Tirén et al. (1996) made a tentative vertical profile across Äspö based on surface and subsurface data located in the "corridor" of boreholes, passing the boreholes KAS02-03, KAS06-08 and KAS16 (Fig. 6-8). Tirén et al. (1996) also included moderately to gently inclined fracture zones striking NE-SW in the SKI structural model of Äspö (Fig. 6-9). The SKN (the National Board for Spent Nuclear Fuel) structural model also includes gently inclined (50° or less) fracture zones, which, when extended, appear at approximately 500 m depth below the central part of Äspö (Tirén, 1996). These sub-horizontal fracture zones were by SKI and SKN interpreted to outcrop on the southeastern part of Äspö and in the water-covered areas just southeast of Äspö. One of these gently dipping fracture zones was by SKI interpreted to be the Ävrö fault zone, which also was believed to intersect KAS07 at 450 mbgl (Cosma et al., 1990) and KAS02 below 800 m depth. When comparing the results from Tirén et al. (1996) (Figs. 6-8 and 6-9) with the interpretation by Talbot and Munier (1989) (Fig. 6-6) and with the generalized geological-tectonical model by Wikberg et al. (1991) (Fig. 6-11), although the two latter are early results, there are obvious similarities, especially at greater depths.

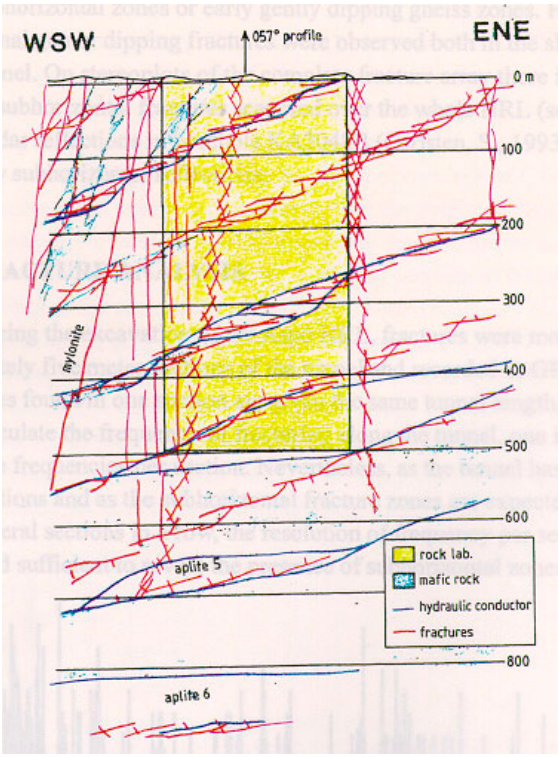

Figure 6-6. *Vertical profile trending 57° through the center of the HRL as proposed by Talbot and Munier (1989). Note that this interpretation have been abandoned after the excavation.*

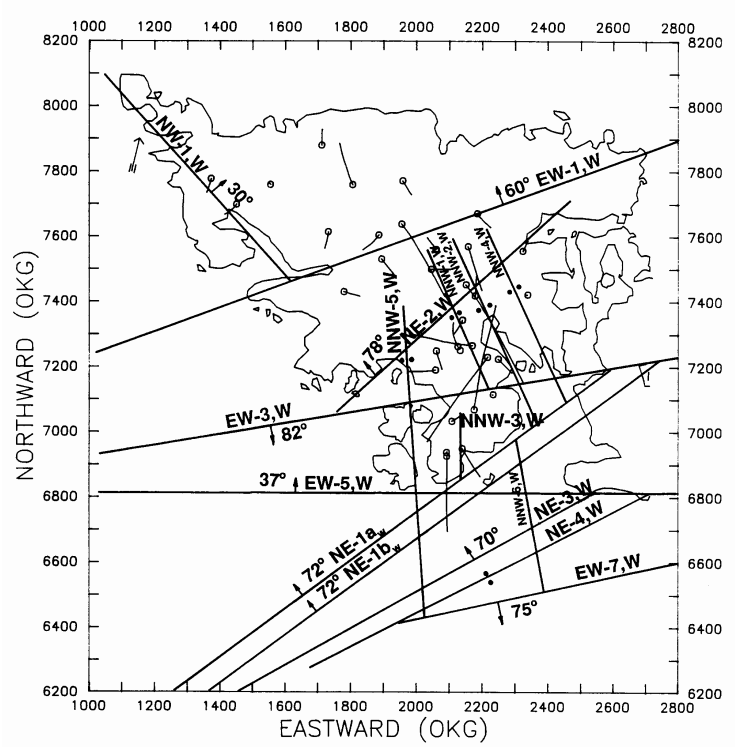

Figure 6-7. *Conductive structures determined mainly by interference tests. Some of the structures in the figure were not seen in the interference test, i.e. gave no response, but are considered to be possible conductors identified from geophysical measurements (Wikberg et al., 1991).*

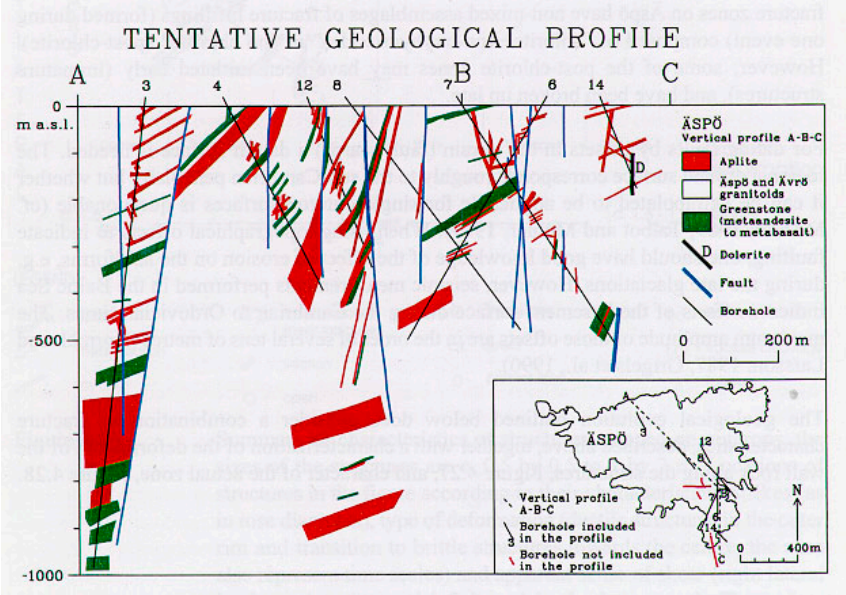

Figure 6-8. *Tentative vertical N-trending profile across Äspö (Tirén et al., 1996).*

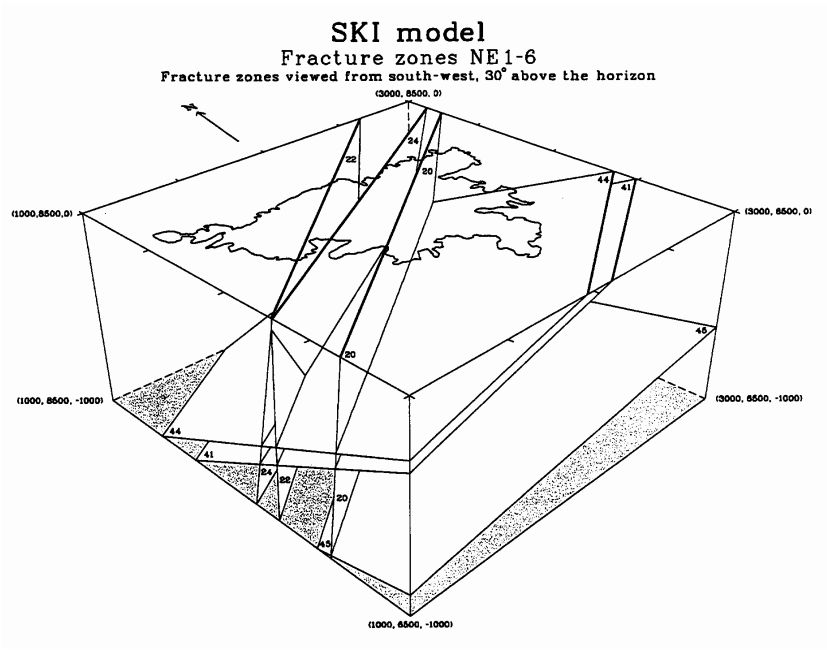

Figure 6-9. *NE-SW striking fracture zones, viewed from a point southwest at an inclination of 30° above the horizon (Tirén et al., 1996).*

Sirat (1999) concluded that GDFs appear to segment the bedrock into sub-horizontal layers and interpolated these zones to be located at 300 (±20) m and 560-600 m depth below the Äspö island.

6.2.3 Hydraulic interference tests

Hydraulic interference tests indicated a major hydraulic conductor oriented NNE-SSW in boreholes KAS07 and KAS08 at 500-600 m borehole length (mbgl) at Äspö (Nilsson, 1989). Rhén (1990) suggested that the response could be explained by the EW-3 zone (Fig. 6-7). In borehole KAS07, this hydraulic conductor coincide with a section of greenstone (450-490 m depth) with a thin inclusion of aplite, approx. 2 m thick, Fig. 6-4 (Stanfors et al., 1997). In borehole KAS08, the bedrock between 460-500 m depth consists of aplite (Fig. 6-5). Also borehole KAS06 has an approximately 80 m long section of aplite at 400-470 m depth, although not reported as a major hydraulic conductor, Fig. 6-3 (Stanfors et al., 1997). The zone at 396-505 m depth in KAS06 is though the most permeable section in the borehole (Nilsson, 1989). Hydraulic interference tests performed in KAS06 (204-277, 304-377, 389-406, and 439-602 mbgl) indicated connections with several boreholes on Äspö (Rhén, 1990). Rhén (1990) used a scale from 1-4, where 1=good hydraulic contact and 4=some contact.

The section at 204-277 mbgl in KAS06 show a good contact with KAS02 (800-854 mbgl) and KAS07 (0-190 mbgl). The conductive structure between KAS06 (218 mbgl) and KAS07 (109 mbgl) was interpreted to strike N28°W and dip 85°E. The pumping at 304-377 mbgl in KAS06 indicated a good contact with KAS02 (346-799 and 800-854 mbgl), KAS05 (320-380 mbgl) and KAS07 (191-290 and 411-500 mbgl). This indicates, using the section in KAS05 and the shallower sections in KAS02 and KAS07, a conductive zone striking N75°E and dipping 35°N (the EW-5 zone, Fig. 6-7). The deeper section in KAS02 and KAS07 was later interpreted to be the Ävrö zone (Tirén, 1996).

The pumping at 389-406 mbgl in KAS06 indicated a good contact with KAS02 (800-854 mbgl) and KAS08 (0-139 and 140-200 mbgl). Finally, the pumping at 439-602 mbgl in KAS06 indicated a good contact with KAS02 (800-854 mbgl) and KAS08 (0-139 mbgl). The geologically defined structure EW-2 may explain the response during the tests at 389-406 and at 439-602 mbgl, as EW-2 may be a hydraulic conductor connecting NNW-1 and NNW-2, Fig. 6-7 (Rhén, 1990).

Hydraulic interference tests performed in KAS03 (Rhén, 1989) indicated a hydraulic zone at 220 m depth striking N50°W and dipping 30°NE. The extension of the zone towards the SE is not clear (Wikberg et al., 1991). A fracture zone was also interpreted at 617 m depth in KAS03 with an orientation of N70°E/60°N (Rhén, 1989, Wikberg et al., 1991). Tests at great depth in KAS02 indicated a channel shaped horizontal structure striking NE-SW.

The lithological and hydraulic data referred to above may be interpreted as indicators of potential sub-horizontal fracture zones associated with aplites at increased fracture frequency providing the hydraulic contact observed. The existence of such zones is also mechanically indicated from the results of the hydraulic fracturing measurements. The aplites in the Äspö region are interpreted to vary in thickness, as they appear from thin dikes and veins to larger irregular bodies (Wikberg et al., 1991). Further, Tirén et al. (1996) interpreted the aplites to break along the E-W and NE-SW shears crossing Äspö (Fig. 6-10), with a vertical displacement of 35-40 m. This implies that the determination of potential sub-horizontal aplite sections may be difficult to identify using e.g. hydraulic interference tests.

6.2.4 Borehole geophysical logs

The aplites have evident signatures on the geophysical logs in boreholes KAS02-03, KAS06-08, and KAS16 (Figs. 6-1 to 5), especially on the magnetic susceptibility and natural gamma logs. The aplites are characterized by a lower content of iron and a higher content of uranium and thorium, as compared to the overall rock. This may be explained as the intruding aplites being enriched in the minimum-melting constituents of granite and containing small amounts of high-melting constituents such as ferromagnesian minerals and calcic plagioclase. Aplites may also contain rarer minerals such as uranium and thorium (Mason and Moore, 1982; Hall, 1987; Stanfors 1988). In average, the magnetic susceptibility in the boreholes of interest is $1.4 \cdot 10^{-2}$ SI, while the aplite sections in these boreholes have a susceptibility of $5.3 \cdot 10^{-3}$ SI. The average natural gamma radiation is 23 μR/H, while the aplite shows a natural gamma radiation of 50 μR/H (Sehlstedt and Triumf, 1988; Sehlstedt and Stråhle, 1989).

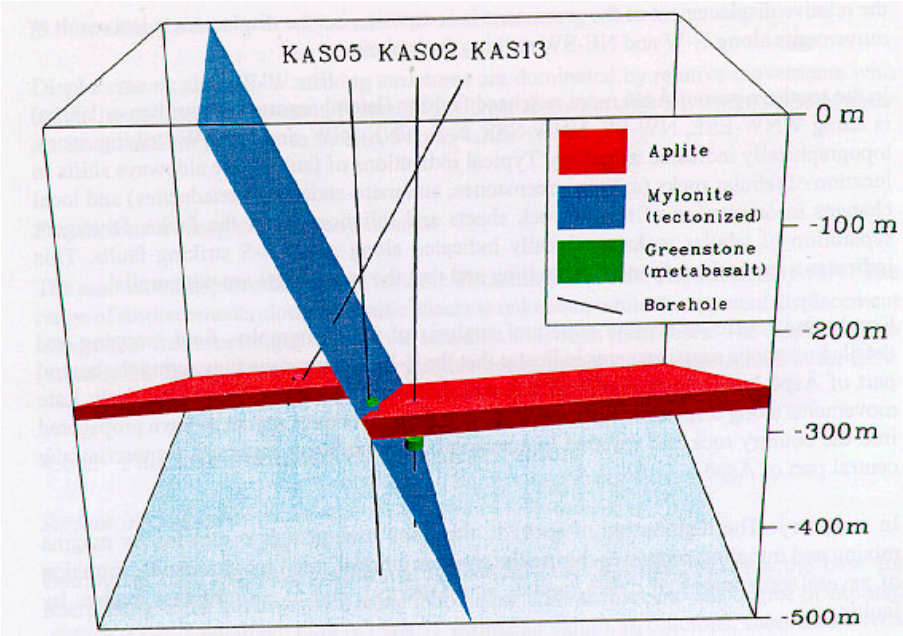

Figure 6-10. *Displacement of an aplite as indicated in boreholes KAS02, KAS05 and KAS13 (After Tirén et al., 1996).*

Ahlbom et al. (1986) suggested that a sub-horizontal zone may function as a hydraulic barrier against draining out and replacement of deep saline water by non-saline water. In the salinity logs this may be expressed as a marked increase in salinity in connection with the zone. Primarily the deep boreholes KAS02 and KAS03 may be analyzed for this effect. Figures 6-1 and 6-2 show an increase in fluid salinity at the level of the potential sub-horizontal discontinuity. In KAS02 the fluid salinity increases steadily from 3000 to 21000 ppm between 150 to 690 m depth. Below 690 m depth, the fluid salinity is stable at 15000 ppm.

In KAS03 the fluid salinity slowly increases between 220-650 m depth followed by a rapid increase from 12000 to 24000 ppm between 650 to 840 m depth (Sehlstedt and Triumf, 1988) (Fig. 6-2). Interestingly, the fluid salinity log indicates fresh water below

840 m depth in KAS03 (3500 ppm). Talbot and Munier (1989) interpreted this fresh water to originate from far inland and that it follows major hydraulic conductors (possibly the Ävrö zone mentioned in Tirén et al., 1996), with outflow far out in the Baltic Sea. Stanfors (1988) concluded that there is an obvious correlation between increased salinity with aplite sections in boreholes KAS02 and KAS03, respectively. Boreholes KAS06 to KAS08 also show an increased fluid salinity in connection with the potential zone. Borehole KAS06 indicates an increase in fluid salinity from 550 m depth to the bottom of the borehole, KAS07 from 410 m depth, and KAS08 from 535 m depth to the bottom of the borehole. However, the logs are inconclusive as the boreholes are not deep enough to cover the effect fully regarding the potential zone.

6.2.5 Seismic reflection studies

Seismic refraction studies (Ploug and Klitten, 1989) indicated two sub-horizontal zones, at 300-500 m respectively at 950-1150 m depth, in two profiles across Äspö. The shallower zone (300-500 m depth) consists of two roughly planar reflectors and the deeper (950-1150 m depth) of a strong reflector in KAS02 (Fig. 6-11).

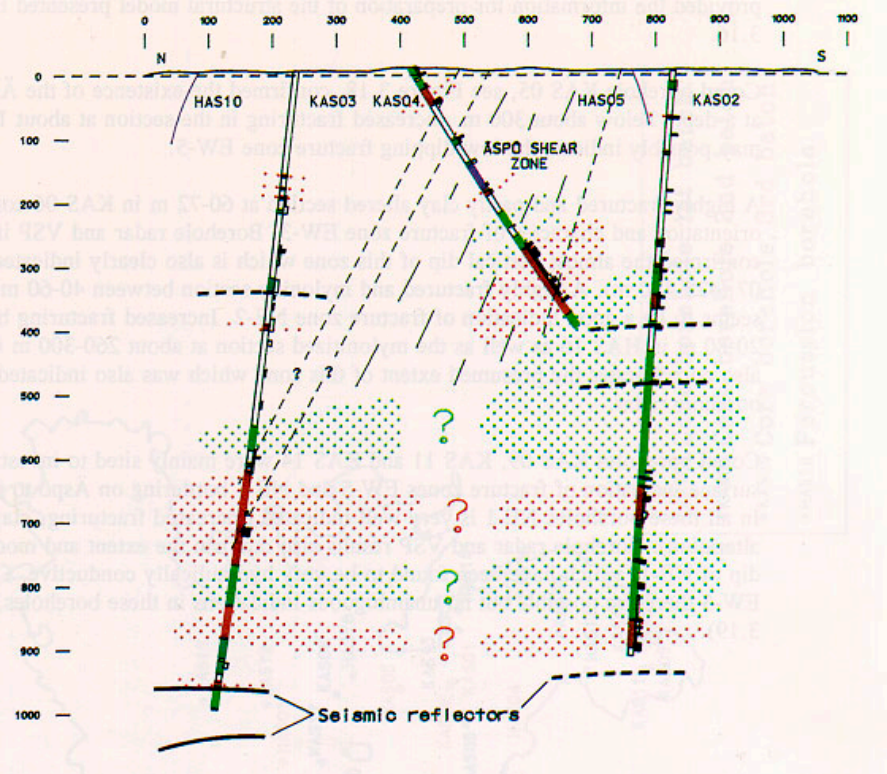

Figure 6-11. *Section trending NW-SE across the Äspö island. Generalized geological-tectonical model based on the first drilling campaign (After Wikberg et al., 1991).*

The reflections are rather short and irregular, which implies that they may correspond to a system of more or less interconnected and irregular heterogeneities in a fractured and weathered rock mass.

These results correspond well with the interpreted characteristics of the aplite in the Äspö area (Wikberg et al., 1991). Talbot and Munier (1989) also suggested that the aplites and their associated hydraulically conducting fracture zones are likely to correspond to these reflectors. Talbot and Munier (1989) also stated that these thrusts may be listric, implying a gentler dip versus depth.

Juhlin (1990) later reevaluated the seismic refraction data from Ploug and Klitten (1989) and found that the two processors used, the Houtex and the University of Manitoba processors respectively, indicated two completely different opinions as to if any reflections are present. The latter indicated numerous reflections, which may be related to zones with a low rock quality index. Juhlin (1990) concluded that the ambiguous results could be resolved only by conducting VSP measurements (e.g. in KAS02 and KAS03) and further seismic experiments in the area.

VSP measurements have been performed in KAS07 (Cosma et al., 1990) and several sub-horizontal zones were indicated: 450 mbgl (strike 320° and dip 35-40°), 580 mbgl (strike 320° and dip 35-45°), 680-700 mbgl (strike 320° and dip 20-40°), and 1050-1100 mbgl (strike 320° and dip 40-45°). Thus, the wave-length is approximately 110 m for the upper zones (the lower also fits this wave-length if we assume that two zones, at approx. 810 and 930 mbgl, were not detected in the survey), which is similar to the results by Talbot and Munier (1989) and Liedholm (1991a, 1991b). The strike is defined as the clockwise angle between the upgoing normal to the reflector and the North. Thus, the dip direction for the reflectors is NW, which is similar to the NNW-NNE suggested by Talbot and Munier (1989).

6.2.6 Borehole radar measurements

Furthermore, results of radar measurements indicate a correlation between boreholes KAS02, KAS03 and KLX01 at 863, 579 and 577 m depth respectively, implying a zone with strike N54°E and dip of 27° towards SE (Stanfors, 1988). However, structures with great extension being interpreted using radar measurements are regarded somewhat uncertain. Stanfors (1988), and Niva and Gabriel (1988) found that radar pulses were delayed, indicating an increased electrical conductivity at 580-635 m borehole length in KAS03. Below this depth, there is a marked change of shape of the radar amplitude curves, indicating a very low electrical conductivity in the rock. Stanfors (1988), and Niva and Gabriel (1988) interpreted this to be the result of a shift from granite to aplite. Stanfors (1988) further states that there is an evident correlation between geophysical borehole measurements and aplite in deeper sections of KAS02 and KAS03. Radar measurements performed by Carlsten (1989) indicated lower radar amplitudes at 530-570 m borehole length in KAS07 and at 540-580 m borehole length in KAS08 implying a higher electrical conductivity in the rock. These sections correspond well with aplite sections in the boreholes. In KAS06, the aplite is found at 400-470 m depth, but in this case the radar amplitude is higher compared to the overall rock. However, immediately above and below this section the radar amplitude is low. Hence, the aplite sections seem to coincide with hydraulic conductors.

6.2.7 Modeling studies

A 3DEC modeling study, based on the SKI structural model, (using 15 respectively 23 major faults and fracture zones) gave that the computed stresses match the measured stresses from KAS02 and KAS03 fairly well (Hansson et al., 1995). However, a major discrepancy occurs at about 600 m depth. The calculated stresses have a variation of ± 10 MPa at 500 m depth, where the magnitude is 20 to 40 MPa. This variation is of the same order of magnitude as the difference between the measured and calculated stresses. Hansson et al. (1995) suggested that the reason for the discrepancy could be: (i) effect of local rock structures; (ii) change of rock type at the local area of the measured site (which was not included in the models); (iii) an inaccurate representation of local stress change by the global stress boundary conditions; (iv) the reduction in the number of major fracture zones in the computational models, which uses far fewer zones than those shown in the structural model (Tirén et al., 1996); (v) the omission of joints in the computational models; and (vi) uncertainties in the estimation of fracture zone properties. Hence, the modeling results could be explained by e.g. the potential zone(s) below the island of Äspö.

6.2.8 Discussion

The stress field along borehole KAS02 can from top to bottom be described by: (A1) an upper section of low increase in stress magnitudes versus depth with magnitudes smaller than those presented in the Fennoscandian Rock Stress Data Base (Ljunggren and Persson, 1995); (A2) a middle section characterized by a large increase of stress magnitudes with depth; (A3) a lower section with no/minor increase in stress magnitudes with depth. In borehole KAS03 the stress field may be described by: (B1) "normal" gradient of stresses down to 550 m depth (note that almost all data are grouped between 470-550 m depth); (B2) a middle section characterized by no/minor increase of stress magnitudes with depth; (B3) a lower section with "normal" increase in stress magnitudes with depth. This non-linear stress distribution versus depth below the island of Äspö could be attributed to a number of reasons:

1. Errors related to the hydraulic fracturing technique, e.g. pore pressure, calculation of S_H (re-opening pressure) and temperature effect.
2. The thrust regime ($\sigma_H > \sigma_h > \sigma_v$) in the upper 400-500 m.
3. Glacial rebound.
4. Change of material properties of the rock.
5. Fracture/fault zones.

These factors are shortly described below.

1. The hydraulic fracturing technique has a few limitations that may partly explain the observed large stress gradient in sections A2 and B3 (and the lower part of B1?). The most important of these is the effect of pore pressure, which has been neglected in the stress calculations in the Äspö region. Hydraulically conductive zones are known to cause pore pressure variations. However, conductive zones are absent at the depth of the largest stress gradient in KAS02 (and KAS03). Moreover, the groundwater level monitoring in these boreholes indicated very small pressure differences versus depth as well as small variations with time (Nyberg et al., 1991). Thus, it seems unlikely that

pore pressure effects are responsible for the large gradient. Measurement errors and theoretical shortcomings involved in the hydraulic fracturing theory have not been investigated.

2. In the upper sections of the boreholes (A1 and B1?), the minimum horizontal stress is close to the vertical stress. This implies that the induced fractures may rotate during the propagation, from a vertical fracture to a horizontal. Thus, the hydraulic fracturing measurements may be a measure of the vertical stress leaving the minimum and maximum horizontal stresses undetermined. This implies that the measurements only give only a lower estimate of the minimum horizontal stress.

3. The low horizontal stresses at Äspö down to 400-500 m depth (sections A1 and B1?) may be an effect of glacial rebound, resulting in relaxation of the stresses in the upper few hundred meters. The larger stress magnitudes below 500 m depth may thus represent the "true" state of stress or perhaps a residual stress field from the glaciation period. An interesting question may then be posed: If the low stresses are an effect of glacial rebound, why is only the upper few hundred meters affected?

4. The relatively large stress gradients observed in section A1 (and the lower part of B1?) may represent a change of material properties (of which the relative stiffness is most important), moving from a less stiff into a more stiff material. Immediately below these sections, sub-horizontal aplite zones appear (A3 and B2). When comparing the Young's modulus of the aplite with the surrounding rock mass, the difference is very small, 258±78 resp. 255±29 GPa, between aplite and Småland Granite (Stille and Olsson, 1996). Thus, the aplites do not have significantly different material properties at the Äspö site.

5. As the aplites are more fractured than the overall rock and also display parallel mylonite structures, these sections (A3 and B2) may cause movement and thereby the observed relaxation of the stresses. The horizontal stress orientations are constant according to the HF measurements, which implies that in this thrust regime the potential movement and relaxation of the stresses must have occurred in the direction of S_H. The aplite layers are dipping towards NW (Tirén et al., 1996), which is in agreement with the direction of maximum horizontal stress. Hence, if movement has occurred in the aplite, the slip would have occurred in the dip direction of the aplite.

Lundholm (2000a and 2000b) made an independent analysis of KAS02 and KAS03 and suggested that mylonite zones are responsible for the non-linear stresses versus depth in KAS02, Fig. 6-12. For KAS03, Lundholm (2000a and 2000b) concluded that no distinct major mylonite zones or other geological zones existed.

A recent study indicated a correlation between stress regimes and orientation of wet fractures (Talbot and Sirat, 2001). The interpreted regimes, based on the hydraulic stress data (Bjarnason et al., 1989), are presented in Fig. 6-13 for borehole KAS02. Talbot and Sirat (2001) analyzed 11000 fractures belonging to six sets with distinctive fracture orientations (GEOTAB) and found that in the upper thrust-prone regime (<240 m),

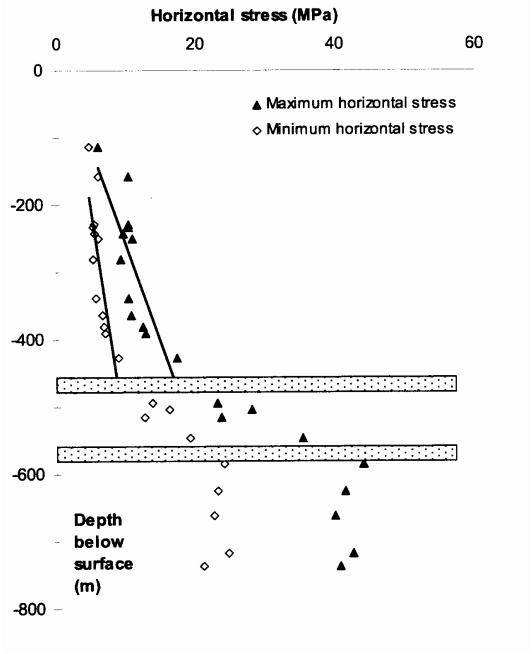

Figure 6-12. *Maximum and minimum horizontal stresses in KAS02 with two zones of mylonite included (After Lundholm, 2000a).*

the dominating wet fracture orientation was sub-horizontal, whereas in the middle wrench-prone regime the dominating fracture orientation was sub-vertical. Thus, the present state of stress seems to cause planar anisotropic hydraulic transmissivity versus depth.

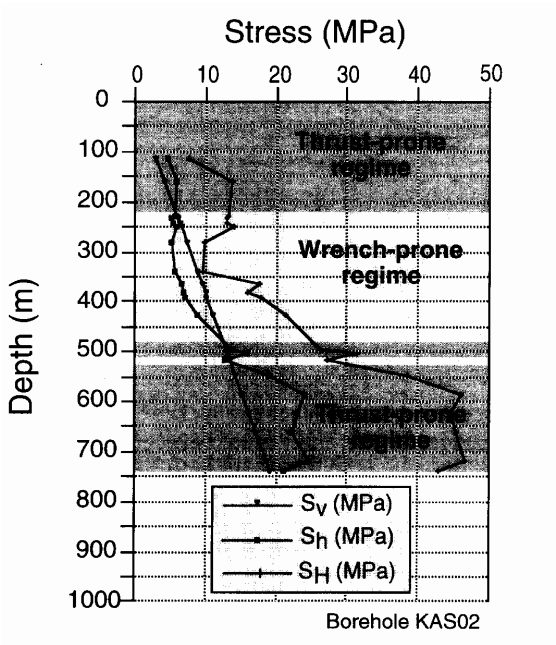

Figure 6-13. *Interpolation of in situ stress measurements in borehole KAS02 at the Äspö HRL (data from Bjarnason et al., 1989) (After Sirat, 1999).*

6.2.9 Conclusion

Based on the hydraulic data, it is suggested that a zone, consisting of more fractured aplites, exist below the island of Äspö. The aplites affect the stress distribution and cause a stress relaxation. However, at this stage, there is no explanation to the observed strong stress gradients above (section A2 and possibly the lower part of section B1) and below the aplite (section B3). A summary of the indications that speak in favor of/against the existence of a potential sub-horizontal aplite zone is presented in Table 6-1.

The potential aplite zone may be one single continuous sub-horizontal layer or several smaller sub-horizontally distributed bodies of aplites. Assuming that the possible zone consists of one continuous layer, intersecting 6 boreholes below the Äspö island (KAS02-03, KAS06-08 and KAS16), the minimum lateral extent would be 900 m. However, the existence of such a zone has not been verified. The orientation of the potential zone is difficult to determine due to (i) the strongly varying thickness of the aplites; (ii) the possible break along the E-W and NE-SW shears crossing Äspö (Tirén et al., 1996); and (iii) the occurrence of two aplite sections in borehole KAS02 (at 652-715 and 858-906 m depth). If the former is extended to the other boreholes, the dip direction is approximately NNW. If, instead, the aplite at 858-906 m depth in KAS02 is extended to the other boreholes, the dip direction is approximately W to WNW. Possibly, the aplite layers appear in cycles with roughly 100 m spacing. Hopefully, future research will confirm/reject this interpretation, see Ch. 8.

Table 6-1. Summary of indications that speak in favor of/against the existence of a potential sub-horizontal zone below the island of Äspö.

Type of indication	In favor of a sub-horizontal zone	Against a sub-horizontal zone
Hydraulic fracturing stress measurements	Zone clearly indicated in KAS02-KAS03.	(No measurements in other boreholes at these depths.)
Geology	Aplites appear in 6 boreholes (KAS02-03, KAS06-08, KAS16).	The aplites are interpreted to vary in thickness.
Geophysical logs: *- Fracture freq.* *- Natural gamma* *- Magn. susc.*	Clearly indicated in 5 boreholes.	Might to some extent be explained by other intersecting fracture zones.
Salinity	Indication in KAS02-03. For KAS06-08 the logs are inconclusive.	Might to some extent be explained by other intersecting fracture zones.
Radar measurements	Gently dipping reflectors KAS02-KAS03.	No correlation found between the other boreholes.
Hydraulic interference tests	Major hydraulic conductor oriented NNE-SSW in boreholes KAS07 and KAS08 at 500-600 mbgl. Conductors found between e.g. KAS02 (346-799 and 800-854 mbgl), KAS06 (304-377 mbgl) and KAS07 (191-290 and 411-500 mbgl) (Rhén, 1990). The deeper sections in KAS02 and KAS07 is interpreted to be the Ävrö zone (Tirén, 1996). A fracture zone was also interpreted at 617 m depth in KAS03 oriented N70°E/60°N.	The correlation between KAS07-KAS08 has been interpreted to be due to the sub-vertical zone NE-1.
Seismic reflection studies	Ploug and Klitten (1989) found sub-horizontal zones at 300-500 m and 950-1150 m depth and Cosma et al. (1990) at 450, 580, 680-700, and 1050-1100 mbgl in KAS07. Talbot and Munier (1989) suggested GDFs (spacing ~100 m) of which two coincided with the seismically indicated zones. This wave-length have been verified by Liedholm (1991a, b) and Cosma et al., 1990). The dip direction of the suggested GDFs (Talbot and Munier, 1989) was verified by the VSP measurements (Cosma et al., 1990).	The seismically indicated zones interpreted by Ploug and Klitten (1989) appear above and below the potential sub-horizontal discontinuity.
Other interpretations and indications	GDFs according to Talbot and Munier (1989) suggests a dip towards NNW. SKI and SKN (Tirén et al., 1996; Tirén, 1996) and Sirat (1999) later confirmed these results.	During the excavation phase, Hermansson (1995) and Munier (1995) found that few gently dipping fracture zones are present in the HRL. The sub-horizontal fractures found appear as fracture swarms rather than fracture zones and have a SW to S dip.

6.3 INFLUENCE OF THE SUB-VERTICAL ZONE EW-1 CROSSING THE ISLAND OF ÄSPÖ ON THE STATE OF STRESS

The influence of the potential sub-horizontal zone was recognized from results in the previous section. The influence of the sub-vertical zone EW-1 (Fig. 6-14) at Äspö was also analyzed. The fracture zone EW-1 has been indicated by airborne geophysical surveys and lineament interpretation. Later, ground geophysical investigations confirmed the extent of EW-1 in more detail. The EW-1 zone is very well indicated topographically (a 50-100 m wide depression in the ground extending many hundreds of meters), geophysically (low-magnetic and low-resistivity zone 200-300 m wide) and geologically in boreholes (mylonites and many highly fractured and altered sections in drill cores). The fracture zone EW-1 is regarded as part of the about 300 m wide low magnetic zone (Äspö shear zone), trending NE, which divides Äspö into two main rock blocks (Rhén et al., 1997b).

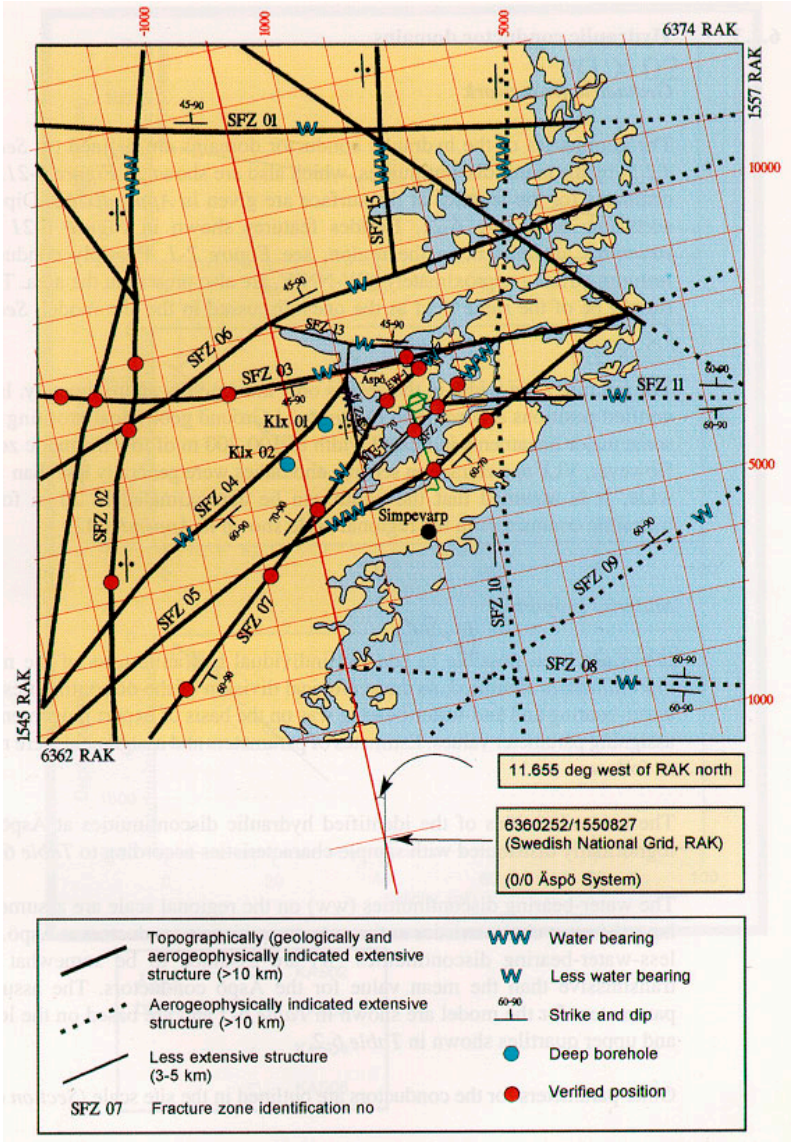

Figure 6-14. *Structural model on regional scale (Rhén et al., 1997b).*

The analysis of EW-1 and its effect on the stress field may be possible through a comparison of the inversion results from boreholes KAS02 and KAS03 situated on different sides of EW-1. By this approach the question whether the EW-1 zone divides the island of Äspö into two stress regions would be enlightened.

The easiest method to investigate this is to plot the inversion results for boreholes KAS02 and KAS03 in the same diagram (Figs. 6-15 and 6-16). The discrepancy between boreholes KAS02 and KAS03 regarding both stress magnitude and orientation is clear. The rock at borehole KAS03 seems to be exposed to higher horizontal stresses at shallow depths than the rock at KAS02. However, this is most likely an overestimation, as most measurement points are located between 450-550 m depth and therefore strongly constrain the inversion result. Borehole KAS03 does not seem to be as strongly affected by the potential sub-horizontal discontinuity as borehole KAS02. But again, this may be explained by the lack of measurements between 150 and 450 m depth in KAS03. The orientation of maximum horizontal stress is, though, rather consistent, NW-SE.

At larger depths, the stress fields in KAS02 and KAS03 are more comparable, although the orientation of maximum horizontal stress is more scattered (average NW-SE).

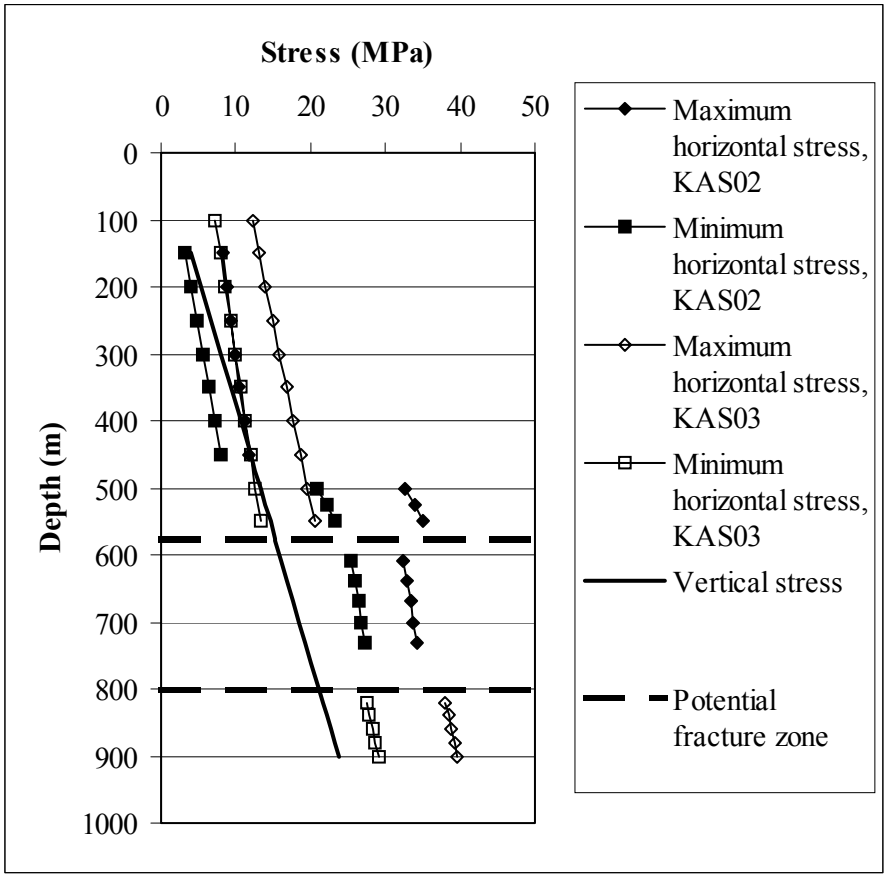

Figure 6-15. *Inversion results for boreholes KAS02 and KAS03, magnitudes.*

In conclusion, the inversion results indicate that the boreholes KAS02 and KAS03 are exposed to different stress regimes, at least at shallow depths. However, at this stage, it is not possible to judge if this is due to: (i) the EW-1 shear zone; (ii) the aforementioned

potential sub-horizontal discontinuity below Äspö (~600-800 m depth); (iii) a combination of the (i) and (ii); or (iv) a result of the location of the measurement points. A fifth alternative to the low horizontal stresses in KAS03 at shallow depth, could be the existence of another more shallow fracture zone that allows movement and relaxation of the stresses. E.g. a mylonitic zone at 390-420 m and several hydraulically conductive sections at 200-400 m depth have been identified (Wikman et al., 1988). A shallow zone is also indicated in the fracture frequency plot. Future work will hopefully contribute to the answer of this question.

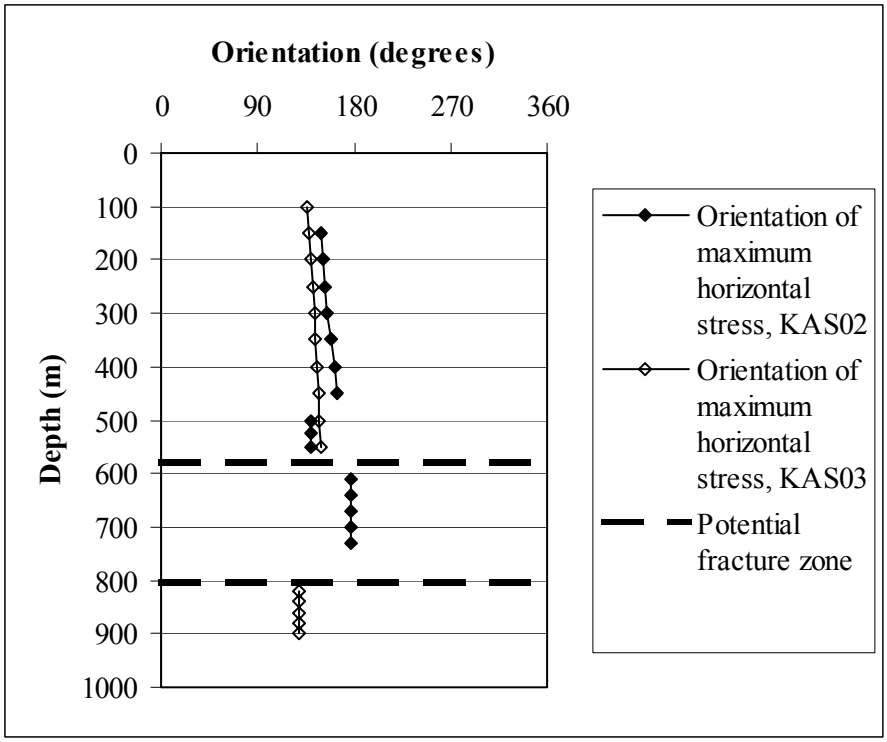

Figure 6-16. *Inversion results for boreholes KAS02 and KAS03, orientation of S_h.*

6.4 INFLUENCE OF STRUCTURES IN BOREHOLE KLX02 ON THE STATE OF STRESS

In KLX02, the bedrock between 700 and 1100 m depth is mainly composed of granite, diorite and thick layers of greenstone (Stanfors et al., 1997) (Fig. 6-17). Eriksson et al. (1997) suggested that a discontinuity, consisting of two intersecting major fracture zones (SFZ04 and SFZ07), is located at 700-1100 m depth (Figs. 6-14 and 6-18). However, a recent seismic study (Bergman et al., 2001), indicates another possibility. Bergman et al. (2001) found two sub-horizontal reflectors at 650 and 900 m depth (dip 0-15° towards East), assuming a p-wave velocity of 5500 m/s (B and G in Fig. 6-19). Hydraulic interference tests between the two deep boreholes KLX02 and KLX01, where pumping was performed in KLX02 in sections 0-805 m and 805-1103 m, indicated an evident correlation with 272-695 m respectively 695-1078 m in KLX01. The former correlation may be explained by a structure with dip direction/dip 273°/39°, surfacing

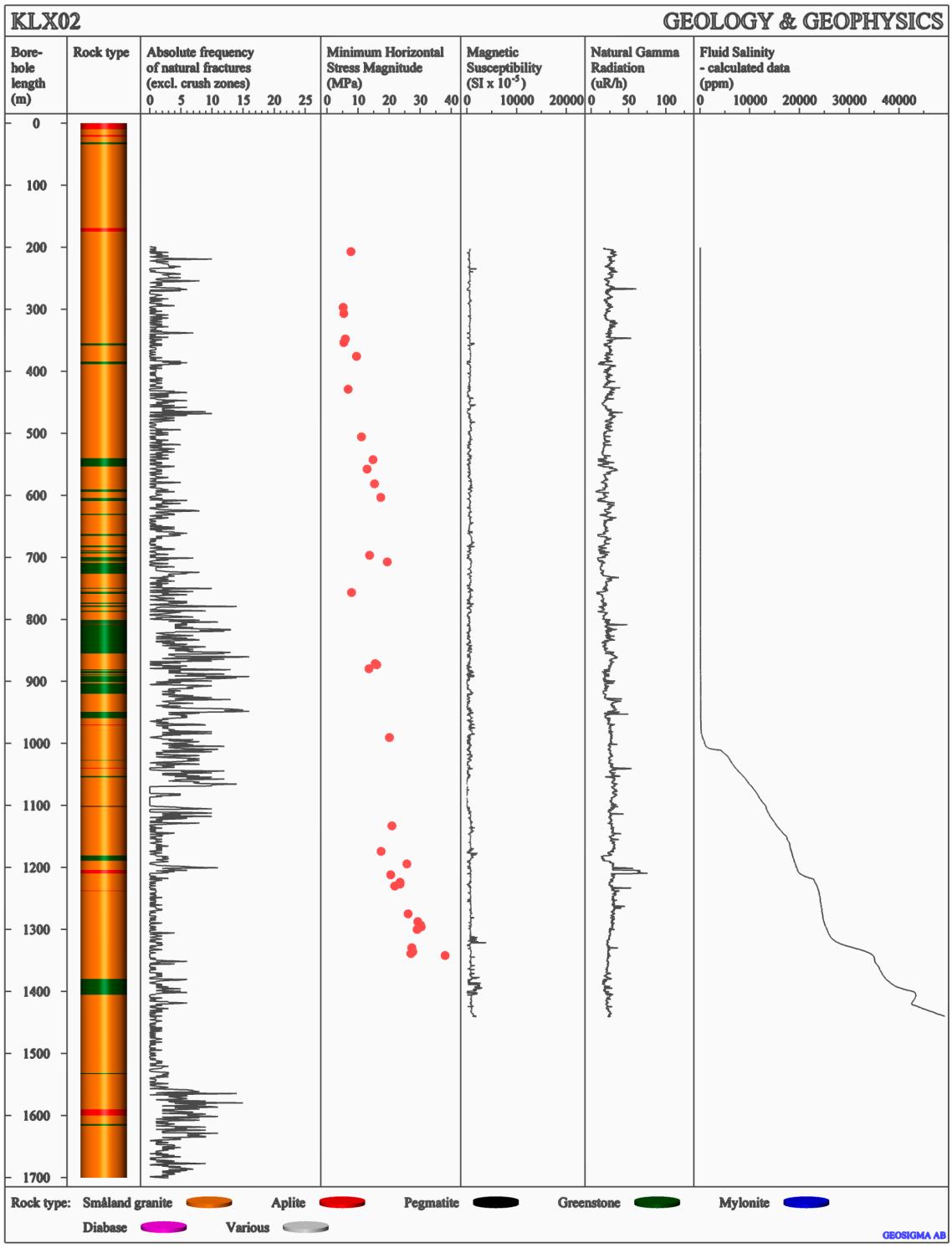

Figure 6-17. *The lithological and geophysical characteristics of borehole KLX02.*

approximately 250 m south of KLX02 (reflector I in Fig. 6-19). The latter correlation corresponds well with greenstone layers in KLX02, which is considered more fractured than the overall rock. The greenstone is interpreted to dip towards east but the extent is not clear. Hence, the suggestions by Bergman et al. (2001) are supported by the hydraulic interference tests.

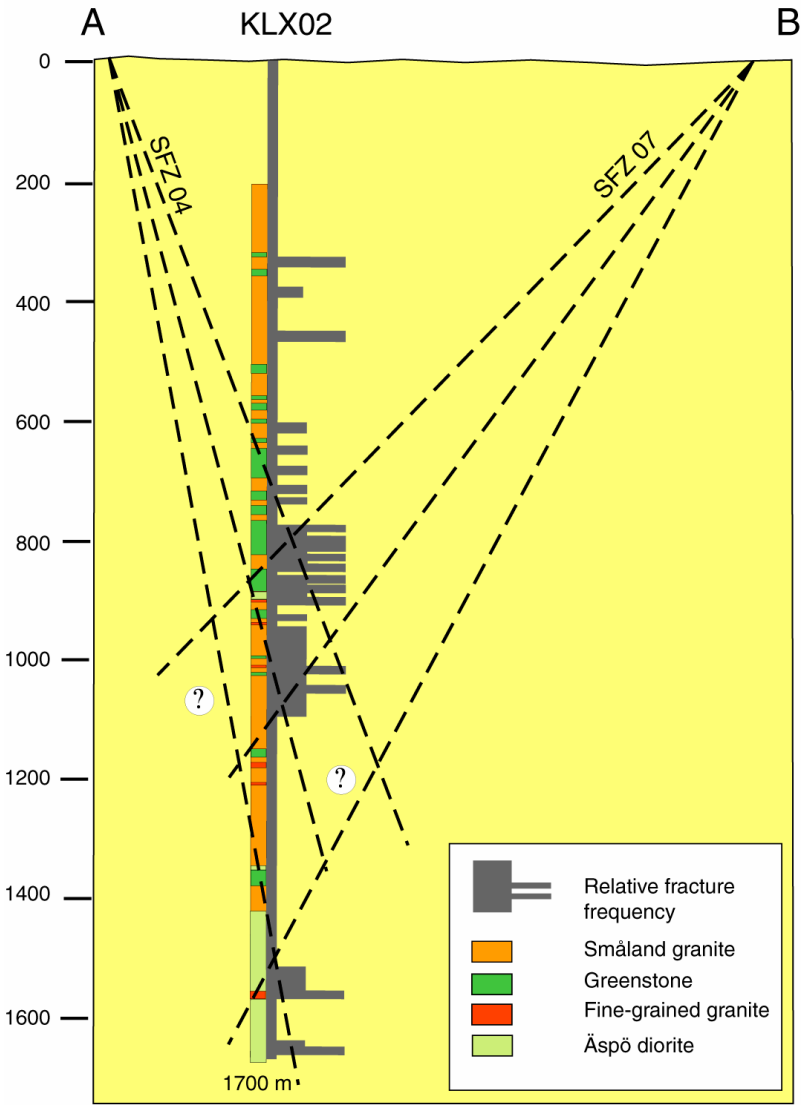

Figure 6-18. *Interpretation of possible connections between fractured sections in borehole KLX02 and surface indicated discontinuities (Ekman, 2001).*

In the hydraulic fracturing measurements the fracture orientations in the deeper section of borehole KLX02 were determined using BIPS-images. The analysis proved to be very difficult, and the determination of fracture orientations are consequently associated with great uncertainties. Firstly, the borehole wall is covered with a dark coating. To some extent this was positive since the impressions of the straddle packer were often visible and the test section more easily recognized. However, the coating also made the fracture determination difficult and subjective. Secondly, the resolution of the BIPS-camera did not allow detection of the small aperture induced fractures except for a few cases. Thirdly, it was not possible to determine if the fracture was hydraulically conductive or sealed. Furthermore, during the BIPS-measurements problems were evident about the orientation of the measuring tool, which means that the fracture orientations are even more uncertain. Therefore, no inversion attempts from the deeper part of KLX02 are presented here and the state of stress is only discussed tentatively.

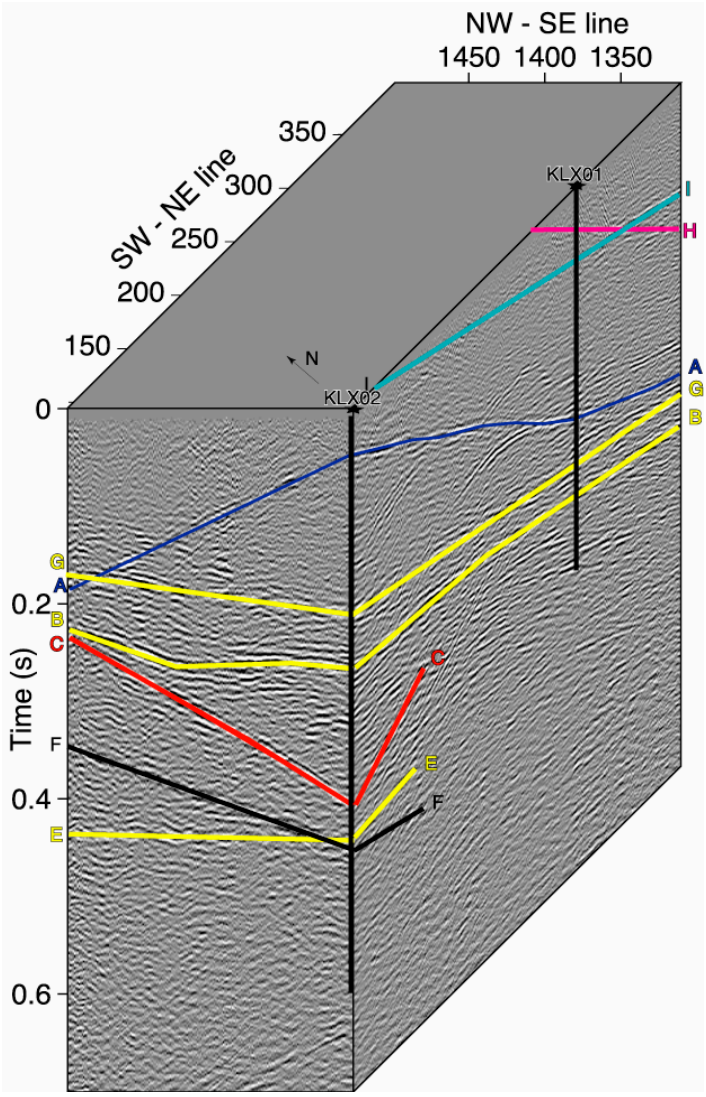

Figure 6-19. *Results from seismic reflection studies at Laxemar. The reflector I, respectively B and G, corresponds well to the results from hydraulic interference tests (Bergman, 2001).*

The analysis of the BIPS-pictures included one possible borehole breakout oriented ENE-WSW at 1341-1342 m depth, indicating a NNW-SSE orientation of maximum horizontal stress. This breakout has also been identified using a forward-viewing camera and has a depth into the borehole wall of approximately 1-2 cm. Another possible borehole breakout was found between 750-820 m depth, oriented NW-S with a maximum depth of 5 mm, i.e. indicating an orientation of maximum horizontal stress approximately ENE-WSW. The dominating elongation is in the NW direction and the less dominant in the S direction (Ask, 1994).

If these suggested breakouts do exist, they may be used to get some constraints of the stress magnitudes at depth in KLX02. If the sub-surface horizontal stresses are unequal, stress concentrations will develop, which may be large enough to cause failure of the borehole wall. Failure will occur when the circumferential compressive stress around the borehole ($\sigma_{\theta,max}=3\sigma_H-\sigma_h$) is larger than the uniaxial compressive strength of the material. The state of stress at the suggested breakout at 750-820 m is approximately

$\sigma_H \approx 20$ MPa and $\sigma_h \approx 10$ MPa, which means $\sigma_{\theta,max}=50$ MPa according to the HF measurement at 753.9 m depth. The bedrock at this depth consists of Småland granite and sections of greenstone (Andersson, 1994; Stanfors, 1995; Ekman, 2001). The Småland granite has a uniaxial compressive strength ranging between 197-275 MPa and the greenstone 121-274 MPa (Stille and Olsson, 1996). At 1350 m depth, the state of stress is approximately $\sigma_H \approx 75$ MPa and $\sigma_h \approx 40$ MPa, implying $\sigma_{\theta,max}=185$ MPa according to the HF measurement at 1336.9 m depth. The bedrock at this depth consists of Småland granite. Consequently, this rough analysis study does not support the hypothesis of a breakout at 750-820 m depth but may well explain the breakout at 1350 m depth since the circumferential compressive stress reaches the lower boundary of the compressive strength. On the other hand, Andersson (1994) reported core discing at 863, 944, 1335, and 1499 m depth, which is an indication of large deviatoric stresses and consequently strengthens the possible occurrence of borehole breakouts (as well as disqualifying the HF measurement at 753.9 m depth).

Furthermore, white colored small aperture fractures (probably calcite filled) appear in the NE-SW direction between 1070-1080 m depth and rotating towards NW-SE with depth down to approximately 1300 m depth in KLX02. Below 1300 m the fractures turn towards NNW-SSE. We suggest that these fractures are drilling induced tensile fractures (DIFs) and may be used to constrain the orientation of maximum horizontal stress. The DIFs develop on opposite sides of the borehole, in theory 180° apart, in a direction parallel to maximum horizontal stress. Stress concentrations exceeding the tensile strength of the borehole wall developing DIFs may be due to circulation of cold drill fluid (e.g. Brudy and Zoback, 1993; Ask, 1998). After Stephens and Voigt (1982); and Ritchie and Sakakura (1956), the thermally induced stress is given by:

$$\sigma_T = -\frac{\alpha_T E \Delta T}{1-\nu} \tag{6-1}$$

where α_T is the thermal expansion, E is Young's modulus, ΔT is the temperature difference between the rock formation and the drill-fluid, and υ is Poisson's ratio. For most common rock types, the generated tensile stress is approximately 1 MPa per 1°C cooling (Brudy and Zoback, 1993). At 1000-1340 m depth in borehole KLX02 the fluid temperature is approximately 26°C (Andersson, 1994). During drilling, the circulation fluid was extracted from the nearby percussion-drilled borehole HLX10 (85 m deep). At 85 m depth, the fluid temperature is approximately 9°C, which means that the temperature difference between the circulation fluid and the fluid at the position of the suggested DIFs is 17°C. This implies that maximum generated tensile stress is 17 MPa, assuming that the rock formation receives the same temperature as the circulation fluid during drilling and that the circulation fluid is not heated (or cooled) during: (i) pumping from HLX10 to KLX02; (ii) temporary storage at the drilling site and; (iii) pumping from ground surface down to actual depth. The tensile strength derived from the HF measurements between 1000 - 1350 m depth is in average 3.5 MPa, indicating that DIFs will develop if the rock formation temperature is lowered 3.5°C during drilling. Reformulated, this means that DIFs will develop if the heating of the circulation fluid plus the effect of heat exchange between the circulation fluid and the formation rock does not exceed 13.5°C.

Further, the suggested DIFs seem to appear as calcite filled small aperture fractures, which implies that the precipitation rate must have been high. However, this may be explained by the fact that the circulation fluid was extracted from the nearby borehole HLX10. During drilling, the circulation fluid is mixed with the groundwater fluid in the drilled borehole and the drilling debris. In the Laxemar area, with a high content of Sodium-Bicarbonate at shallow to intermediate depths and a high content of Calcium-Chloride at large depths in the groundwater, this situation may lead to an over-saturation and fast precipitation of calcite (hours) on the borehole walls (Laaksoharju et al., 1995; Laaksoharju, personal communication).

A simple but interesting analysis can be made using these results. Suppose that the suggested breakouts and DIFs, and the sub-horizontal zone at 650-900 m depth dipping gently towards East is correct (Bergman, 2001). In this case, the S_H orientation rotates from NW to ENE-E and back to NW when passing the zone in the borehole direction. The orientation of S_H within the zone is almost perpendicular to the zone indicated by Bergman (2001) which means that it is a plane of small or zero shear stress, a principal plane. If a slip has occurred and the slip-plane became free from shear stress, it may cause the observed rotation of the stresses as well as explain the low stress magnitudes at these depths.

Conclusively, it is suggested that the zone at 700-1100 m depth (either a wide sub-horizontal zone (Bergman et al., 2001) or due to the intersection of SFZ04 and SFZ07 (Eriksson et al., 1999)) causes a strong re-orientation of the stress field, from NW orientation of the maximum horizontal stress above the zone to ENE-WSW within the zone and back to NW below the zone. Below 1300 m depth the orientation of maximum horizontal stress turns towards NNW. Due to the uncertainties in the BIPS-analysis and the contradictory results concerning the orientation of maximum horizontal stress in the deeper section of KLX02 compared to Ljunggren and Klasson (1997), and the suggested occurrence of borehole breakouts and tensile fractures, it is recommended that further research is conducted to verify/reject this suggestions, see Ch. 8.

7 DISCUSSION

There is generally a reasonable agreement between the results from the inversion analysis and the existing hydraulic fracturing data. However, all inversions are associated with uncertainties, in some cases rather large, which means that the results at this stage should be regarded only as guidelines concerning the state of stress in the Äspö region.

The inversion results indicate that the magnitude of minimum horizontal stress is very close to the vertical stress down to approximately 400-500 m depth. The orientation of maximum horizontal stress is NW-SE. In boreholes KAS02 and KAS03, thrust regimes are indicated at least down to approximately 900 m depth.

The study indicates that the first shut-in pressure is preferable when using the integrated stress determination method. Perhaps this is due to the fact that the fracture connects with other fractures, thereby changing the hydraulic response resulting in erroneous fracture normal stress, during the propagation in the following pumping cycles. Another explanation may be found in that more fractures in the test section are opened during the propagation phase. A third possibility is that the fracture turns from vertical to horizontal as it propagates away from the borehole (Zoback et al., 1977; Evans et al., 1989).

The most probable reason for the relatively poor results of the inversion analysis of hydraulic stress data is that the number of hydraulic fracturing data greatly exceeds the number of HTPF data. Normally, when applying the integrated stress analysis method (Cornet and Valette, 1984), which is based on the HTPF method, the relationship between the number of hydraulic fracturing and HTPF measurements is the opposite. In order to solve for example a six-parameter model, the fractures need to be located at different depths and have different orientations. The number of fractures must, in theory, be at least 6, but usually between 8 to 10 fractures are used to solve a six-parameter model. Consequently, the major drawback when using a majority of hydraulic fracturing measurements is that the induced fractures are all vertical or close to vertical and have similar orientations. During the coarse of inversion analysis, it was evident that the resolution of the unknown parameters becomes greatly improved with increasing number of tests on inclined fractures.

Another reason for the relatively poor result using hydraulic stress data may be found in the fact that many hydraulic fracturing tests were performed in sections that included more than one fracture. This implies that several fracture combinations had to be tested and more important, the fracture normal stress may not be representative since it includes pumping in two or more fractures simultaneously. The occurrence of the induced and pre-existing fracture were probably the result of the high flow rate pumping tests involved in the hydraulic fracturing method. Most probably, the pre-existing fracture was sealed at the beginning of the test and opened simultaneously as the induced fracture. The following pumping test subsequently involved both the induced

and pre-existing fracture and the data was in some cases rejected as outlyers during the inversion analysis.

Additionally, the analysis of existing hydraulic data reveals existence of chevron notches. The occurrence of chevron notches indicates that the borehole axis is not precisely parallel to a principal stress direction or that the induced fracture turns from vertical to horizontal as it propagates away from the borehole. The latter implies that the shut-in pressure may only afflict the vertical stress and the minimum horizontal stress. Thus, the maximum horizontal stress remains undetermined (Zoback et al., 1977; Evans et al., 1989). In the Äspö region, the minimum horizontal stress is close to the vertical stress down to approximately 400-500 m depth according to the in-situ HF measurements. Thus, if a thrust regime ($\sigma_H>\sigma_h>\sigma_v$) prevails, there is a possibility that the induced vertical fractures will turn to the horizontal as it propagates away from the borehole. Note that if the vertical stress (σ_v) is smaller than the minimum horizontal stress (σ_h), a vertical fracture may still be induced. This is explained by the use of straddle packers, which applies a normal load to the borehole wall, thereby reducing the stress concentration at the corners between the straddle packer and the open hole (Haimson, 1968). Data indicating chevron notches was however not deviating strongly from the remainder of the data set and consequently that did not have to be excluded during the inversion analysis. They are though still a source of uncertainty.

Furthermore, the majority of the stress measurements at Äspö are hydraulic fracturing measurements, which means that the normal high flow rate pumping test has been used. However, this pumping procedure does not give as well defined fracture normal stress as compared to the low flow rate hydraulic jacking tests, which in turn effects the resolution of the unknown parameters during inversion. This introduces a source of uncertainty in the analysis.

All inversion results are compared with the results from hydraulic fracturing measurements. However, it should be remembered that this type of measurement is associated with several uncertainties. Schmitt and Zoback (1989) found major differences in the classical formulas regarding the calculation of maximum horizontal stress depending on if the material is porous, non-porous and whether the fluid is penetrating or not. To overcome this problem, Schmitt and Zoback (1989) proposed a modified effective stress law for extensional failure. The introduction of the modified effective stress law may be extended implying that in low-permeability, hard granitic rocks, the pore pressure effect can be neglected. In the HF measurements in the Äspö region, the pore pressure effect has been neglected which may, if the assumption is incorrect, result in an exaggerated maximum horizontal stress. Later, Schmitt and Zoback (1992) showed in a laboratory study that during a fast flow rate HF test the pore pressure diminishes. They concluded that the pore pressure perturbation could not reach equilibrium over the time scale of a fast flow rate HF test resulting in possible overestimation of the maximum horizontal stress.

Also the interpretation regarding the reopening pressure is questionable. Ito et al. (1999) and Rutqvist etal. (2000) found discrepancies regarding the true and apparent (i.e. detected) reopening pressure, which they related to equipment compliance and the effect of fluid penetration of the fracture plane. If these effects were not corrected for, the result could be a possible underestimation of σ_H.

The stress fields in all surface drilled boreholes (KAS02, KAS03 and KLX02) are disturbed by discontinuities. Below the island of Äspö it is suggested that the disturbance is caused by a potential discontinuity consisting of a layer of fractured aplite. This suggestion is strengthened by the possible appearance of the zone also in four other deep boreholes on Äspö, KAS06-08 and KAS16 at 500-600 m depth. In KLX02, two contradictory suggestions have been made concerning the structures between 700-1100 m depth. Eriksson et al. (1997) suggested that a discontinuity, consisting of two intersecting major fracture zones (SFZ04 and SFZ07), is located at 700-1100 m depth. However, Bergman et al. (2001) found two sub-horizontal reflectors at 650 and 900 m depth (dip 0-15° towards East), assuming a p-wave velocity of 5500 m/s. Bergman et al (2001) also suggested that the fracture zone at 1550-1700 m borehole length is due to a structure dipping 48°-53° towards south and that yet another zone at great depth (3 km) exists, dipping approximately 9° towards north. Further research is needed to verify/reject these suggestions.

The study of sub-vertical geological structures at Äspö (EW-1) and it's effect on the stress field is not of the quality that firm conclusions may be drawn. However, the analysis of the potential sub-horizontal structure below the island of Äspö indicates an interesting result. Above the discontinuity, the bedrock in boreholes KAS02 and KAS03 seems to be exposed to different states of stress. Within and below the potential sub-horizontal discontinuity a more comparable state of stress seems to prevail. This could be interpreted as that the bedrock behaves like a block structure down to approximately 600 m depth and below this depth the bedrock behaves more like a continuum.

The fracture orientations in the deeper sections of borehole KLX02 were determined using BIPS-pictures. The analysis proved to be very difficult and the determination of fracture orientations are consequently associated with great uncertainties. Thus, no inversion attempts from the deeper part of KLX02 were made and the state of stress is only discussed tentatively. In summary, it is suggested that the zone in KLX02 causes a strong re-orientation of the stress field, from NW orientation of maximum horizontal stress above the zone to ENE-WSW within the zone and back to NW below the zone. Below 1300 m depth the orientation of maximum horizontal stress turns towards NNW. Due to the uncertainties in the BIPS-analysis and the contradictory results concerning the orientation of maximum horizontal stress in the deeper section of KLX02 compared to Ljunggren and Klasson (1997), and the suggested occurrence of borehole breakouts and tensile fractures, it is suggested that further research is conducted to verify/reject these suggestions, see Chap. 8.

8 RECOMMENDATIONS FOR FUTURE RESEARCH

The in-situ stress measurements conducted in the Äspö region, mainly hydraulic fracturing and overcoring stress measurements, indicate different states of stress, especially regarding the magnitudes versus depth. In order to improve the interpretation of the regional stress field an integrated stress analysis approach is made. The objective is to develop an inversion program where different stress measurement techniques and stress indicators are combined, thereby determining a stress field that fits a much larger amount of data obtained from different sources. When combining the stress data, misfit functions will be included to avoid that one kind of stress data overshadows the others because they are more numerous. Thus, the recommendations for future research at Äspö involve the following:

1. Evaluation of overcoring stress data and development and calibration of a three-dimensional inversion program for overcoring stress data.

2. Integration and calibration of the programs for combination of overcoring and hydraulic stress data and development of misfit functions.

3. Further research concerning the breakouts and the possible tensile fractures in the deeper section of borehole KLX02 is recommended. The breakouts could be detected and mapped using an acoustic borehole televiewer (BHTV), which at present is the best tool for measuring borehole breakouts. In addition, this tool provides data on pre-existing fractures (if they have an acoustic and/or depth contrast with respect to the borehole wall). Furthermore, slip along pre-existing fault surfaces generated during drilling may be mapped in detail from which the stress tensor can be constrained further (e.g. Célérier, 1988). BHTV-measurements may be performed though a collaboration with Dr. Philippe Pezard, ISTEEM (CNRS), France.

4. Inclusion of other sources of stress data, e.g. borehole breakouts, tensile fractures, focal mechanisms, and core discing in the integration procedure.

5. Further investigation of the influence of geology and discontinuities (major fracture zones) on the local stress field are suggested. This could be performed through:
   a) VSP measurements in KAS02 and KAS03 to verify/reject the potential sub-horizontal zone below the island of Äspö.
   b) Modeling studies to determine the relative stiffness of zones.
   c) Further studies of the structures in borehole KLX02.

ACKNOWLEDGEMENTS

The research was made possible through financial support from the Swedish Nuclear Fuel and Waste Management Co. (SKB) and the Swedish Natural Science Council (NFR). We would like to acknowledge Dr. Christer Ljunggren, SwedPower, for sharing a paper copy of his inversion program from his publication jointly by Ljunggren and Raillard (1987), for sharing the primary data from the hydraulic stress measurements and for reviewing the manuscript. We also would like to acknowledge Mr. Rolf Christiansson, SKB, for reviewing the manuscript, Mr. Per Askling, GEOSIGMA, for helping us with color pictures and Mr. Lennart Ekman, LE Geokonsult, Mr. Sven Tirén, GEOSIGMA, Dr. Maria Ask, Stockholm University, Mr. Björn Sjödin, Comsol AB, Dr. Marcus Laaksoharju, Intera KB, the Division of Engineering Geology, KTH, and the Département de Sismologie, IPGP, for valuable comments.

REFERENCES

Ahlbom, K., Andersson, P., Ekman, L., Gustavsson, E., and Smellie, J. Preliminary investigations of fracture zones in the Brändan area, Finnsjön study site. SKB Technical Report 86-05, Stockholm, 1986, 155 pp.

Andersson, J. Statistisk analys av bergspänningsdata - En inledande studie av vertikalspänningars och töjningars djupberoende på Äspö. SKB Utveckling, Arbetsrapport U-96-33, Stockholm, 1996, 21 pp.

Andersson, J. Statistiska ansatser för att studera skillnader mellan hydraulisk spräckning och överborrning. SKB Utveckling, Arbetsrapport U-97-04, Stockholm, 1997, 12 pp.

Andersson, O. Deep drilling KLX02, Drilling and documentation of a 1700 m deep borehole at Laxemar, Sweden. SKB Technical Report 94-19, 1994, 45 pp.

Angelier, J., Tarantola, A., Valette, B. och Manoussis, S. Inversion of field data in fault tectonics to obtain the regional stress field - I. Single fault populations: a new method of computing the stress tensor. *Geophys. J. R. astr. Soc.*, Vol. **69**, 1982, pp. 607-621.

Amadei, B. and Stephansson, O. *Rock Stress and Its Measurements*, Chapman and Hall Publ., London, 1997, 490 pp.

Ask, D., Cornet, F.H., and Stephansson, O. Analysis of overcoring rock stress data in the Äspö region. *Proceeding of the 38th U.S. Rock Mechanics Symposium,* Washington, USA. A.A. Balkema Publisher, 2001b, 5 pp.

Ask, M.V.S. In-situ and laboratory stress investigations using borehole data from the North Atlantic Ocean. Doctoral thesis. Royal Institute of Technology, Stockholm, 1998, 48 pp.

Ask, M.V.S. Unpublished material, 1994.

Askling, P. Undersökning av sprickriktningar i valda avsnitt samt jämförelse med sprickdata från kärnborrhål på Äspö. Drilling KLX02-Phase 2, Lilla Laxemar, Oskarshamn. SKB Progress Report 95-44, Stockholm, 1995, 18 pp.

Bergman, B., Juhlin, C., and Palm, H. Reflektionsseismiska studier inom Laxemarområdet. SKB Report R-01-07, Stockholm, 2001, 48 pp.

Bjarnason, B. and Torikka, A. Field instrumentation for hydrofracturing stress measurements. Documentation of the 1 000 m hydrofracturing unit at Luleå University of Technology. SKB Technical Report 89-17, Swedish Nuclear Fuel and Waste Management Co., Stockholm, 1989, 24 pp.

Bjarnason, B., Klasson, H., Leijon, B., Strindell, L. and Öhman, T. Rock stress measurements in boreholes KAS02, KAS03 and KAS05 on Äspö. SKB Progress Report 25-89-17, Stockholm, 1989, 59 pp.

Bredehoeft, J.D., Wolff, R.G., Keys, W.S., and Schuter, E. Hydraulic fracturing to determine the regional stress field, Piceance Basin, Colorado. *Bull. Geol. Soc. Am.*, **87**, 1976, pp. 250-258.

Brudy, M. and Zoback, M.D. Compressive and tensile failure of borehole arbitrary-inclined to principal stress axes: application to the KTB borehole, Germany. *Int. J. Rock Mech. Min. Sci. & Geomech. Abstr.*, Vol. **30**, 1993, pp.1035-1038.

Carlsten, S. Results from borehole radar measurements in KAS05, KAS06, KAS07 and KAS08 at Äspö - Interpretation of fracture zones by including radar measurements from KAS02 and KAS04. SKB Progress Report 25-89-10, Uppsala, 1989, 32 pp.

Célérier, B. How much does slip on a reactivated fault plane constrain the stress tensor. *Tectonics*, **7** (6), 1988, pp. 1257-1278.

Cornet, F.H. and Burlet, D. Stress field determinations in France by hydraulic tests in boreholes. *J. Geophys. Res.*, **97**, 1992, pp. 11829-11849.

Cornet, F.H. and Jianmin, Y. Analysis of induced seismicity for stress field determination and pore pressure mapping. *Pageoph.*, Vol. **145**, No 3/4, 1995, pp. 677-700.

Cornet, F.H. and Valette, B. In situ determination from hydraulic injection test data. *J. Geophys. Res.*, **89**, 1984, pp. 11527-11537.

Cornet, F.H. The HTPF and the integrated stress determination methods. *Comprehensive Rock Engineering*, Vol **3**. (J. Hudson, Ed.). Pergamon Press, Oxford, 1993a, pp. 413-432.

Cornet, F.H. Stresses in rock and rock masses. *Comprehensive Rock Engineering*, Vol **3**. (J. Hudson, Ed.). Pergamon Press, Oxford, 1993b, pp. 297-327.

Cosma, C., Heikkinen, P., Keskinen, J., and Kormonen, R. VSP-survey including 3-D interpretation in Äspö, Sweden. Borehole KAS07. SKB Progress Report 25-90-07, Stockholm, 1990, 34 pp.

*Ekman, D. Rock stress, hydraulic conductivity and stiffness of fracture zones in the Laxemar borehole, Småland, Sweden. Master of Science Thesis, Royal Institute of Technology, Stockholm, Sweden, 1997, 52 pp.

*Ekman, D., Rutqvist, J. and Ljunggren, C. Determination of hydromechanical parameters down to 1 340 m depth in borehole KLX02 in Laxemar, Sweden. Paper presented at Rock Mechanics Meeting in Stockholm March 12, 1997 (Ed. C. Bachman). Swedish Rock Engineering Research (SveBeFo), Stockholm, 1997a, pp. 39-61.

*Ekman, D., Rutqvist, J., Stephansson and Nilsson, T. Laboratory compliance tests of the Vattenfall Hydropower Co multihose field unit. In SKB Project Report U-97-26, 1997b, 17 pp.

*Ekman, D., now Ask, D.

Ekman, L. Project deep drilling KLX02 Phase-2. Scope of activities and results. Summary report. SKB Report in press, 2001.

Enever, J., and Chopra, P.N. Experience with hydraulic fracturing stress measurements in granites. *Proceeding International Workshop on Rock Stress and Rock Stress Measurements* (Stephansson Ed.), Stockholm. Centek Publisher, Luleå, 1989, pp. 411-420.

Eriksson, L., Johansson, R., Thunehed, H., and Triumf, K-A. Metodtester ytgeofysik 1996. Bestämning av berggrundens bulkresistivitet och djupet till salint grundvatten med halvregional resistivitetsmätning, elektrisk sondering samt transient elektromagnetisk sondering. SKB Projekt Rapport D-98-01, 1998, 83 pp.

Evans, K.F., Engelder, T. and Plumb, R.A. Appalachian stress study 1. A detailed description of in situ stress variations in devonian shales of the Appalachian Plateau. *J. Geophys. Res.*, Vol. **94**, 1989, pp. 7129-7154.

Follin, S. Djupborrning KLX02 - Etapp 2. Lilla Laxemar, Oskarshamns kommun. Interpretation of the hydraulic testing of KLX02. SKB Progress Report U-96-32, 1996, 11 pp.

Gronseth, J.M. and Kry, P.R. Instantaneous shut-in pressure and it's relationship to the minimum in-situ stress. *Proceeding from the Hydraulic fracturing Stress Measurements*, Monterey, National Academy Press, Washington DC, 1983, pp. 55-60.

Haimson, B.C. Hydraulic fracturing in porous and nonporous rock and its potential for determining in situ stresses at great depth. Unpublished PhD Thesis, University of Minnesota, 1968, 234 pp.

Hall, A. *Igneous petrology*, Longman Group UK Limited, London, 1987, 573 pp.

Hallbjörn, L., Ingevald, K., Martna, J., and Strindell, L. New automatic probe for measuring triaxial stresses in deep boreholes. *Tunneling Underground Space Technology*, Vol. **5**, No. 1/2, 1990, pp. 141-145.

Hansson, H., Stephansson, O. and Shen, B. Site-94, Far-field rock mechanics modelling for nuclear waste disposal. SKI Report 95:40, Stockholm, 1995, 83 pp.

Hardy, M.P. Fracture mechanics applied to rock. Unpublished PhD Thesis, University of Minnesota, Minneapolis, 1973.

Hayashi, K. and Sakurai, I. Interpretation of hydraulic fracturing shut-in curves for tectonic stress measurements. *Int. J. Rock Mech. Min. Sci. & Geomech. Abstr.*, **26**, 1989, pp 477-482.

Hermansson, J. Structural geology of water-bearing fractures, SKB Progress Report, 25-95-23, Stockholm, 1995, 63 pp.

Hubbert, M.K. and Willis, D.G. Mechanics of hydraulic fracturing. *Pet. Trans.* Vol. **210**, pp. 153-168

Hudson J.A. and Cooling, C.M. In situ rock stresses and their measurements in the UK-Part 1. The current state of knowledge. *Int. J. Rock Mech. Min. Sci. & Geomech. Abstr.*, Vol. **25**, 1988, pp. 363-370.

Ito, T., Evans, K., Kawai, K., and Hayashi, K. Hydraulic fracturing reopening pressure and the estimation of maximum horizontal stress. *Int. J. Rock Mech. & Min. Sci.*, Vol. **36**, 1999, pp. 811-826.

Juhlin, C. Evaluation of reprocessed seismic refraction data from Äspö. SKB Progress Report 25-90-02, Stockholm, 1990, 12 pp.

Julien, Ph. Och Cornet, F.H. Stress determination from aftershocks of the Campania-Lucania earthquake of November 23, 1980. *Ann. Geophys.*, Vol. **5B**, 1987, pp. 289-30.

Klasson, H. Interpretation of pressure versus time in hydrofracturing stress measurements. Unpublished MSc Thesis, Luleå University of Technology, Luleå, 1989, 53 pp.

Kornfält, K.-A. and Wikman, H. Drilling KLX02-Phase 2 Lilla Laxemar, Oskarshamn. Petrological classification of core samples and drill cuttings. SKB Progress Report 94-50, Lund, 1994, 8 pp.

Klasson, H., Persson, M., Ljunggren, C. and Bergsten, K-Å. SKB Report in press, 2001.

Laaksoharju, M., Smellie, J., Nillson, A.-C. and Skårman, C. Groundwater sampling and chemical characterization of the Laxemar deep borehole KLX02. SKB Technical Report 95-05, Stockholm, 1995, 74 pp.

Lee, M.Y. and Haimson, B.C. Statistical evaluation of hydraulic fracturing stress measurement parameters. *Int. J. Rock Mech. Min. Sci. & Geomech. Abstr.*, Vol. **26**, 1989, pp. 447-56.

Lee, M. and Stillborg, B. Äspö virgin stress measurement results in sections 1050, 1190 and 1620 m of the access ramp. SKB Progress Report 25-93-02, Stockholm, 1993, 117 pp.

Lee, M., Hewitt, T. and Stillborg, B. Äspö virgin stress measurement results. Measurements in boreholes KA1899A, KA2198A and KA2510A. In SKB Progress Report 25-94-02, Stockholm, 1994, 66 pp.

Leijon, B. Summary of rock stress data from Äspö. SKB Progress Report 25-95-15, Stockholm, 1995, 12 pp.

Liedholm, M. Conceptual modeling of Äspö, Technical notes 1-17. General geological, hydrogeological and hydrochemical information. SKB Progress Report 25-90-16a, Stockholm, 1991a, 12 pp.

Liedholm, M. Conceptual modeling of Äspö, Technical notes 18-32. General geological, hydrogeological and hydrochemical information. SKB Progress Report 25-90-16b, Stockholm, 1991b, 12 pp.

Litterbach, N., Lee, M. Struthers, M. and Stillborg, B. Virgin stress measurement results in boreholes KA2870A and KA3068A. SKB Progress Report 25-94-32, Stockholm, 1994, 26 pp.

Ljunggren, C. and Bergsten, K-Å. Rock stress measurements in KA3579G, prototype repository. SKB Progress Report HRL-98-09, Stockholm, 1998, 25 pp.

Ljunggren, C., Chang, Y. och Andersson, J. Bergspänningsmätningars representativitet - Mätnoggrannhet och naturliga variationer vid hydraulisk spräckning och överborrning. SveBeFo Rapport 37, Stockholm, 1998, 79 pp.

Ljunggren, C. and Klasson, H. Deep hydraulic fracturing rock stress measurements in borehole KLX02, Laxemar, Drilling KLX02-Phase 2, Lilla Laxemar, Oskarshamn. SKB Utveckling, Project Report U-97-27, Stockholm, 1997, 33 pp.

Ljunggren, C. and Klasson H. Rock stress measurements at Zedex test area, Äspö HRL. Äspö Hard Rock Laboratory, Technical Note TN-96-08z, Stockholm, 1996, 34 pp.

Ljunggren, C. och Persson, M. Beskrivning av databas - Bergspänningsmätningar i Sverige. SKB Djupförvar, Projekt Rapport PR D-95-017, Stockholm, 1995, 21 pp.

Ljunggren, C. and Raillard, G. Rock stress measurements by means of hydraulic tests on pre-existing fractures at Gideå site, Sweden. *Int. J. Rock mech. Min. Sci. & Geomech. Abstr.*, Vol. **24**, 1987, pp. 339-345.

Lundholm, B. Analysis of rock stress and rock stress measurements with application to Äspö HRL. Licentiate Thesis, Luleå University of Technology, Luleå, 2000a, 125 pp.

Lundholm, B. Rock stress and rock stress measurements at Äspö HRL. SKB International Progress Report IPR-00-24, Stockholm, 2000b, 64 pp.

Mason, B. and Moore, C.B. *Principles of geochemistry*, John Wiley and Sons Inc., Hong Kong, 1982, 344 pp.

Menke, W. *Geophysical Data Analysis: Discrete Inverse Theory*, Academic Press, Inc., Orlando, Florida, 1984, 260 pp.

Munier, R. Studies of geological structures at Äspö. Comprehensive summary of results. SKB Progress Report 25-95-21, Stockholm, 1995, 155 pp.

Myrvang, A.M. Evaluation of in-situ rock stress measurements at the Zedex test area. SKB, Progress Report HRL-97-22, 1997, 14 pp.

Nilsson, G., Litterbach, N., Lee, M., and Stillborg, B. Virgin stress measurement results, borehole KZ0059B. Äspö Hard Rock Laboratory, Technical Note TN-97-25g, Stockholm, 1997, 3 pp.

Nilsson, L. Hydraulic tests at Äspö, KAS05-KAS08, HAS13-HAS17. Evaluation. SKB, Progress Report 25-89-20, Stockholm, 1989, 85 pp.

Nisca, D.H. Geophysical laboratory measurements on core samples from KLX01, Laxemar and KAS02, Äspö. SKB, Progress Report 25-88-06, Stockholm, 1988, 24 pp.

Niva, B. and Gabriel, G. Borehole radar measurements at Äspö and Laxemar - Boreholes KAS02, KAS03, KAS04, KLX01, HAS02, HAS03 and HAV07. SKB Progress Report 25-88-03, Stockholm, 1988, 23 pp.

Nyberg, G., Jönsson, S., and Ekman, L. Groundwater level program. Report for the period 1987-1989. SKB Progress Report 25-90-18, Stockholm, 1991, 37 pp.

Patchett, P.J., Todt, W., and Gorbatschev, R. Origin of continental crust of 1.9-1.7 Ga age; Nd-isotopes in the Svecofennian orogenic terrains of Sweden. *Precambrian Research*, Vol. **35**, 1987, pp. 145-160.

Ploug, C. and Klitten, K. Shallow reflection seismic profiles from Äspö, Sweden. SKB Progress Report 25-89-02, Stockholm, 1989, 12 pp.

Ratigan, J.L. The use of the fracture reopening pressure in hydraulic fracturing stress measurements. *Rock Mech. Rock Eng.*, **25**, 1992, pp. 225-136.

Rhén, I. SKB-Swedish Hardrock Laboratory. Transient interference tests on Äspö 1988, Evaluation. SKB Progress Report 25-88-13, Stockholm, 1989, 163 pp.

Rhén, I. Transient interference tests on Äspö 1989 in KAS06, HAS13 and KAS07. SKB Progress Report 25-90-09, Stockholm, 1991, 242 pp.

Rhén, I., Gustavsson, G. and Wikberg, P. Äspö HRL-Geoscientific evaluation 1997/4. Results from pre-investigations and detailed site chracterization. Comparison of predictions and observations. Hydrogeology, groundwater chemistry and transport of solutes. SKB Technical Report 97-05, Stockholm, 1997a, 321 pp.

Rhén, I., Gustavsson, G., Stanfors, R. and Wikberg, P. Äspö HRL-Geoscientific evaluation 1997/5. Models based on site characterization 1986-1995. SKB Technical Report 97-06, Stockholm, 1997b, 428 pp.

Ritchie, R.H. and Sakakura, A.Y. Asymptotic expansions of solutions of the heat conduction equation in internally bounded cylidrical geometry. *J. Appl. Phys.*, Vol. **27**, 1956, pp. 1453-1459.

Rutqvist, J. Coupled stress-flow properties of rock joints from hydraulic field testing. Doctoral thesis. Royal Institute of Technology, Stockholm, 1995, 31 pp.

Rutqvist, J., Tsang, C.-F., *Ekman, D. and Stephansson, O. Evaluation of in-situ hydromechanical properties of rock fractures at Laxemar in Sweden. *Proceeding of the 1st Asian Rock Mechanics Symposium*, ARMS '97, Seoul, Korea. A.A. Balkema Publisher, 1997, pp. 619-24.

*Ekman, D., now Ask, D.

Rutqvist J., Tsang C.-F , and Stephansson, O. Uncertainty in the principal stress estimated from hydraulic fracturing measurements due to the presence of the induced fracture. *Int. J. Rock Mech. Min. Sci. & Geomech. Abstr.*, Vol. **37**, 2000, pp. 107-120.

Schmitt, D.R. and Zoback, M.D. Poroelastic effects in the determination of the maximum horizontal principal stress in hydraulic fracturing tests - A proposed breakdown equation employing a modified effective stress relation for tensile failure. *Int. J. Rock Mech. Min. Sci. & Geomech. Abstr.*, Vol. **26**, 1989, pp. 499-506.

Schmitt, D.R. and Zoback, M.D. Diminished pore pressure in low-porosity crystalline rock under tensional failure: Apparent strengthening by dilatancy. *Int. J. Rock Mech. Min. Sci. & Geomech. Abstr.*, Vol. **97**, 1992, pp. 273-288.

Scotti, O. and Cornet, F.H. In-situ stress fields and focal mechanism solutions in central France. *Geophys. Res. Lett.*, Vol. **21**, nb. 22, 1994, pp. 2345-2348.

Sehlstedt, S. and Triumf, C-A. Interpretation of geophysical logging data from KAS02-KAS04 and HAS08-HAS12 at Äspö and KLX01 at Laxemar. SKB, Progress Report 25-88-15, Stockholm, 1988, 20 pp.

Sehlstedt, S. and Stråhle, A. Geological core mapping and geophysical borehole logging in the boreholes KAS05-08 at Äspö. SKB, Progress Report 25-89-09, Stockholm, 1989, 25 pp.

Shen, B. Mechanics of fractures and intervening bridges in hard rocks. Doctoral thesis, Div. Eng. Geol. KTH, Stockholm, 1993, 38 pp.

Sirat, M. Structural and neural network analyses of fracture systems at the Äspö Hard Rock Laboratory, SE Sweden. Doctoral thesis, Faculty of Science and Technology, Uppsala University, 1999, 153 pp.

Smellie, J. and Laaksoharju, M. The Äspö Hard Rock Laboratory: Final evaluation of the hydrogeochemical pre-investigations in relation to existing geologic and hydraulic conditions. SKB Technical Report 92-31, Stockholm, 1992, 239 pp.

Stanfors, R., Erlström, M. and Markström, I. Äspö HRL-Geoscientific evaluation 1997/1. Overview of site characterization 1986-1995. SKB Technical Report 97-02, Stockholm 1997, 153 pp.

Stanfors, R. Drilling KLX02 - Phase 2, Lilla Laxemar, Oskarshamn. Brief geological description of the cored borehole KLX02. SKB Progress Report 95-37, 1995, 17 pp.

Stanfors, R. Geological borehole description: KAS02, KAS03, KAS04 and KLX01. SKB, Progress Report 25-88-18, Stockholm, 1988, 88 pp.

Stephansson, O. The importance of rock stress measurement and it's interpretation for rock disposal of hazardous waste. *Proceeding of the international symposium on rock stress*, Kumamoto, Japan. A.A. Balkema Publisher, 1997, pp. 3-13.

Stephens, G. and Voigt, B. Hydraulic fracturing theory for condition of thermal stress. *Int. J. Rock Mech. Min. Sci. & Geomech. Abstr.*, Vol. **19**, 1982, pp. 279-284.

Stille, H. and Olsson, P. Summary of rock mechanical results from the construction of Äspö Hard Rock Laboratory. SKB Progress Report HRL-96-07. 1996, 24 pp.

Talbot, C.J. and Munier, R. Faults and fracture zones in Äspö. SKB, Progress Report 25-89-11, Stockholm, 1989, 58 pp.

Talbot, C.J. and Sirat, M. Stress control of hydraulic conductivity in fracture-saturated Swedish bedrock. *Engineering Geology*, in press 2001.

Tarantola A. and Valette B. Generalized non-linear inverse problem solved using the least square criterion. *Rev. Geophys. Space. Phys.*, **20**, 1982, pp. 219-32.

Tirén, S.A. Comparison of the SKI, SKB and SKN geological and structural models of the Äspö area. SKI Report 97:19, Stockholm, 1996, 81 pp.

Tirén, S.A, Beckholmen, M., Voss, C., and Askling, P. Development of a geological and structural model of Äspö, southeastern Sweden. SKI Report 96:16, Stockholm, 1996, 198 pp.

Wikberg, P., Gustavsson, G., Rhén, I., and Stanfors, R. Äspö Hard Rock Laboratory. Evaluation and conceptual modeling based on the pre-investigations 1986-1990. SKB Technical Report 91-22, Stockholm, 1991, 213 pp.

Wikman, H., Kornfält, K-A., Raid, L., Munier, R. and Tullborg, E-L. Detailed investigation of drillcores KAS02, KAS03 and KAS04 on Äspö island and KLX01 at Laxemar. SKB Progress Report 25-88-11, Stockholm 1988, 102 pp.

Yin, J.M. and Cornet, F.H. Integrated stress determination by joint inversion of hydraulic tests and focal mechanisms. *Geophys. Res. Lett.*, Vol. **21**, nb. 24, 1994, pp. 2645-2648.

Zoback, M.D., Healy, J.H. and Roller, J.C. Preliminary stress measurements in Central California using the hydraulic fracturing technique. *Pageoph.*, Vol. **115**, 1977, pp. 135-152.

APPENDIX

Table A-1. Results from hydraulic stress measurements in borehole KAS02 (Bjarnason and Klasson, 1989, Ljunggren and Klasson, 1997, Ekman, 1997, Ekman et al., 1997).

Vertical Depth	Ps_1	Ω_{Ps1}	Ps_2	Ω_{Ps2}	ϕ	Ω_ϕ	θ	Ω_θ
KAS02								
155,2	9,1	1,0	7,5	0,5	230	3	90	1
228,8	9,1	0,7	7,6	0,3	238	3	90	3
232,9	8,5	0,9	6,2	0,2	237	1	90	2
					231	3	82	4
					302	4	67	5
243,1	8,9	0,9	6,8	0,5	251	1	90	4
					92	2	81	3
250,2	9,0	0,8	7,4	0,4	234	6	90	2
					209	3	18	2
					133	2	23	4
279,9	9,8	1,5	6,4	0,7	257	1	90	2
339,4	10,4	1,8	7,0	0,6	236	1	90	2
					70	3	88	4
346,0	10,9	1,1	9,0	0,6	263	1	90	2
					57	2	69	1
363,7	10,3	0,9	9,1	0,8	238	3	90	4
					267	3	90	2
					231	4	89	4
380,7	10,5	0,9	7,9	0,5	250	2	90	2
389,8	9,0	0,8	8,1	0,5	213	6	90	4
					209	2	84	3
425,6	11,2	0,7	10,5	0,3	227	1	90	1
494,9	19,6	1,4	18,4	1,4	231	1	90	2
					158	1	36	1
504,1	21,5	1,4	20,1	0,5	234	1	90	1
521,8	21,2	2,1	17,9	1,5	230	1	90	1
547,0	23,9	1,5	22,0	1,0	216	4	90	2
610,7	32,9	1,9	28,7	0,7	202	4	38	3
					250	1	28	3
624,8	31,1	1,1	28,8	1,5	227	1	90	2
					19	2	77	1
643,0	26,2	2,1	22,9	1,1	203	1	90	2
660,7	27,8	2,0	27,5	2,0	240	1	90	1
718,5	32,6	1,6	30,2	1,2	200	1	90	2
734,0	29,2	1,1	28,2	1,0	158	1	56	1
					160	2	56	3

Table A-2. Results from hydraulic stress measurements in borehole KAS03 (Bjarnason and Klasson, 1989, Ljunggren and Klasson, 1997, Ekman, 1997, Ekman et al., 1997).

Vertical Depth	Ps_1	Ω_{Ps1}	Ps_2	Ω_{Ps2}	ϕ	Ω_ϕ	θ	Ω_θ
KAS03								
131,2	7,6	1,4	5,3	0,8	235	1	90	1
153,5	10,3	2,1	6,0	0,6	266	2	88	2
346,6	10,5	2,0	8,1	1,1	29	2	15	1
					40	2	42	1
					40	2	28	1
480,3	13,8	1,5	12,1	0,5	260	3	90	2
493,6	13,8	1,2	12,5	0,4	217	2	90	1
					188	2	81	2
513,9	17,3	1,7	14,4	1,1	216	2	90	1
					150	1	53	1
532,8	13,0	0,4	12,5	0,1	238	1	90	1
534,7	16,0	1,1	13,4	0,4	244	1	90	1
544,6	14,6	1,0	12,5	0,4	214	1	90	1
546,6	13,9	0,9	11,7	0,6	219	6	90	3
549,6	13,6	0,7	12,3	0,4	233	1	90	1
662,5	12,6	1,5	9,7	0,7	240	4	90	1
					178	3	28	5
664,5	11,5	1,3	10,5	0,6	238	2	90	1
736,8	15,4	1,1	15,2	0,3	256	2	90	1
					237	2	88	3
818,0	30,0	1,5	29,4	1,5	190	2	85	3
820,4	29,2	1,6	26,4	0,5	253	2	74	2
875,4	27,4	1,8	23,8	0,7	230	2	75	2
878,4	29,0	1,9	24,5	0,5	216	4	90	3
883,3	29,2	1,5	25,5	0,2	212	6	90	2
					193	3	77	2
					259	3	24	3
891,2	32,2	1,7	27,4	0,5	251	2	75	2
					241	5	90	5
960,6	30,5	0,7	27,8	0,2	283	2	31	2

Table A-3. Results from hydraulic stress measurements in borehole KLX02 (Bjarnason and Klasson, 1989, Ljunggren and Klasson, 1997, Ekman, 1997, Ekman et al., 1997).

Vertical Depth	Ps_1	Ω_{Ps1}	Ps_2	Ω_{Ps2}	ϕ	Ω_ϕ	θ	Ω_θ
KLX02								
206,4	8,6	0,8	7,9	0,6	267	1	90	1
265,4	7,6	0,3	10,8	0,2	259	2	66	2
266,0	6,3	0,4	6,8	0,5	230	5	65	3
272,5	7,9	1,5	5,9	0,9	356	2	44	2
288,2	7,5	0,9	4,7	0,4	210	3	8	1
305,8	8,9	1,5	6,8	1,0	91	1	62	1
					104	1	90	1
314,5	7,8	0,5	4,4	0,3	31	1	61	2
					254	2	54	1
					25	2	80	3
315,2	7,8	0,3	4,4	0,3	26	1	60	1
336,6	6,6	0,5	3,9	0,5	226	1	27	1
					269	1	63	1
337,2	8,2	0,2	7,8	0,5	234	3	50	1
					99	4	81	1
					214	1	7	1
346,7	9,1	2,7	7,7	1,2	198	2	56	1
					230	3	61	2
352,7	11,2	2,4	9,9	1,9	51	2	52	2
					59	3	56	3
					63	2	69	3
					223	2	90	2
427,4	9,8	1,1	9,1	1,1	234	3	90	2
504,1	18,0	2,0	12,8	0,9	230	2	90	1
					334	1	68	1
					92	1	40	1
540,5	17,5	1,4	16,2	1,1	237	1	87	2
					239	1	90	2
					237	1	83	2
555,7	15,8	1,2	13,3	0,9	223	1	76	1
					120	1	90	1
579,5	18,7	0,9	16,7	0,7	256	1	90	1
601,2	17,1	0,9	16,7	0,6	119	1	90	1
641,8	22,0	2,1	19,5	0,5	50	2	61	1
					294	4	41	8
704,8	22,0	1,2	19,2	0,9	238	1	90	1
753,9	13,8	1,0	12,5	0,7	90	2	61	1
					90	1	58	3
					114	1	90	1
868,2	17,2	1,1	16,7	1,1	350	4	28	4
					37	2	48	2
					255	*5*	*90*	*2*
					178	*4*	*39*	*4*
870,0	18,1	1,4	17,6	1,4	84	1	30	1
					85	*5*	*49*	*5*
					20	*5*	*67*	*5*

Vertical Depth	Ps_1	Ω_{Ps1}	Ps_2	Ω_{Ps2}	ϕ	Ω_ϕ	θ	Ω_θ
KLX02								
876,3	17,2	1,6	15,6	1,6	154	3	83	4
					210	*1*	*90*	*1*
					180	*3*	*50*	*3*
					35	*5*	*61*	*5*
986,8	22,3	0,6	21,3	0,6	90	2	78	3
					306	3	47	5
1070,9	19,8	2,6	-	-	225	2	56	2
					171	2	16	2
					153	3	35	3
					173	3	35	3
					163	3	43	3
1128,7	22,9	1,4	22,0	1,2	*169*	*3*	*48*	*5*
					172	*5*	*50*	*5*
					136	*5*	*31*	*5*
					298	*5*	*66*	*5*
					246	*5*	*90*	*5*
1169,5	19,5	1,2	18,8	1,1	283	2	78	2
					33	2	11	2
					299	2	74	2
1190,0	28,9	1,1	26,7	0,7	*354*	*5*	*81*	*5*
					74	*5*	*48*	*5*
					249	*5*	*90*	*5*
					215	*5*	*90*	*5*
1207,4	22,9	1,2	21,6	0,8	*337*	*5*	*61*	*5*
					4	*5*	*69*	*5*
					235	*5*	*90*	*5*
1219,3	25,5	1,0	24,4	0,5	*231*	*3*	*90*	*3*
1222,3	26,6	1,2	24,2	1,0	*98*	*5*	*30*	*5*
					198	*5*	*37*	*5*
					139	*5*	*18*	*5*
					196	*5*	*42*	*5*
1225,3	25,1	1,0	23,3	1,0	24	1	81	2
1270,1	28,9	1,2	27,1	0,7	347	2	25	2
					236	2	9	2
					335	5	53	5
					11	5	24	5
1282,6	29,8	1,1	30,2	0,4	*150*	*2*	*65*	*3*
					119	*5*	*76*	*5*
					178	*5*	*79*	*5*
					250	*5*	*90*	*5*
1288,1	32,3	1,1	30,9	0,5	*0*	*5*	*61*	*5*
					351	*5*	*58*	*5*
					20	*2*	*19*	*2*
					281	*5*	*4*	*5*
1291,1	31,7	0,8	31,3	0,6	143	1	79	1
					248	1	49	1
1295,1	30,4	1,1	29,8	1,3	*153*	*5*	*81*	*5*
					257	*2*	*50*	*2*
					205	*5*	*75*	*5*
					324	*1*	*83*	*1*
1324,4	32,3	1,6	29,4	1,2	225	2	65	2
					233	5	90	5
					18	3	36	2
					48	3	21	3

Vertical Depth	Ps_1	Ω_{Ps1}	Ps_2	Ω_{Ps2}	ϕ	Ω_ϕ	θ	Ω_θ
KLX02								
1330,9	31,9	1,4	29,7	0,9	*224*	*5*	*43*	*5*
					11	*5*	*51*	*5*
					357	*5*	*57*	*5*
					20	*5*	*49*	*5*
1333,9	30,0	1,0	29,4	0,5	203	2	73	2
					235	*5*	*90*	*5*
					303	3	45	3
1336,9	40,4	1,7	40,8	1,7	*135*	*5*	*62*	*5*
					283	*5*	*39*	*5*
					325	*5*	*16*	*5*
					354	*5*	*39*	*5*

Fracture orientations in italic are associated with very large uncertainties.